

NASA TECHNICAL
MEMORANDUM

NASA TM X-53693

January 11, 1968

NASA TM X-53693

A COLLECTION OF PAPERS RELATED TO
PLANETARY METEOROLOGY

Edited by Don K. Weidner
Aero-Astroynamics Laboratory

NASA

*George C. Marshall
Space Flight Center,
Huntsville, Alabama*



FACILITY FORM 602

N 68-18836	N 68-18847
(ACCESSION NUMBER)	(THRU)
180	1
(PAGES)	(CODE)
TMX-53693	30
(NASA CR OR TMX OR AD NUMBER)	(CATEGORY)

NASA - GEORGE C. MARSHALL SPACE FLIGHT CENTER

Technical Memorandum X-53693

January 11, 1968

A COLLECTION OF PAPERS RELATED TO PLANETARY METEOROLOGY

Edited by

Don K. Weidner

SPACE ENVIRONMENT BRANCH
AEROSPACE ENVIRONMENT DIVISION
AERO-ASTRODYNAMICS LABORATORY
RESEARCH AND DEVELOPMENT OPERATIONS

PREFACE

The science of planetary meteorology has developed very rapidly during the last decade. Impetus from the data obtained during initial planetary atmosphere experiments has stimulated research for more detailed representations of the planetary atmospheres that are essential to future, more refined experiments. Specifically, this research has entailed the development of more refined data acquisition techniques and the establishment of theoretical and empirical atmospheric models.

The scientific papers contained in this document represent a one-year effort of the MSFC planetary atmosphere study program. Emphasis was placed upon the Mars atmosphere because of MSFC involvement in the Voyager program, but in view of the decline in interest for planetary exploration, the emphasis is now being placed upon the upper earth atmosphere. However, since the planetary atmosphere study program was established with versatility in mind, the techniques used in generating Mars atmospheric information may also be applied to the earth's atmosphere.

The first three papers, which are concerned with atmospheric processes, provide theoretical concepts of the Mars atmospheric composition and temperature. Techniques used in computing the ground surface temperature and generating model atmospheres are described in papers 4 and 5, respectively. The next two papers provide empirical models of the Mars atmosphere and are followed by a paper on the atmosphere of Mercury. The feasibility of obtaining Martian atmospheric information from vacuum chamber simulation experiments is discussed in the last three papers.

The editor wishes to express his sincere appreciation to S. Hightower and I. Dolin for their efforts in preparing this document for publication.

Don K. Weidner

Aerospace Environment Division
Aero-Astroynamics Laboratory
George C. Marshall Space Flight Center
Huntsville, Alabama

TABLE OF CONTENTS

<u>Paper No.</u>	<u>Title</u>	<u>Page</u>
1	CHEMICAL KINETICS AND COMPOSITION OF THE MARS ATMOSPHERE - M. Bortner and F. Alyea.....	1 ✓
2	A TEMPERATURE PROFILE OF THE UPPER MARTIAN ATMOSPHERE FROM A KINETIC VIEWPOINT - James W. Johnson.....	29 ✓
3	A METHOD FOR THE PREDICTION OF THE MARTIAN TEMPERATURE AND SOME APPLICATIONS OF METEOROLOGICAL ANALYSIS - Y. S. Lou.....	35 ✓
4	PREDICTION OF MARTIAN SURFACE TEMPERATURE - F. B. Tatom, P. B. Deshpande, and F. T. Hung.....	49 ✓
5	THE MSFC PLANETARY ATMOSPHERE COMPUTER PROGRAM - John Chambers and Ed Seely.....	69 ✓
6	MARTIAN ATMOSPHERIC MODELS - Don K. Weidner.....	81 ✓
7	OUTER ATMOSPHERE STRUCTURE OF MARS - Don Vachon and K. Lichtenfeld.....	87 ✓
8	MODEL ATMOSPHERES OF MERCURY - Otha H. Vaughan...	109 ✓
9	LIMITATIONS IN KNOWLEDGE OF THE THERMODYNAMIC PROPERTIES OF THE MARTIAN ATMOSPHERE - Wallace W. Youngblood.....	131 ✓
10	SIMULATION STUDY OF MARTIAN ATMOSPHERIC CONDITIONS - T. S. Chang.....	149 ✓
11	SIMULATION OF THE TRANSPORTATION AND DEPOSITION OF DUST AND SAND BY MARTIAN ATMOSPHERIC PROCESSES - W. C. Lucas and W. W. Youngblood.....	155 ✓

CHEMICAL KINETICS AND COMPOSITION OF THE MARS ATMOSPHERE

By

M. Bortner and F. Alyea*

SUMMARY

N68-18837

The composition of the Martian atmosphere as a function of altitude is dependent upon the chemical kinetics. A complex chemical system has been developed, and the chemical kinetics involved have been calculated. These calculations resulted in a predicted steady-state atmosphere which gives the concentrations of eighteen species as a function of altitude. (The calculations involved fifty chemical reactions, ten of which were photochemical.) A total density distribution and three elemental compositions (corresponding to those given by 80 percent CO_2 , 20 percent N_2 ; 90 percent CO_2 , 10 percent N_2 ; and 100 percent CO_2) were assumed. Mean and extreme solar flux values were used to evaluate the effect of solar activity on the atmosphere. Although no account was taken of diffusion, it is an important factor which should be considered in a subsequent study.

Based on the results obtained for the neutral species, it is found that CO_2 is more than 50 percent dissociated at all altitudes above 60 km. Above this CO and O are major constituents. Ozone is present in mole fractions comparable to those in the Earth's atmosphere. Nitrogen oxides probably do not build up in large concentrations.

Charged species are more difficult to predict. Above 80 km electrons are the only important negatively charged species. Below this, negative ions, especially CO_3^- , become important but none build up to large concentrations. The major positive ions are O^+ , N^+ and CO^+ at high altitudes and NO^+ at lower altitudes.

*The authors are associated with the General Electric Corporation, Missile and Space Division, Valley Forge, Pennsylvania. This paper was prepared for MSFC under contract number NAS8-22603.

I. INTRODUCTION

For some experiments which have been suggested for Mars atmosphere exploration to be successful, it is important to have well founded predictions of the atmospheric composition as a function of altitude. The major component indicated by available data is carbon dioxide. However, at high altitudes where solar flux in the effective wavelength range of from 1300 to 1650 Å is available, the carbon dioxide is largely dissociated. It is therefore not sufficient to know that the Mars atmosphere is largely CO₂ and that N₂ is present; it is also necessary to know the major species to be expected at each altitude. The fraction of CO₂ dissociated at various altitudes depends not only upon the solar flux but also on a number of reactions, some of which involve minor species. Only a thorough chemical kinetics investigation involving such minor species and many reactions can establish these primary features.

In this study, the possible importance of a number of minor species and many reactions was tested. Previous studies, which used only an extremely simple chemical system, probably resulted in somewhat erroneous compositions because of these simplifications. The present study has been conducted to be as complete in its chemical kinetics as necessary to avoid this problem. Other features can be added in the future so that the present study can be made more comprehensive.

II. ATMOSPHERIC DATA

The predictions of the atmospheric composition must be based on available data and must agree with them within their limits of uncertainty. Such available data, which have been described and discussed in detail (e.g., Fjeldo et al. [8], Chamberlain [4], Chamberlain and McElroy [5], Spinrad et al. [13], Owen [12], and Edelson [7]), are limited primarily to pressure, spectra, and electron density measurements. The information acquired from these measurements give direct usable estimates of pressure as a function of altitude, pressure scale height, electron density as a function of altitude, and total CO₂ content. From these, indirect estimates of number density, temperature, and certain other quantities have been made. The indirect estimates involve certain assumptions which introduce considerable uncertainty in the derived quantities. Since some of these quantities are used in the calculations to be described, these calculations will involve similar uncertainties. However, the results of this study might possibly help in reducing the uncertainty in quantities that are indirectly derived from future Mars atmospheric measurements.

The data which are used in the calculations are the number density as a function of altitude, the relative elemental composition, and of lesser importance, temperature. The number densities were taken from Fjeldbo et al. [9].

Since the CO₂ content of the Mars atmosphere, as determined by spectral measurements, appears to be nearly as large as the total density derived from the pressure measurements, the composition of the atmosphere has been assumed to be at least 80 percent CO₂ and perhaps as much as 100 percent CO₂. For cases where the composition consists of less than 100 percent CO₂, the remaining material is usually assumed to be nitrogen. The latter assumption was accepted in performing the calculations, but a further study with other gases as the remaining material would seem in order. The elemental compositions assumed for the calculations were

- (a) 0.8 C; 1.6 O; 0.4 N
- (b) 0.9 C; 1.8 O; 0.2 N
- (c) 1 C; 2 O.

The total density as a function of altitude is shown in figure 1.

The solar flux at the top of the Mars atmosphere was obtained by modifying the corresponding values obtained for the Earth, through use of correction factors [1] to account for the different heliocentric distances.

III. CHEMICAL SYSTEM AND CHEMICAL KINETICS

A. Chemical Species

The steady-state concentrations have been calculated as a function of altitude. The concentrations are those of eighteen species comprising seven neutral species, free electrons, seven positive ions, and three negative ions. The specific species considered were as follows:

CO ₂	CO ₂ ⁺	O ⁻
N ₂	N ₂ ⁺	O ₂ ⁻
N	N ⁺	O ₃ ⁻
CO	CO ⁺	e
O	O ⁺	
O ₂	O ₂ ⁺	
O ₃	NO ⁺	

The concentrations calculated were steady-state concentrations for an average solar flux and for a flux increased by a factor of 2.3 at all wavelengths. Although time-varying concentrations should be calculated using normal flux variations, such calculations were considered to be outside the scope of the present study.

The calculations included the various photochemical processes and the other chemical reactions which appreciably affect the concentrations of the major species of interest. The attenuation of the flux through the atmosphere was calculated along with the changes in concentrations resulting from the photochemical processes.

B. The Chemical Processes

The flux at the top of the Mars atmosphere was calculated by comparing it with that at the top of the Earth's atmosphere. Calculations were started at 150 km, an altitude sufficiently high that the attenuation above it would be negligible. The total number density was determined at this altitude from the calculations described in paragraph IIIA. At this and at each succeeding lower altitude, the rates per reacting particle of each of the various photoionization and photodissociation processes were determined by integrating the product of the solar flux and the effective cross section over the wavelength range of importance. These integrals are then first-order rate constants since each, when multiplied by the appropriate concentration, gives the rate of the process. These and the other chemical processes were then used to determine steady-state concentrations, which would be expected to be reached only after considerable time. At altitudes where diffusion can play a role, steady-state conditions would actually never be reached. (The consideration of diffusion is another modification which should be carried out in the future, but which is considered outside the scope of the present study.)

Forty-four reactions were included in the chemical kinetics calculations, and included photoionization, photodissociation, photo-detachment, three-body neutral-neutral recombinations, neutral rearrangement, dissociative ion-electron recombination, three-body electron attachment, dissociative attachment, associative detachment, ion-ion recombination, positive-ion charge transfer and charged rearrangement reactions. These are listed in table I along with constants used in the study.

The rate constants used were taken from various reference sources. Some of them are known with an uncertainty of perhaps 20 percent, but others are only estimated. Obviously, this will introduce uncertainties

TABLE I

Chemical Reactions and Rate Constants Used in the Chemical Kinetics Calculations

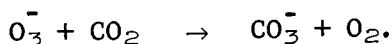
Reactions	Rate Constants (sec)	Reactions	Rate Constants (sec)
Photoionization		Charge transfer, positive ion	
$\text{CO}_2 + h\nu \longrightarrow \text{CO}_2^+ + e$		$\text{N}_2^+ + \text{CO}_2 \longrightarrow \text{N}_2 + \text{CO}_2^+$	9×10^{-10}
$\text{N}_2 + h\nu \longrightarrow \text{N}_2^+ + e$		$\text{N}_2^+ + \text{CO} \longrightarrow \text{N}_2 + \text{CO}^+$	7×10^{-10}
$\text{CO} + h\nu \longrightarrow \text{CO}^+ + e$		$\text{N}_2^+ + \text{N} \longrightarrow \text{N}_2 + \text{N}^+$	1×10^{-12}
$\text{O} + h\nu \longrightarrow \text{O}^+ + e$		$\text{N}_2^+ + \text{O}_2 \longrightarrow \text{N}_2 + \text{O}_2^+$	2×10^{-10}
$\text{O}_2 + h\nu \longrightarrow \text{O}_2^+ + e$		$\text{N}^+ + \text{CO}_2 \longrightarrow \text{N} + \text{CO}_2^+$	1.3×10^{-9}
$\text{N} + h\nu \longrightarrow \text{N}^+ + e$			
Photodissociation		Charge transfer, positive ion	
$\text{CO}_2^+ + h\nu \longrightarrow \text{CO} + \text{O}$		$\text{CO}^+ + \text{O} \longrightarrow \text{CO} + \text{O}^+$	1×10^{-11}
$\text{O}_2 + h\nu \longrightarrow \text{O} + \text{O}$		$\text{CO}^+ + \text{CO}_2 \longrightarrow \text{CO} + \text{CO}_2^+$	1.1×10^{-9}
$\text{O}_3 + h\nu \longrightarrow \text{O} + \text{O}_2$		$\text{CO}_2^+ + \text{O} \longrightarrow \text{CO}_2 + \text{O}^+$	1×10^{-11}
Photodetachment		Charged rearrangement, positive ion	
$\text{O}^- + h\nu \longrightarrow \text{O} + e$		$\text{CO}_2^+ + \text{N} \longrightarrow \text{NO}^+ + \text{CO}$	1×10^{-11}
		$\text{CO}_2^+ + \text{O} \longrightarrow \text{O}_2^+ + \text{CO}$	1×10^{-11}
		$\text{O}^+ + \text{CO}_2 \longrightarrow \text{O}_2^+ + \text{CO}$	1.2×10^{-9}
		$\text{O}^+ + \text{N}_2 \longrightarrow \text{NO}^+ + \text{N}$	3×10^{-12}
		$\text{O}_2^+ + \text{N} \longrightarrow \text{NO}^+ + \text{O}$	2×10^{-10}
Dissociative recombination		Charge transfer, negative ion	
$\text{CO}_2^+ + e \longrightarrow \text{CO} + \text{O}$	2.5×10^{-7}	$\text{O}_2^- + \text{O}_3 \longrightarrow \text{O}_2 + \text{O}_3^-$	3×10^{-10}
$\text{N}_2^+ + e \longrightarrow \text{N} + \text{N}$	3.0×10^{-7}	$\text{O}^- + \text{O}_3 \longrightarrow \text{O} + \text{O}_3^-$	7×10^{-10}
$\text{NO}^+ + e \longrightarrow \text{N} + \text{O}$	5.0×10^{-7}		
$\text{O}_2^+ + e \longrightarrow \text{O} + \text{O}$	2.9×10^{-7}		
Ion-ion recombination		Three-body neutral recombination	
$\text{CO}_2^+ + \text{O}^- \longrightarrow \text{CO}_2 + \text{O}$	3×10^{-7}	$\text{CO} + \text{O} + \text{M} \longrightarrow \text{CO}_2 + \text{M}$	1×10^{-35}
$\text{CO}_2^+ + \text{O}^- \longrightarrow \text{CO} + \text{O} + \text{O}$	3×10^{-7}	$\text{O} + \text{O} + \text{M} \longrightarrow \text{O}_2 + \text{M}$	9.8×10^{-33}
$\text{NO}^+ + \text{O}_3^- \longrightarrow \text{N} + \text{O} + \text{O}_3$	3×10^{-7}	$\text{N} + \text{N} + \text{M} \longrightarrow \text{N}_2 + \text{M}$	1.1×10^{-32}
$\text{CO}_2^+ + \text{O}_3^- \longrightarrow \text{CO}_2 + \text{O}_2$	3×10^{-7}	$\text{O} + \text{O}_2 + \text{M} \longrightarrow \text{O}_3 + \text{M}$	1.8×10^{-33}
$\text{O}_2^+ + \text{O}_3^- \longrightarrow \text{O}_2 + \text{O}_3$	3×10^{-7}		
Attachment		Neutral rearrangement	
$\text{O} + e + \text{M} \longrightarrow \text{O}^- + \text{M}$	1×10^{-32}	$\text{O} + \text{O}_3 \longrightarrow \text{O}_2 + \text{O}_2$	7.7^{-16}
$\text{O}_2 + e + \text{M} \longrightarrow \text{O}_2^- + \text{M}$	1×10^{-30}		
$\text{O} + e \longrightarrow \text{O}^- + h\nu$	1.3×10^{-15}		
Associative detachment			
$\text{O}_2^- + \text{O} \longrightarrow \text{O}_3 + e$	3×10^{-10}		
$\text{O}^- + \text{CO} \longrightarrow \text{CO}_2 + e$	8×10^{-10}		

in the calculations. A major source of uncertainty in these rate constants is the temperature effect. This is due to lack of accurate data on the temperature variation of the rate constants and to the uncertainty in the temperature itself. All rate constants were evaluated at 200 °K although the temperature may be appreciably lower at some altitudes. Since the value of rate constants at lower temperatures, especially those of the order of 100 °K, is not known, the use of values at 200 °K for all altitudes appeared reasonable.

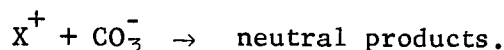
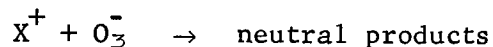
After the concentrations of the eighteen species are calculated at each altitude, the rates of six other reactions not included in the iterative calculations are calculated to permit an estimation of their importance and the effect of their omission. The reactions and the rate constants used were as follows:

<u>Reactions</u>	<u>Rate Constants (sec)</u>
$N_2^+ + O^- \rightarrow N_2 + O$	3×10^{-7}
$N_2^+ + O \rightarrow N_2 + O^+$	1×10^{-12}
$N_2^+ + O \rightarrow NO^+ + N$	2.5×10^{-10}
$N^+ + CO_2 \rightarrow NO^+ + CO$	1×10^{-11}
$O_3^- + CO_2 \rightarrow CO_3^- + O_2$	4×10^{-10}
$N + O + M \rightarrow NO + M$	1.3×10^{-32}

Although the system of eighteen species and fifty reactions appears to be rather complex, a closer examination shows that other species and other reactions are also important. For example, the major negative ion at low altitudes is none of the three included in the fifty reactions but rather CO_3^- , formed by the reaction



This species was not included in the basic calculations in order to permit simplification. An estimate of the amount of O_3^- , derived from the amount of CO_3^- , is being provided later in this report. Deriving the amount of O_3^- from the amount of CO_3^- is reasonable since the major mechanism by which either is removed is ion-ion recombination.



C. Kinetics of Individual Species

As mentioned previously, the concentrations of the important species depend upon numerous reactions some of which involve minor species.

CO_2 is dissociated and ionized by solar flux and is also consumed by several charge exchange reactions. Although it is reformed by the three-body recombination of CO and O, other reactions involving ions (mainly O^+ and various negative ions) provide faster production of CO_2 . This is shown schematically in the flow diagram in figure 2. At low altitudes there is little dissociation since the effective flux is absorbed at higher altitudes. At higher altitudes, CO_2 is largely dissociated because the reactions forming CO_2 are slow. At intermediate altitudes, there is a steady-state in which several reactions are important.

The kinetics of CO and of O are shown schematically in figures 3 and 4, respectively. The reactions shown are those which appear to be the most important in controlling the various concentrations of interest. The chemical kinetics of N_2 are shown schematically in figure 5.

IV. METHOD OF CALCULATION

The rates of all the reactions were calculated using any set of trial concentrations which were required only to fit the elemental composition assumed. Then the ratio, for each specie, of the rate at which it is being formed to the rate at which it is being consumed was calculated. The individual concentrations were then changed to bring them closer to the steady-state values, by making the ratios nearer unity by a factor of as much as 1.5. Several concentrations (including one carbon-containing species, one oxygen-containing species, one nitrogen-containing species, and one negatively charged species) were calculated by balance so that the total number of atoms

and the elemental composition would not be changed. The species so calculated were usually those of the highest concentration. The procedure was then iterated a number of times until the ratios were all very close to unity. The attenuation of flux, as a function of wavelength, was then calculated for a five-kilometer altitude interval, assuming the composition and flux attenuation to be constant over that altitude range and equal to that in the middle of the altitude range. The flux so determined was then used as the initial flux for the calculation of conditions at an altitude five kilometers lower. The procedure was repeated for each 5-kilometer altitude increment down through the atmosphere. This same calculation was carried out for each of the assumed atmospheres, that is, for each of the three assumed elemental compositions and for two different fluxes. A flow diagram of the computer program is shown in figure 6.

V. ATMOSPHERIC COMPOSITION

A. Neutral Species

The calculated atmospheric composition provides the concentrations of the eighteen species listed in paragraph IIIA.

Figures 7, 8, and 9 graphically give the results for the neutral species.

The calculations predict CO_2 to be more than half dissociated at altitudes above 60 km. This is a somewhat lower altitude than given in other predications (Fjeldbo et al. [8,9] and Chamberlain [4]), but the data should be reliable because they are calculated from a consideration of the detailed flux and its attenuation through the atmosphere. CO and O are the major species initiating from CO_2 and have approximately equal concentrations down to about 80 km. Below this, CO continues to increase to a peak at about 60 km while O decreases due to the formation of O_2 which is important in the 50 to 90 km range. Ozone is present in concentrations of as large as about one part per million peaking at about 65 km.

In the atmospheres considered where nitrogen was included, it was found to be largely dissociated above 85 km. Data on reactions not included in the iterative calculations indicate that nitrogen oxides are not important, although a more complete investigation would be required to eliminate this possibility completely. It appears that some NO may be formed, but would be consumed rapidly by $\text{N} + \text{NO}$ reaction. The data obtained are sufficient to make a more complete analysis of certain facets of the kinetics such as the nitrogen oxide effects. This should be done when time permits.

The three atmospheres considered did not give drastically different results for the neutral species. The preceding findings appear to hold for all three compositions. Other than the obvious change in nitrogen content, there is little variation of the altitude of the peaks or even of their magnitude among the three cases.

B. Charged Species

The results of the calculations of the charged species are less reliable than those of the neutral species. The data obtained showed total charge densities which were much higher than the available experimental data indicate. However, it is believed that the relative concentrations of the charged species are reliable. The data, therefore, are presented in this form; that is, concentration relative to the electron density. The data are shown in figures 10, 11 and 12. The charged species data below 85 km are not reliable since the electron density is extremely low and all ion kinetics are dependent upon the electron density. Above 125 km there is also some doubt about certain of the species, although in general they appear reasonable.

Because of the difficulties in obtaining charged species concentrations above 125 km, the location of the electron density peak could not be decided with high accuracy. However, in all cases, the electron density dropped off below 125 km and when any data were obtained above this, a decrease was indicated. This would agree with the findings of Fjelbdo, et al. [8]. It is noticed that diffusion would tend to change the electron densities rather than to shift the peak.

In most cases considered, O^+ is the major ion present. With appreciable nitrogen included in the atmosphere, NO^+ does become important at low altitudes and even becomes the predominant ion at 85 km in the 20 percent N_2 case. The importance of O_2^+ and CO_2^+ was found to increase at low altitudes.

No negative ions become important at altitudes below 85 km; e.g., O^- is present in the largest concentration but only amounts to about 10^{-6} of that of the free electrons. O_2^- is important only in leading to other negative ions, and this is of minor significance. O_3^- is found to build up at low altitudes but not to significant concentrations. It is probable that some negative ions are present at altitudes below 85 km. These are mainly CO_3^- (probably over 90 percent) with some O_3^- . However, it is unlikely that the ion densities at lower altitudes are large enough to be important.

C. The Solar Flux

The solar flux is attenuated as it passes through the atmosphere. The flux as a function of wavelength is shown for several altitudes in figure 13 for the 80 percent CO_2 - 20 percent N_2 atmosphere and as a function of altitude for several wavelengths in figure 14. The attenuation above 110 km is small. Below this altitude, the flux at wavelengths below 900 Å is rapidly attenuated and is essentially completely absorbed by 85 km. Since this is the most important radiation for ionization, there is little ionization below this, as indicated in paragraph VB. The flux between 900 and 1350 Å persists to slightly lower altitudes, as illustrated by the dotted lines which represent a maximum and minimum in the CO_2 cross section. The flux from 1350 to 1600 Å is effective in dissociating CO_2 . Because the absorption coefficients (cross sections) for dissociation are smaller than for ionization, the effective flux persists to slightly lower altitudes than does the radiation of less than 900 Å, which is completely absorbed by the time it reaches an altitude of a little below 80 km.

The flux attenuation for the other atmospheres is not greatly different from that given above. In the case of the higher flux used, the attenuation was at about the same rate although the curves in figure 13 would be moved to higher intensities; the relative results of figure 14 would not be changed. Thus, examination of the results for the two cases indicates that the degree of ionization and dissociation would be increased for the species O_2 , N_2^+ , N^+ , O^- , NO^+ , O^+ , CO^+ , O_3^- and e but would not change significantly for the species CO , O , CO_2 , N_2 , N , CO_2^+ , O_2^+ , O_2^- and O_3 .

D. The Diffusion Problem

Major uncertainties in the preceding calculations arise from the omission of any diffusion processes. Considerable work was done on this problem, and a method of including diffusion in the calculations has been detailed. The following describes this work.

In addition to photochemical processes, the structure of the Mars atmosphere is controlled by diffusion. At high altitudes, this can be illustrated by the fact that, as the pressure decreases, the molecular diffusion coefficient increases. Thus, in comparison with the decreasing chemical reaction rates, molecular diffusion becomes dominant. On the other hand, at low altitudes the interaction of the planetary surface with the atmosphere causes winds and related phenomena to smooth chemical variations by turbulent mixing. The following discussion presents a mathematical model of the diffusing Mars atmosphere and qualitatively examines the altitude regions which are controlled by diffusion and chemistry.

In a dynamic atmosphere, the flux of the diffusing species is related to the chemical production rates by the species continuity equations.

$$\frac{dN_i}{dh} = S_i^+ - S_i^- \quad (1)$$

where

N_i = particle flux of species i (particles/cm² sec)

h = altitude

S_i^+ = sum of the rates of all reactions producing species i
(particles/cm³ sec)

S_i^- = sum of the rates of all reactions removing species i
(particles/cm² sec).

Because the charge neutrality is preserved, the summation of N_i over all charged species must be zero. Thus, if there are L species considered in an atmospheric model, there are $L-1$ independent equations in the set, equation (1), and a charge balance

$$\sum_i Z_i N_i = 0 \quad (2)$$

where

Z_i = charge on species i .

The Stefan-Maxwell relations as generalized to a multicomponent mixture relate the diffusion fluxes to the concentration, pressure, and electric field driving forces present in the model atmosphere. These equations, well documented in the literature, were obtained from Hirshfelder, et al. [10].

$$\sum_j \frac{X_j N_i - X_i N_j}{nD_{ij}} = \frac{dX_i}{dh} + X_i \left(1 - \frac{M_i}{\bar{M}} \right) \frac{d \ell_n P}{dh} - \frac{X_i Z_i E}{kT} \quad (3)$$

$$\sum_i \sum_j \frac{X_j N_i - X_i N_j}{n D_{ij}} = 0 \quad (4)$$

where

X_i = mole fraction of species i

n = total number density

D_{ij} = binary diffusion coefficient of species i and j

M_i = molecular weight of species i

\bar{M} = average molecular weight of gas

P = pressure

E = electric field induced by charge separation

k = Boltzmann constant

T = temperature.

Charge balance then supplies the equation for the induced electric field.

$$\frac{E}{kT} \sum_j X_j Z_j^2 = - \sum_j \frac{X_j Z_j M_j}{\bar{M}} \frac{d \ln P}{dh} - \sum_j \frac{Z_j}{n} \sum_i \frac{X_j N_i - X_i N_j}{D_{ij}} \quad (5)$$

Notice that the above equations do not use binary, ambipolar diffusion coefficients since these are not applicable to a multicomponent mixture per se. (Blanc's law must be employed.) However, this effect has been considered by the inclusion of the induced electric field. Several auxiliary relationships necessary to complete the model include the hydrostatic equation:

$$\frac{dp}{dh} = -\rho g = -\frac{P}{H} \quad (6)$$

where

ρ = mass density

g = acceleration due to gravity

H = scale height,

and the equation of state

$$P = nkT$$

or

$$P = \frac{R}{\bar{M}} \rho T. \quad (7)$$

Examination of equations (1) through (7) indicates a coupled set of differential and algebraic equations which relate the diffusion fluxes and species concentrations to the solar flux (photochemistry) and the gravitational attractive force of the planet. As mentioned above, the dominant terms in the equations are a strong function of altitude with diffusion controlling the upper atmosphere and chemistry important near the Mars surface. It is of interest to qualitatively determine the altitude region where both effects are of the same order.

Rearrangement of the left-hand side of equation (3) results in the approximate expression

$$\sum_j \frac{X_j N_i - X_i N_j}{nD_{ij}} \approx \frac{N_i}{nD_{ij}}. \quad (8)$$

An approximate flux for species i can be obtained by neglecting the chemical loss terms, S_i^- , and integrating equation (1) over altitude

$$N_i \approx \int_h^\infty S_i^+ dh \quad (9)$$

thus combining equations (3), (8) and (9)

$$\frac{dX_i}{dh} \approx \frac{\int_h^\infty S_i^+ dh}{nD_{ij}} - \frac{X_i}{H} \left(1 - \frac{M_i}{\bar{M}} \right). \quad (10)$$

Examination of the two terms on the right-hand side of equation (10), using the results of the previously described nondiffusing atmospheres, indicates that a very sharp distinction between diffusion and chemical dominance is achieved between 85 and 105 km. This is illustrated for electrons in table II using the results for the 90 percent CO₂ 10 percent N₂ atmosphere.

TABLE II
Comparison of Diffusion and Chemical Dominance

Altitude (km)	Chemistry	Diffusion
	$\frac{\int_h^\infty S_i^+ dh}{nD_{ij}}$	$\frac{X_i}{H} \left(1 - \frac{M_i}{\bar{M}} \right)$
85	1.4×10^{-9}	2.8×10^{-13}
90	1.2×10^{-9}	1.1×10^{-9}
95	6.5×10^{-10}	1.1×10^{-9}
100	3.7×10^{-10}	5.1×10^{-9}
105	2.1×10^{-10}	1.9×10^{-8}
110	1.3×10^{-10}	3.7×10^{-8}
115	7.2×10^{-11}	7.2×10^{-8}

Thus, it can be concluded that diffusion will play a major role in determining the profile of the electron density. Notice that diffusion will not alter the position of the peak significantly. However, the maximum concentration would be expected to decrease.

VI. CONCLUSIONS

Based on the results obtained for the neutral species, it is found that CO_2 is more than 50 percent dissociated at all altitudes above 60 km and CO and O are the major constituents. Ozone is present in quantities of as much as one part per million. Nitrogen oxides probably do not build up in large concentrations.

Charged species are more difficult to predict. Above 80 km, electrons are the only important negatively charged species. Below this, negative ions, especially CO_3^- , become important but none build up to large concentrations. The major positive ions are O^+ , N^+ and CO^+ at high altitudes and NO^+ at lower altitudes.

REFERENCES

1. Allen, C. W., Astrophysical Quantities, Athlone Press, London, 1963.
2. Bortner, M. H., DASA Reaction Rate Handbook, DASA No. 1948, 1967a.
3. Bortner, M. H., "A Critical Review of Rate Constants in High Temperature Air," NBS NSRDS Report, to be published, 1967.
4. Chamberlain, J. W., *Ap. J.* 136, 582, 1962.
5. Chamberlain, J. W. and M. McElroy, *Science* 152, 21, 1966.
6. Craig, R. A., The Upper Atmosphere, Academic Press, New York, 1965.
7. Edelson, S., private communication, 1967.
8. Fjeldbo, G., W. C. Fjeldbo and V. R. Eshelman, *J. Geophys. Res.* 71, 2307, 1966a.
9. Fjeldbo, G., W. C. Fjeldbo and V. R. Eshelman, *Science* 153, 1518, 1966.

REFERENCES (Continued)

10. Hirshfelder, J. O., C. F. Curtiss, and R. B. Bird, Molecular Theory of Gases and Liquids, John Wiley, 1954.
11. Loeb, L. B., Basic Processes of Gaseous Electronics, University of California Press, 1955.
12. Owen, T., Ap. J. 146, 257, 1966.
13. Spinrad, H., R. A. Schorn, R. Moore, L. P. Giver and H. J. Smith, Ap. J. 146, 331, 1966.

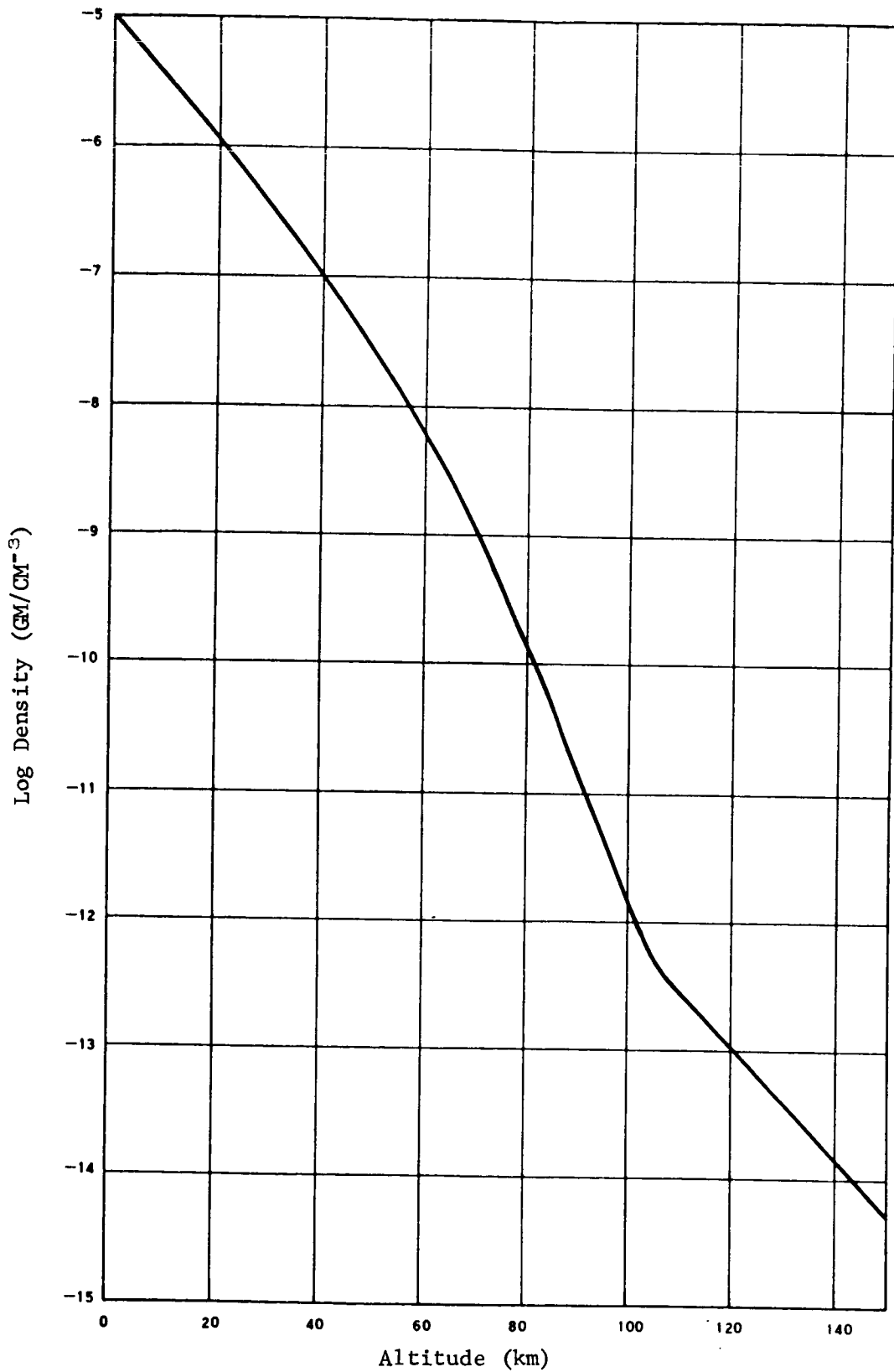


Figure 1. Density of Martian Atmosphere as a Function of Altitude

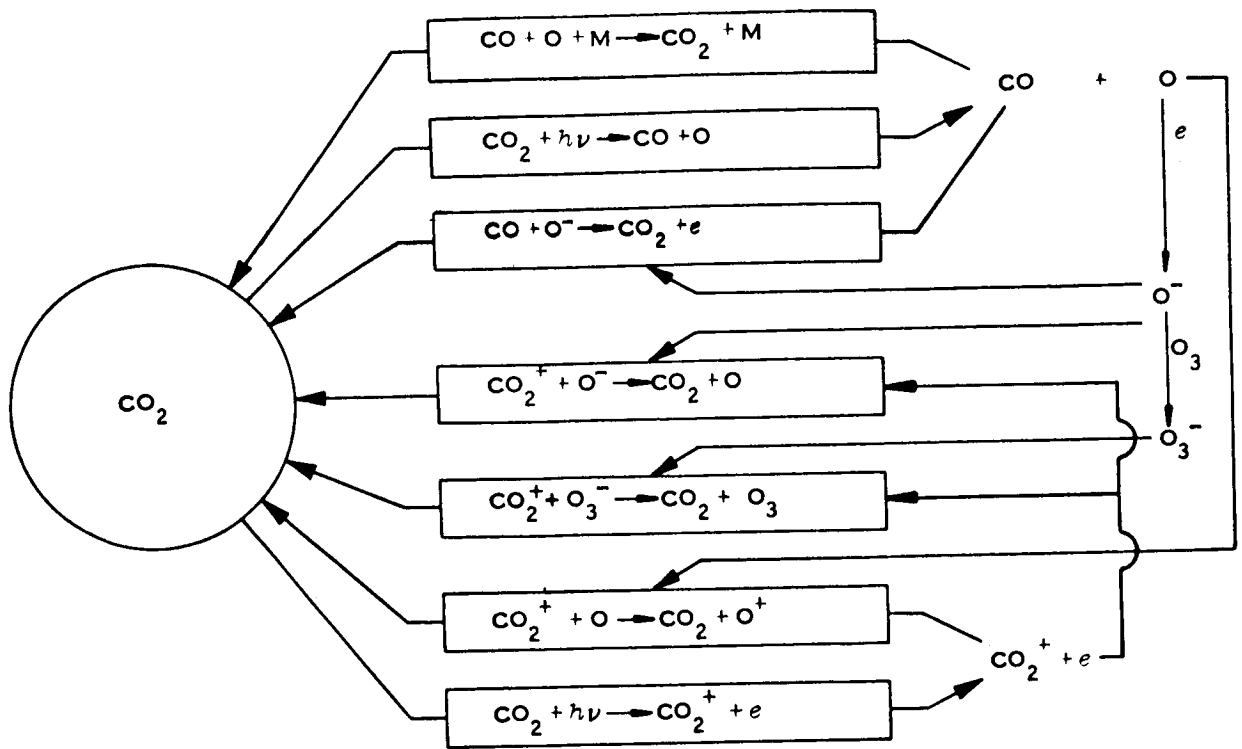


Figure 2. Schematic Representation of CO_2 Kinetics in Martian Atmosphere

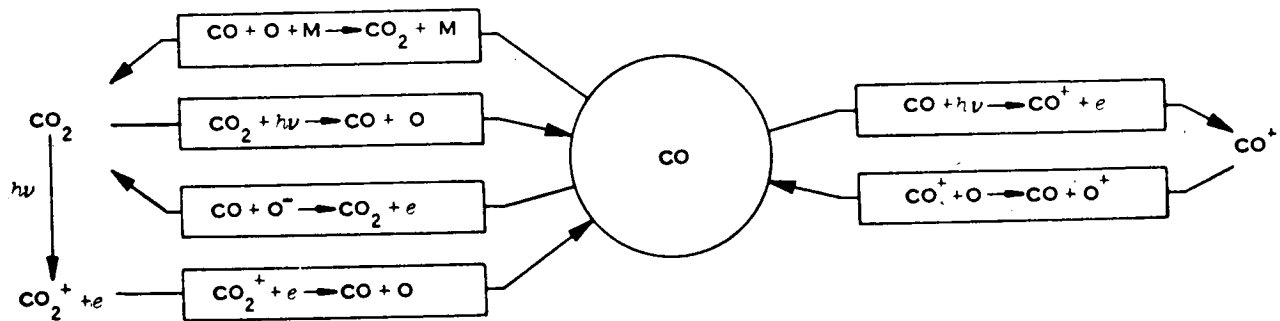


Figure 3. Schematic Representation of CO Kinetics in Martian Atmosphere

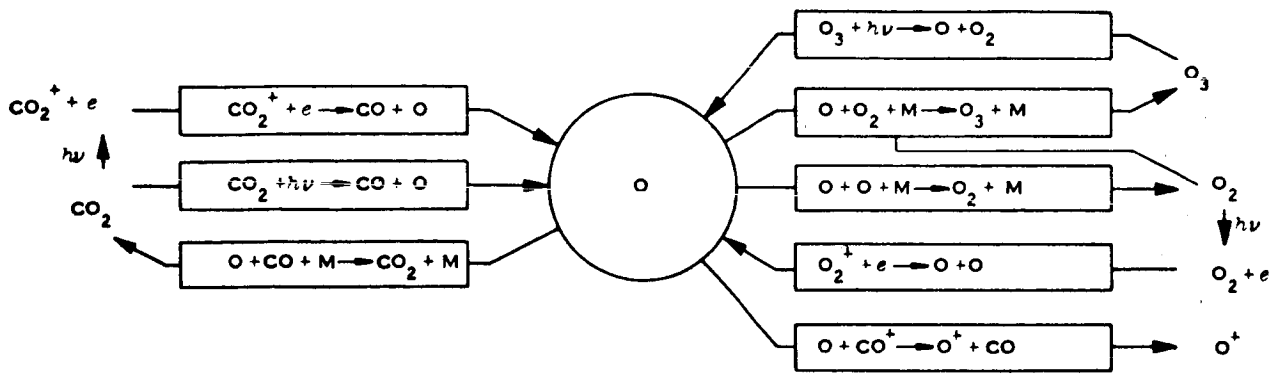


Figure 4. Schematic Representation of Chemical Kinetics of Atomic Oxygen in Martian Atmosphere

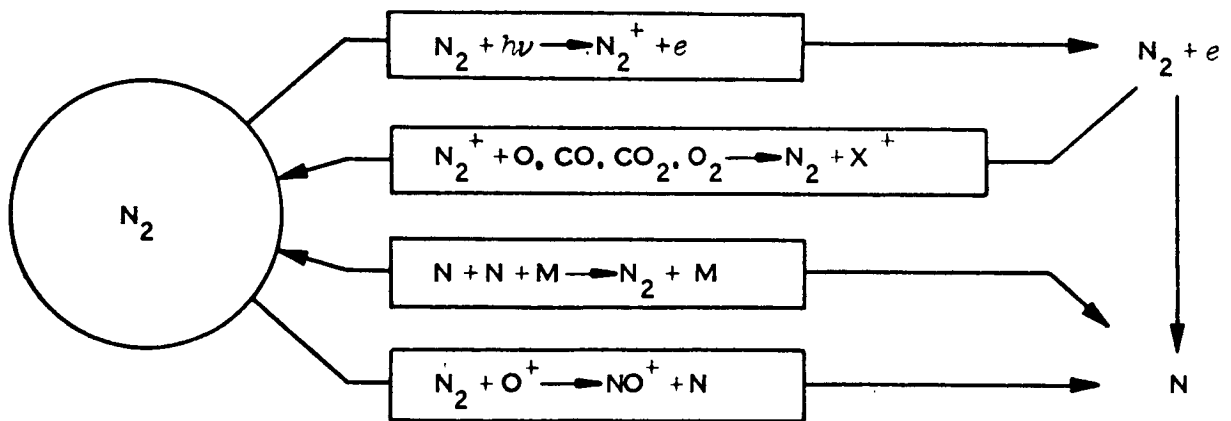


Figure 5. Schematic Representation of Chemical Kinetics of N_2 in Martian Atmosphere

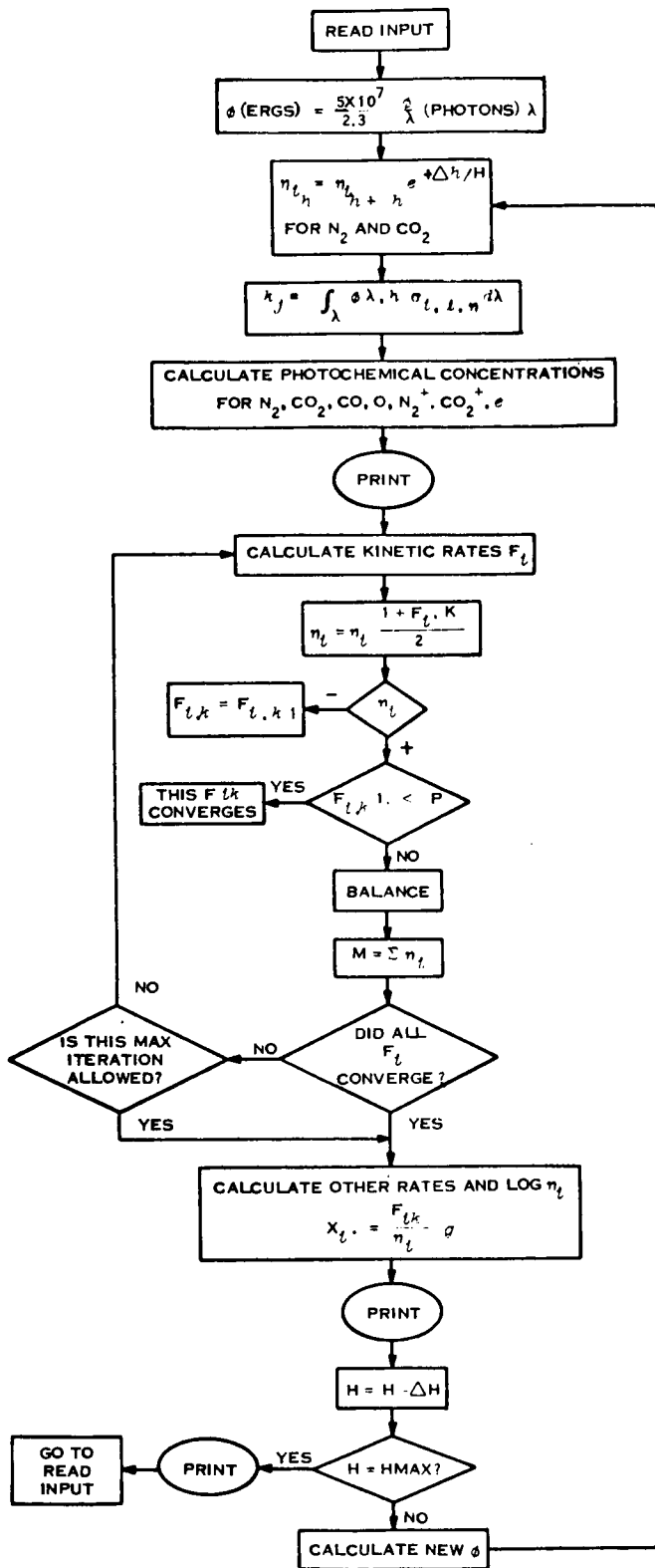


Figure 6. Flow Diagram of Computer Program Used for Martian Atmosphere Composition Calculations

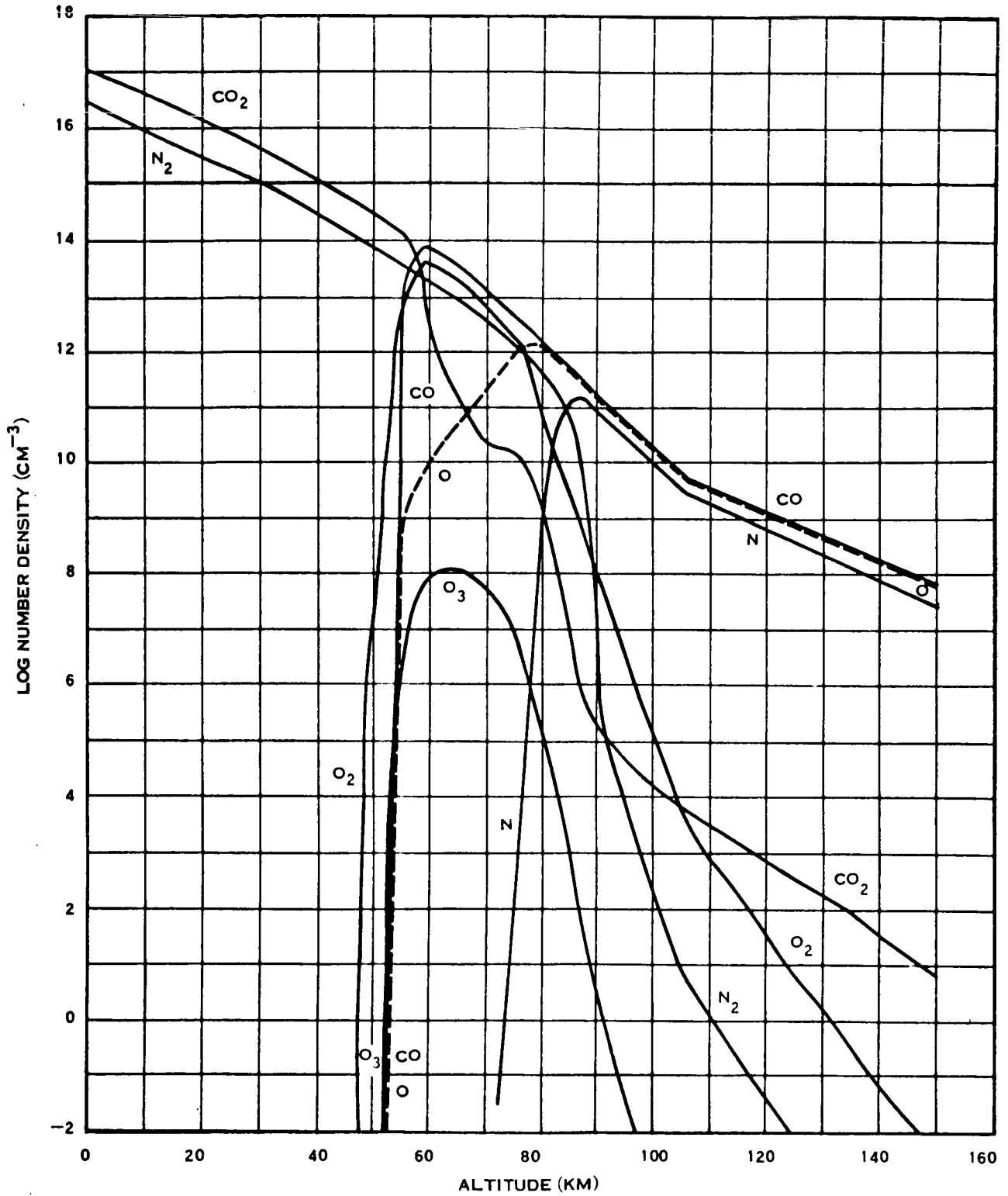


Figure 7. Calculated Neutral Species Concentrations (80% CO₂, 20% N₂)

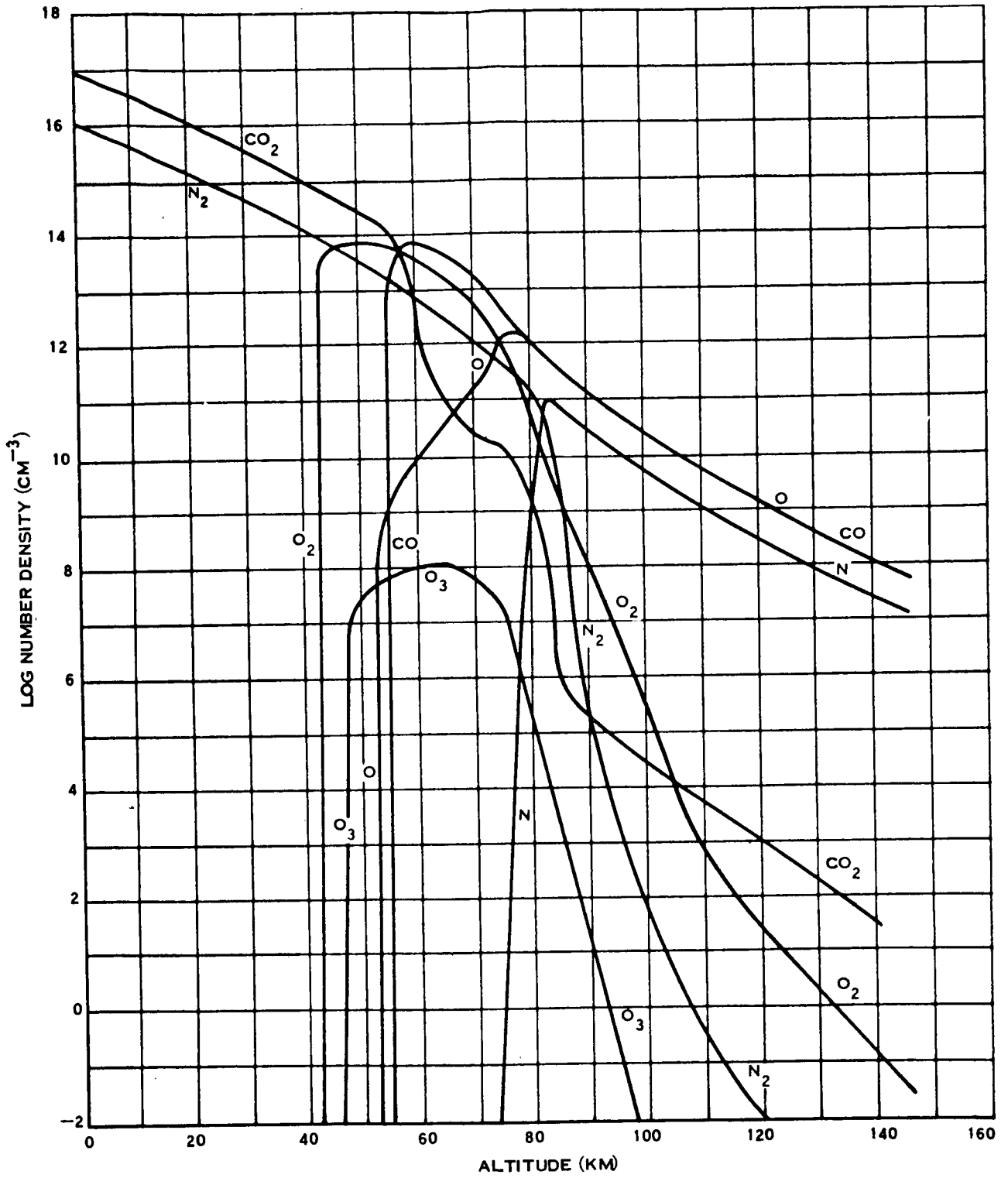


Figure 8. Calculated Neutral Species Concentrations (90% CO₂, 10% N₂)

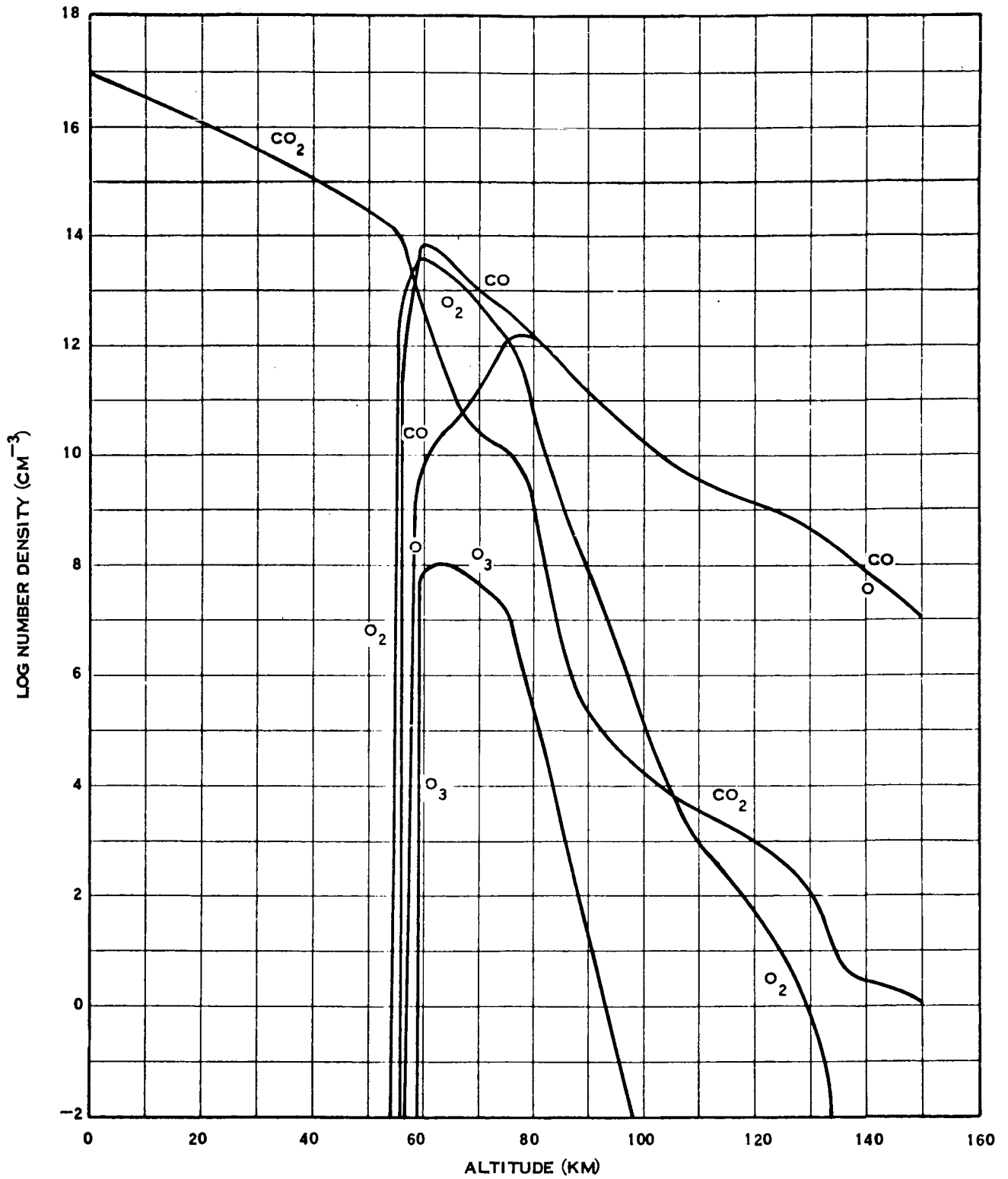


Figure 9 Calculated Neutral Species Concentrations (100% CO₂)

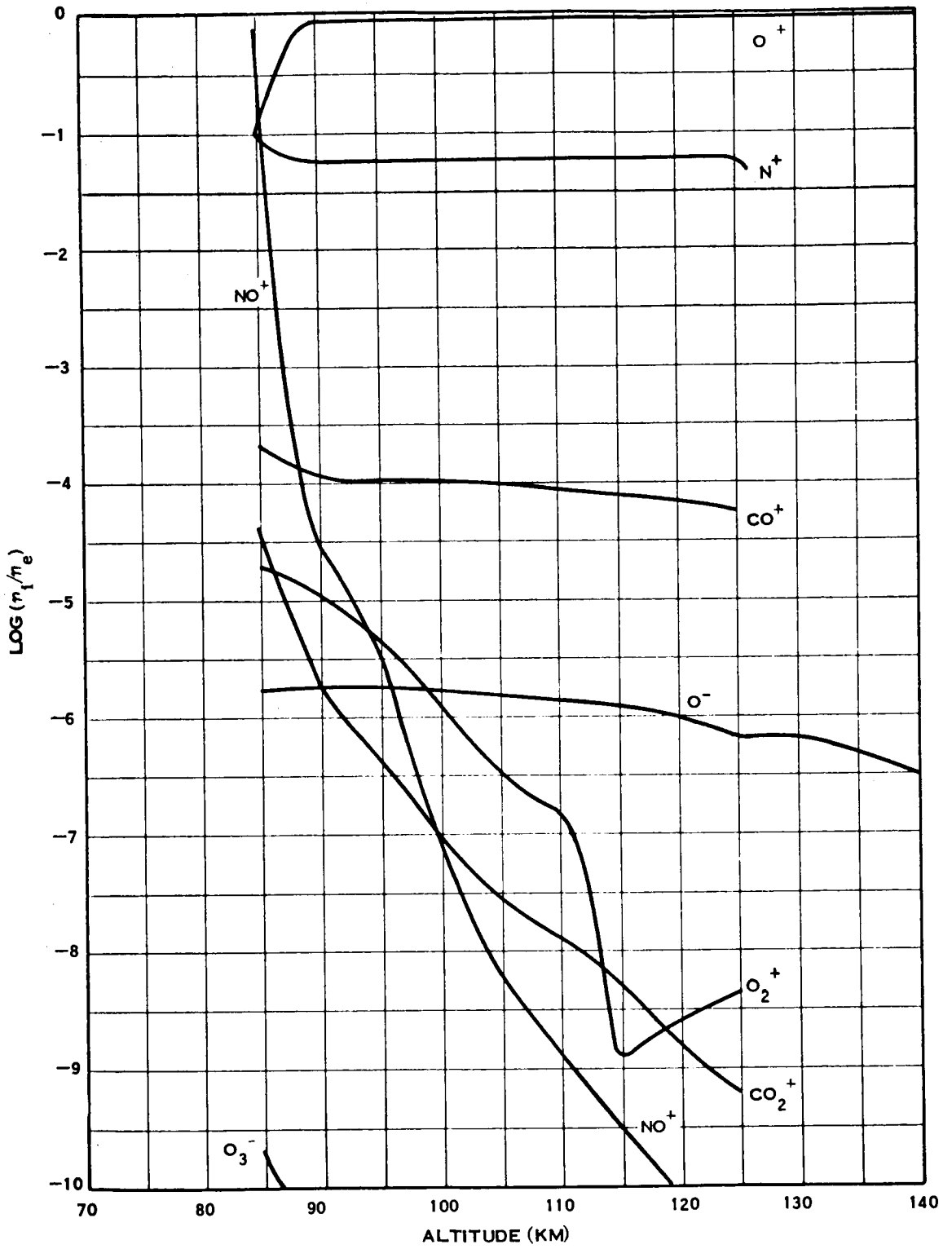


Figure 10. Ion Concentrations Relative to Electron Density (80% CO_2 , 20% N_2)

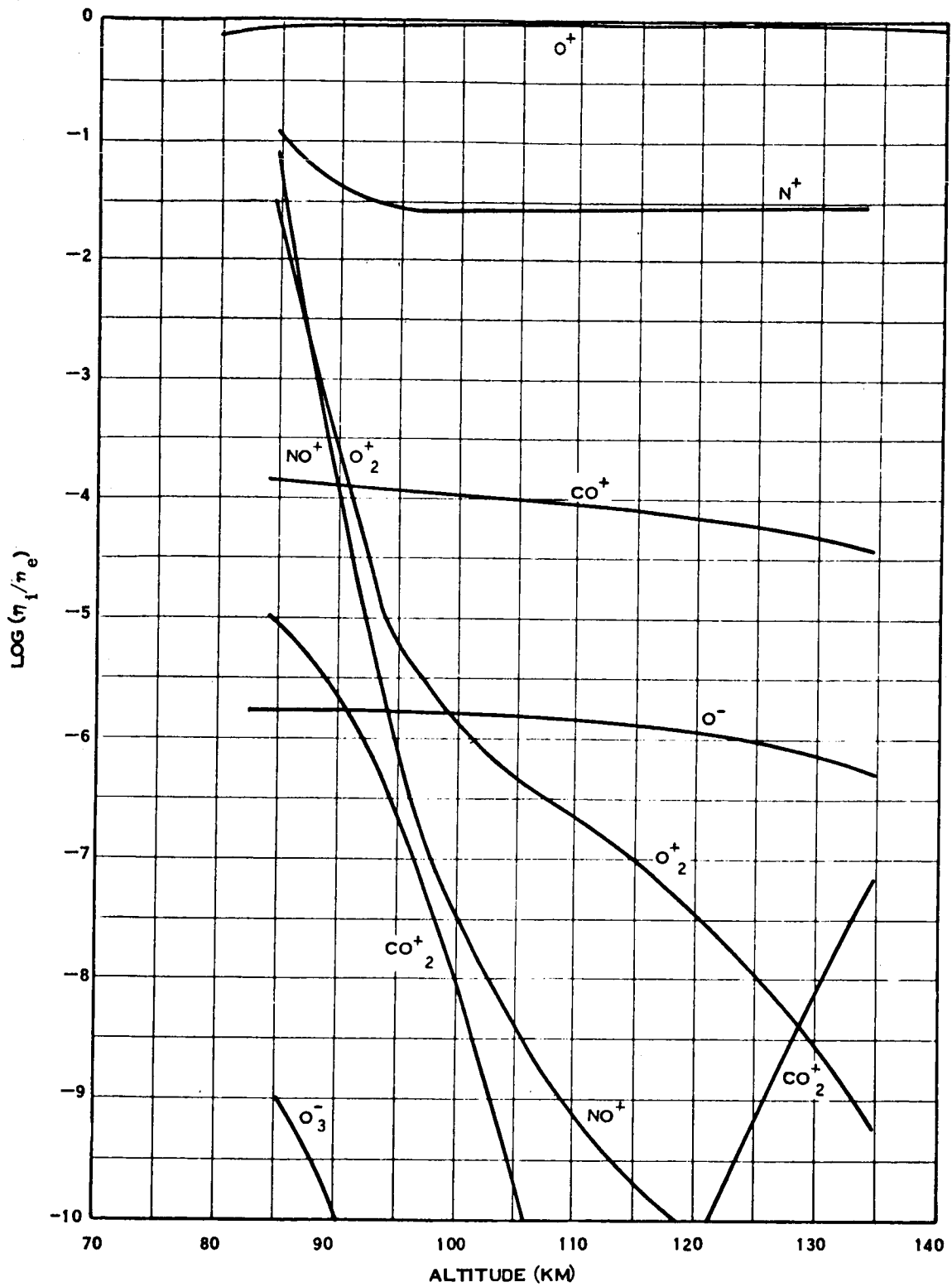


Figure 11. Ion Concentrations Relative to Electron Density (90% CO_2 , 10% N_2)

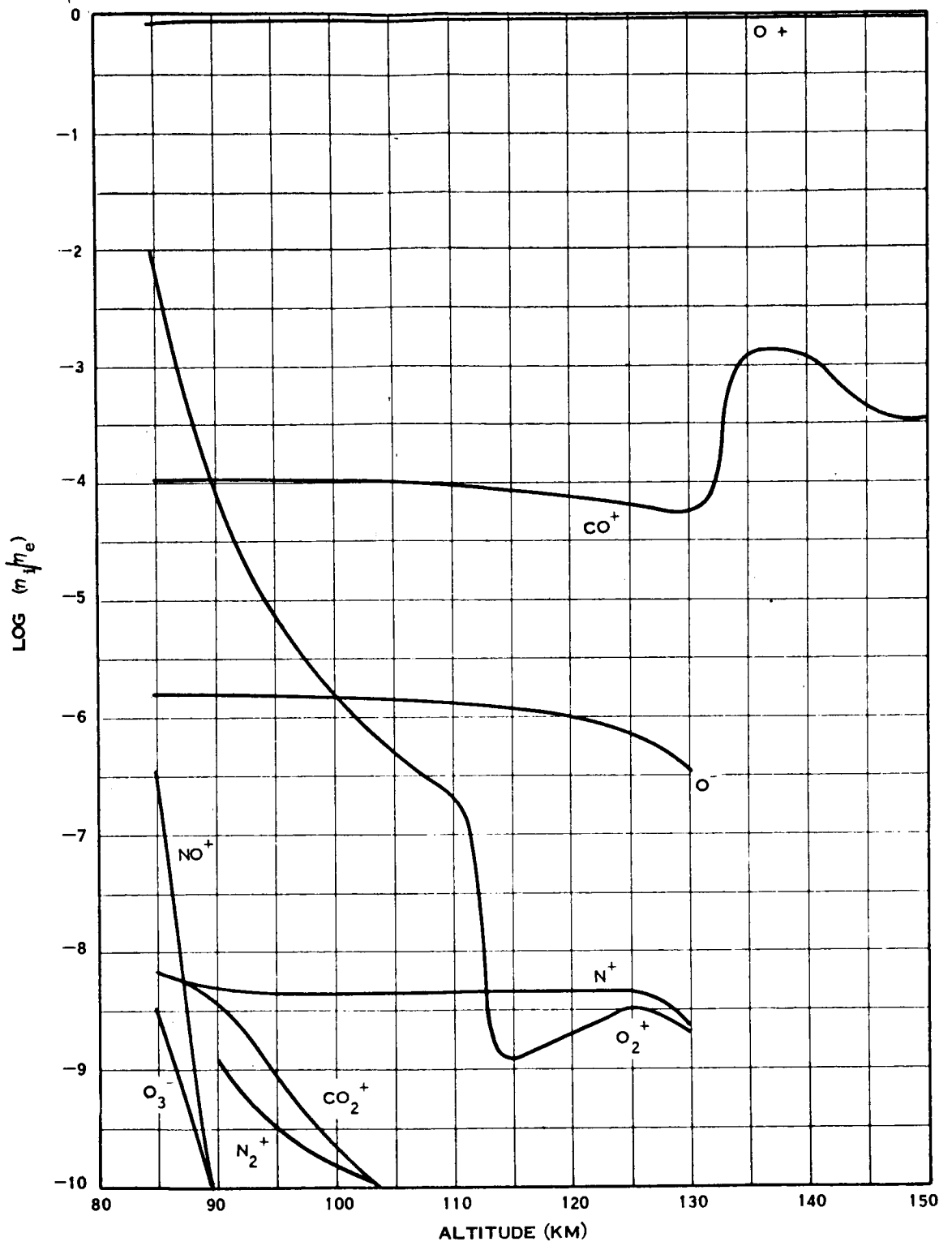


Figure 12. Ion Concentrations Relative to Electron Density (100% CO₂ - 0.1 PPM N₂)

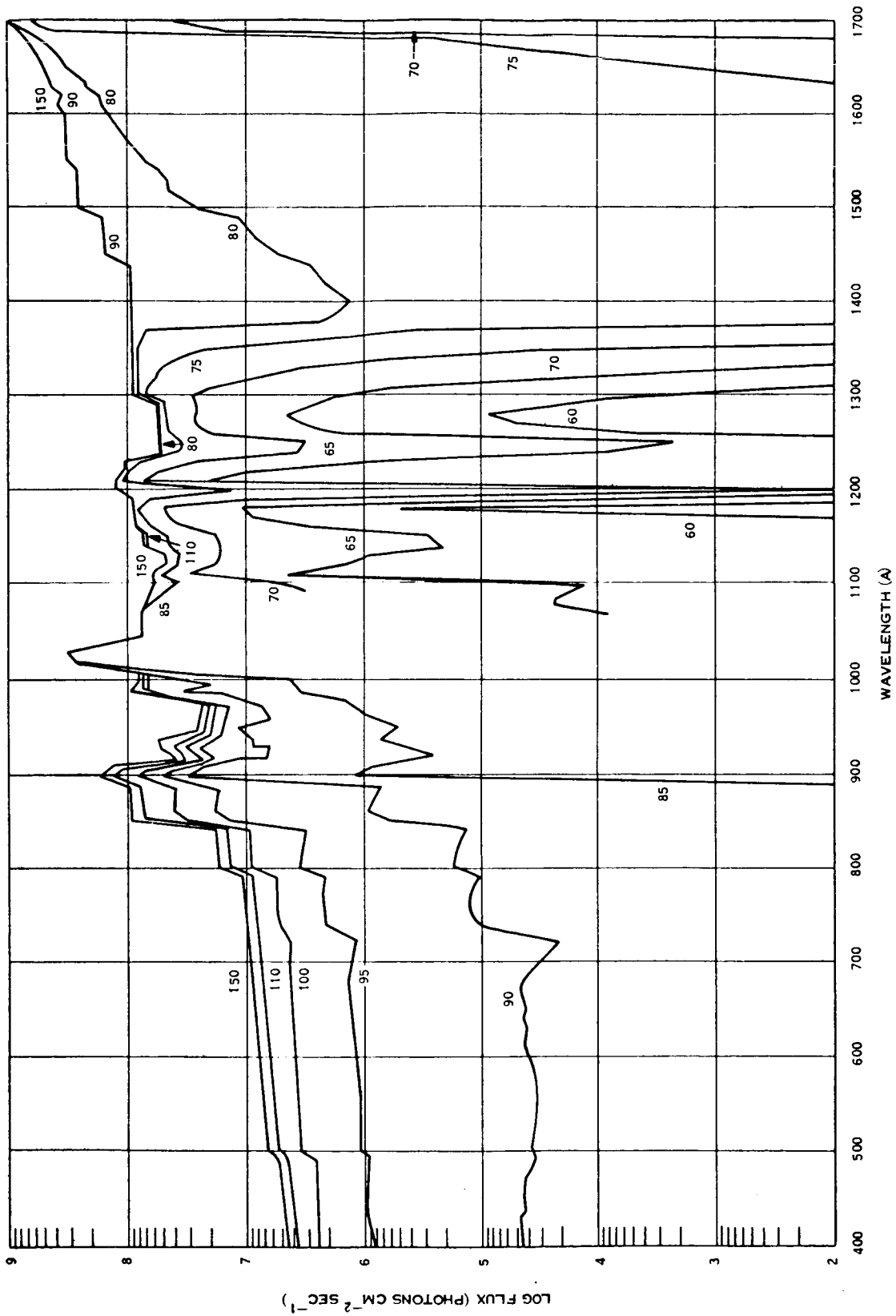


Figure 13. Flux at Various Altitudes as a Function of Wavelength (80% CO₂, 20% N₂)

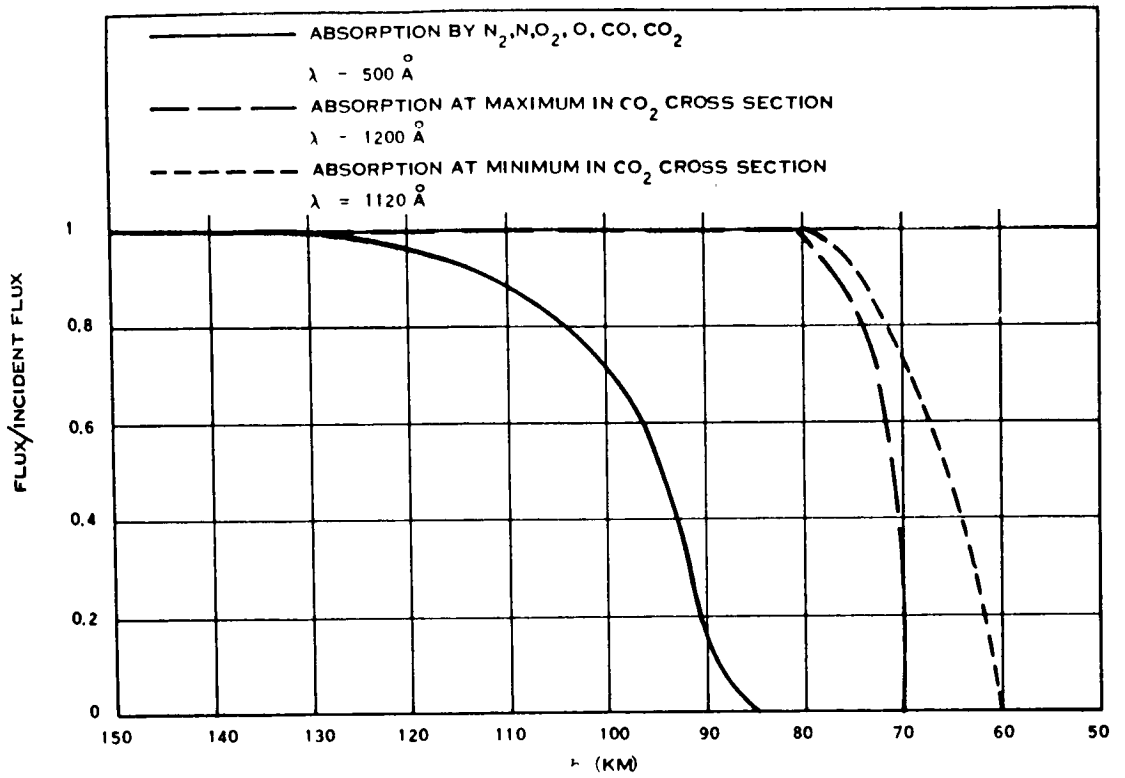


Figure 14. Flux/Incident Flux Versus Altitude

A TEMPERATURE PROFILE OF THE UPPER MARTIAN ATMOSPHERE
FROM A KINETIC VIEWPOINT

by

James W. Johnson

Aerospace Environment Division
Aero-Astroynamics Laboratory
George C. Marshall Space Flight Center
Huntsville, Alabama

N 68-18838

SUMMARY

To provide a model for the overall structure of the Martian atmosphere, the methods of kinetic theory are applied to the case of an ideal gas in a gravitational force field. For the lower atmosphere, the distribution function of molecular velocities can be easily obtained because the motion of the molecules comprising the system can be considered to be perfectly random. However, in the upper atmosphere, the molecular velocities are no longer isotropic, and the distribution is not easily obtained except in a certain limiting case in which collisions are so infrequent that they can be neglected altogether.

If this assumption is made, the temperature profile may then be derived from a calculated atmospheric constituent distribution function. Once an adequate treatment from the kinetic viewpoint is obtained, chemical and radiative processes might possibly be regarded as perturbations.

I. INTRODUCTION

The structure of a planetary atmosphere cannot be described by any one simple scheme. Many processes, such as chemical decomposition and recombination, radiative processes, conduction and convective currents, solar activity, and planetary motion will, in general, influence the behavior of a planet's atmosphere [1]. However, simple considerations from kinetic theory are particularly useful in providing a first order approximation to the overall structure of planetary atmospheres. With all other factors disregarded, the problem of planetary atmospheres becomes one of calculating the distribution of molecules of an ideal gas in a gravitational force field.

For the lower atmosphere the number density of the molecules is such that the gas can be treated using a Maxwellian distribution function, and its various properties can easily be calculated. Under these conditions it is found that the number density and pressure variations with altitude obey the hydrostatic equation, and the temperature remains constant. Deviations from these predicted results for the lower atmosphere can be explained by taking into account radiative and chemical processes and the fact that under these circumstances the atmosphere behaves

somewhat as a fluid. In contrast, the upper atmosphere does not lend itself to such a simple theoretical scheme.

The basic difficulty arises from the fact that, since the mean free path of the molecules is large, the motion of the system is no longer random. Indeed, above a certain height, namely, that height at which the mean free path becomes greater than the scale height, the molecules move as tiny satellites in the central force field of the earth since the effects of collisions become insignificant [2]. The region between these two extremes represents a kind of limbo for the theoretician that cannot be adequately described within the scope of this paper. Here a simple description of the upper atmosphere extreme will be given. This model readily lends itself to application to the Martian atmosphere since its relatively insignificant magnetic field will not appreciably affect the streaming of charged particles into space.

II. PROCEDURE

To provide a model from which the temperature profiles of the upper Martian atmosphere can be calculated, it is assumed that there exists an exospheric boundary below which the molecules constituting the atmosphere follow a Maxwellian distribution and above which the molecules are essentially collisionless. The motions of molecules streaming from the boundary of the exosphere are governed by the principle of conservation of energy and the principle of conservation of angular momentum taken about the center of the planet. These provide two equations which relate the variables at the base of the exosphere [3]. The two equations so obtained may be used as transformation equations to obtain a distribution of molecular speeds at any point above the base of the exosphere from the assumed Maxwellian distribution at the base. These transformation equations may be written as

$$r^2 = V_0^2 + \frac{2 GM}{Rr} (r - R)$$

and

$$V \sin \theta = V_0 \frac{R}{r} \sin \theta_0$$

where G is the universal gravitational constant and M is the mass of the planet. The other symbols are defined in Figure 1. The differential volume element at some point in the portion of phase space above the exospheric boundary is related to that at the base of the exosphere in the following fashion:

$$dV_0 d\theta_0 d\phi_0 = J \left(\frac{V_0, \theta_0, \phi_0}{V, \theta, \phi} \right) dV d\theta d\phi ,$$

where J is the Jacobian of the transformation and is given by

$$J \left(\frac{V_0, \theta_0, \phi_0}{V, \theta, \phi} \right) = \frac{v^2 r \cos \theta}{V_0^2 R \cos \theta_0} .$$

Integrating over the angular coordinates θ and ϕ with limits of integration consistent with the values of θ_0 and ϕ_0 , we obtain a distribution function of molecular speeds for a single atmospheric component at any point r above the boundary of the exosphere

$$dN_V = AV (V^2 + B)^{1/2} \exp \left[- \frac{M}{2kT_0} (V^2 + B) \right] dV ,$$

where

$$B = \frac{2 GM (r - R)}{Rr} ,$$

and A is a constant. The kinetic temperature is defined by the relation

$$T = \frac{M \langle V^2 \rangle}{3k} ,$$

where the mean value of the square of the molecular speed at any level r , $\langle V^2 \rangle$, is obtained from the above distribution function and the usual method of obtaining the average value of a continuum.

$$\langle V^2 \rangle = \frac{\int_0^\infty V^2 dN_V}{\int_0^\infty dN_V} .$$

Notice that the molecules which do not reach the height $h = r - R$ are neglected by taking the lower limit of the integrals to be $v = 0$. The result of this integration is

$$T \doteq T_0 \left(1 + \frac{z}{3} \right) ,$$

where

$$z = 2 \left(\frac{mg}{kT_0} \right) R \left(\frac{h}{R + h} \right) ,$$

and h is the distance above the exosphere. Figure 2 gives a temperature profile for $T_0 = 320^\circ\text{K}$ and $R = 200$ km. This procedure may readily be extended to the case where the exosphere is composed of more than one type of molecule. For an exospheric boundary containing two constituents of masses m_1 and m_2 , the temperature is given by

$$T \doteq T_0 + \frac{2g Rh}{3K(R + h)} \left(\frac{m_1 + K m_2}{1 + K} \right),$$

where

$$K = \frac{n_2}{n_1} \left(\frac{m_2}{m_1} \right)^{1/2} \exp \left(- \frac{m_2}{m_1} \right),$$

and n_1 and n_2 are the number of molecules of each constituent per unit volume at the base of the exosphere. An extension to more than two constituents is also possible.

III. CONCLUSIONS

The primary objection to using this approach is in assuming that there exists a well-defined boundary between multiple-collision and collisionless regions. This boundary could not exist for any appreciable time since the diffusive characteristics of the gas would rapidly cause such a discontinuity to vanish. Nevertheless, neglecting chemical and radiative processes, it can be safely assumed that this temperature curve represents an upper bound for the actual temperature profile for Mars in the region immediately above the exosphere and approaches the actual temperature profile at very large altitudes. The effect of collisions will cause the lapse rate to be smaller than is predicted here since the proportion of molecules at high speeds will be reduced by "shielding" effects and momentum exchange processes. So that an acceptable temperature profile can be obtained, an analysis of systems which differ slightly from perfectly random motion must be made. The profile so obtained must approach a constant value for the temperature as predicted from a Maxwellian distribution at the base of the exosphere and the profile given here at large distances above the exosphere. In any event, the temperature of the upper atmosphere of Mars increases with altitude.

REFERENCES

1. Kuiper, G. P. (1952). Planetary atmospheres and their origins, Atmospheres of the Earth and Planets, University of Chicago Press, Chicago.
2. Opik, E. J., and S. F. Singer (1961). Distribution of density in a planetary exosphere, Physics of Fluids 4(2): 221-233.
3. Jeans, J. H. (1925). Aerostatics and Planetary Atmospheres, The Dynamical Theory of Gases, p. 334, Cambridge University Press, London.

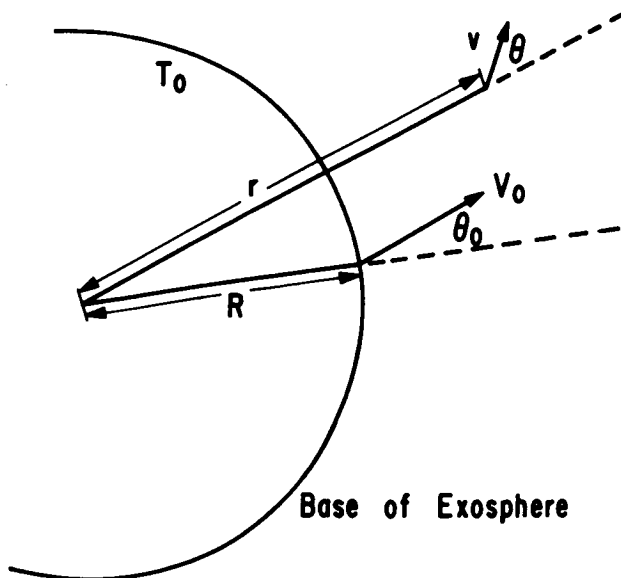


FIG. 1. EXOSPHERE OF MARS

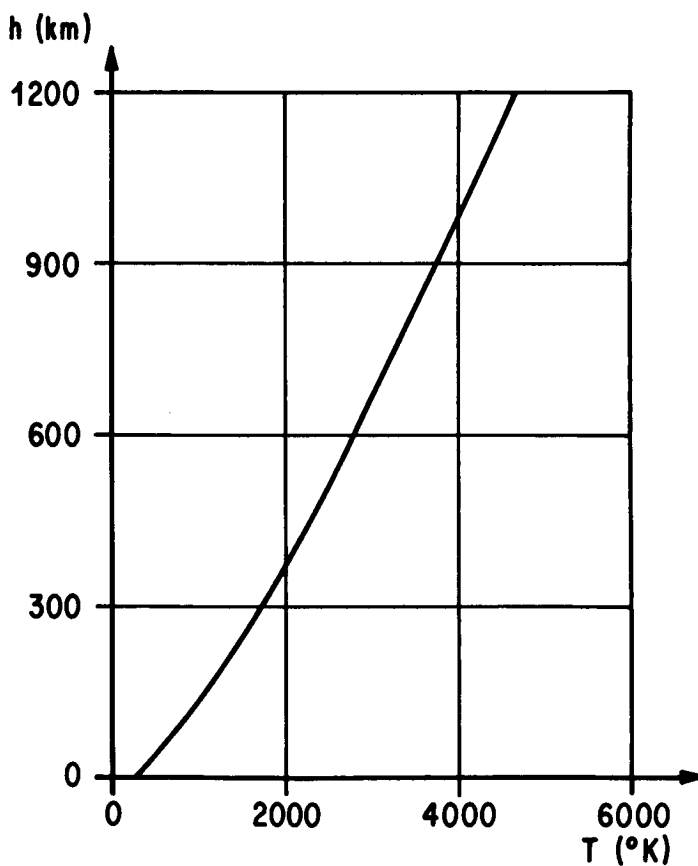


FIG. 2. TEMPERATURE PROFILE OF THE UPPER MARTIAN ATMOSPHERE

A METHOD FOR THE PREDICTION OF THE MARTIAN
TEMPERATURE AND SOME APPLICATIONS OF
METEOROLOGICAL ANALYSIS

by

Y. S. Lou

Nortronics-Huntsville
Huntsville, Alabama

N68-18839

SUMMARY

A modified radiative-convective model is established for the prediction of the surface and atmospheric temperatures at a given point on Mars in terms of Earth dates. Other atmospheric parameters can be calculated from this model with the aid of the proper concept or theory. Calculations may be made at points laid out in a grid over a specific region of interest on the Martian surface, and synoptic maps of isotherms and contours can be constructed. These maps may be used to estimate the motions of the Martian atmosphere, both horizontally and vertically. It is likely that the results obtained from this modified model would show an approximate structure of the atmosphere, but further work is required to justify the validity of the model, since circulation has not been taken into account and the Martian atmosphere has been assumed to be steady state.

I. INTRODUCTION

In the future exploration of Mars, it is necessary to predetermine the environmental conditions to be encountered by any space vehicle penetrating the Martian atmosphere and landing on the Martian surface. Our present knowledge of the Martian atmosphere is limited by many undetermined factors, both physical and dynamic. Because routine observation cannot be conducted, the actual structure of the atmosphere still remains in question. However, it is possible to construct a model atmosphere from theoretical considerations of radiative-convective transfer when the active constituents of the atmosphere are quantitatively known.

Early studies of the radiative equilibrium of a non-gray atmosphere have been carried out by Gowan [1], Goody [2], King [3, 4], Yamamoto [5], Moller and Manabe [6], and others. Because of the complete disregard for atmospheric motion in the computations, the general characteristic of the purely radiative equilibrium calculation is that it tends to overestimate the surface temperature on one hand, and to underestimate the upper tropospheric temperature on the other hand. To overcome this defect the process of a convective adjustment to approximate the upward heat transfer by atmospheric

motions must be considered. It is expected that this process of convective adjustment will transfer heat energy from the surface of the planet into the lower and upper troposphere and thereby permit more realistic temperatures to occur throughout the troposphere. This type of study has been made for the Earth's atmosphere by Manabe and Strickler [7], in which the whole atmosphere is divided into eighteen layers. They indicated that it is possible to obtain a vertical distribution of the atmospheric temperature, which almost exactly satisfies the condition of radiative or thermal equilibrium, as the asymptotic steady state of the initial value problem. Other similar studies were made for the Martian atmosphere by Prabhakara and Hogan [8], and Leovy [9], in which the atmosphere from the surface up to 100 km altitude is considered to be fifty layers of equal geometric thickness and two layers of equal pressure difference. The results of their calculation again showed a fairly good approximation of the thermal structure of the Martian atmosphere.

A good theoretical model of the atmospheric structure should not only include the process of radiative transfer, but all the important dynamic processes as well. Therefore, it is worthwhile to consider a radiative-convective model which can not only provide a practical means for determining the environmental conditions of a specific region on Mars during a specific time period in the past or future, but can also be incorporated in an advanced general circulation model of the atmosphere.

In this study, a modified radiative-convective model is established for calculations of surface and atmospheric temperature at a given point on Mars in terms of Earth dates. Other atmospheric parameters can then be calculated from this model with the aid of proper concepts or theory. If the calculations were made at a grid of points laid out over a large portion of the Martian surface area, then the synoptic maps of isotherms (lines of equal temperature) and contours (lines of equal height) could be drawn, which would approximately represent the structure of the Martian atmosphere in three dimensions. Although the initial condition of the atmosphere is assumed to be steady state, i. e., no circulation has been taken into account in the computations, the horizontal wind field, because of the differential heating on a rotating planet, can be derived from the synoptic maps. A further application of the model, in addition to serving as the basis of a dynamic model, is to calculate the vertical motion of the air.

II. THE RADIATIVE-CONVECTIVE MODEL

To establish a numerical model for the calculation of temperature on Mars, the thermal structure of the atmosphere must be considered from both the empirical and the theoretical viewpoints. A model should be established in such a way that it is not only supported by theory but is also in agreement with observations.

There is a considerable amount of information in the literature on the thermal structure of Mars; among these documents, the data obtained by radiometric and spectroscopic means provide reasonably good temperature measurements. More reliable information was recently obtained from the Mariner IV occultation experiment, from which several possible models of temperature height profiles have been derived (Johnson [10], Chamberlain and McElroy [11], Fjeldbo [12],

and Smith [13]). These were based on differing theoretical assumptions concerning the main ionization layer in the Martian atmosphere over Electris, near 50°S, 177°E at 1300 hours local time in late winter. Three different names (E, F1, and F2) were given to these profiles based on Earth analogy. Among these models, Johnson's F2 hypothesis [10] seems preferable. In this model, photo-dissociation of CO₂ and diffusive separation result in an atomic oxygen upper atmosphere, with O⁺ being the principal ion in the isothermal top side of the ionosphere [14]. The low particle concentration associated with the identification of the peak ionization as an F2 peak requires that the atmosphere be very cold. The low density observed by Mariner IV near the surface indicates that the atmosphere consists almost entirely of CO₂. The E and F1 hypotheses both require mixing or negligible dissociation of CO₂ in order to avoid the preponderance of atomic oxygen in the region where the data show a constant plasma scale height [12 and 14].

Previous investigations have also been made to obtain the temperature distribution of Mars from theoretical calculations based on the radiative-convective concept. In addition to those mentioned in the previous section, Ohring [15] and Neubauer [16] have also contributed a large amount of information on the thermal structure of Mars. However, for simplicity Leovy's two-layer model is considered in this study because it is suitable as a basis of an advanced dynamic model such as the one Mintz [17] has proposed.

In this study, the Martian atmosphere from the surface to 100-km altitude is considered. Johnson's F2 hypothesis [10] and Leovy's radiative-convective model [9] were modified to develop a new model. Figure 1 illustrates the assumed structure of the model in which the Martian atmosphere is divided into two layers. The lower layer (from level 3 to G) contains half of the tropospheric air mass; the upper layer (from the top of the atmosphere to level 3) contains half of the tropospheric air mass and the mass above the tropopause. The principal features of this model are: the Martian surface pressure is 8 mb; the atmosphere is considered to be entirely carbon dioxide with a molecular weight of 44.0 near the surface; it would change from a purely mixed medium to a gas undergoing strong dissociation and diffusive equilibrium at about 60-km altitude [18]; the vertical temperature profile first follows a near adiabatic lapse rate from surface to tropopause, then decreases linearly upward to 100-km altitude where the temperature is constant at 85°K; and there is a very thin subsurface layer near the surface (from level 4 to G in Figure 1) into which the temperature is also assumed to be continuous.

Since the Martian atmosphere is largely transparent to solar radiation, most of the incoming solar energy is not absorbed directly in the atmosphere but rather at the surface. This energy is carried into the soil by conduction and then upward into the atmosphere mainly by turbulent convection. Some of the energy is emitted from the surface directly to space, and the energy that the atmosphere receives by turbulent convection is lost in the form of long-wave radiation. Thus, the thermal structure of the Martian atmosphere is controlled by radiative, convective, and conductive processes. In our model, variation of temperature below 100 km is taken into account, but the thermal structure above 100 km is assumed to be unchanging.

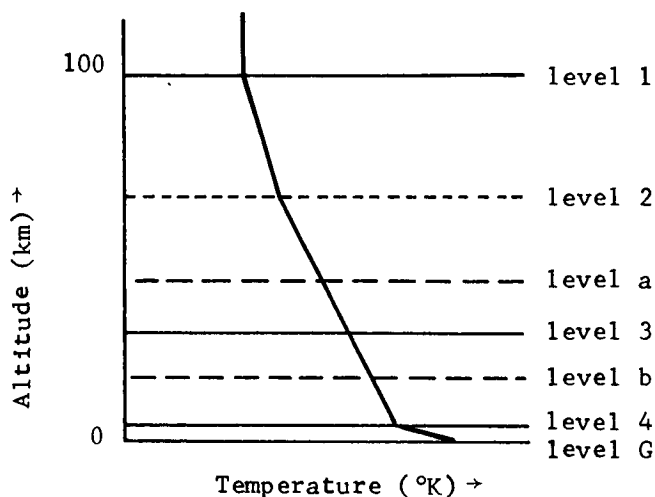


TABLE 1. ASSUMED PRESSURE AT EACH LEVEL

Level	Pressure (mb)
1	0.00191
2	1.64
a	3.23
3	4.82
b	6.41
4	8.00
G	8.00

Figure 1. NOMENCLATURE USED IN THE MODEL

The equations governing the temperature variations of the atmospheric layers are

$$\frac{dT_a}{dt} = \left(\frac{g}{C_p \Delta p} \right)_a \left[(S_0 - S_3) + (F_3 - F_0) + C_3 \right] \quad (1)$$

and

$$\frac{dT_b}{dt} = \left(\frac{g}{C_p \Delta p} \right)_b \left[(S_3 - S_4) + (F_4 - F_3) + (C_4 - C_3) \right] \quad (2)$$

where T is temperature, t is time, $\frac{C_p \Delta p}{g}$ is the heat capacity per unit area of each layer, S is solar energy flux, F is infrared radiative energy flux, and C is convective heat flux.

The heat conduction equation applying at subsurface levels is given by

$$\frac{\partial T}{\partial t} = k \frac{\partial^2 T}{\partial Z^2} \quad (3)$$

where k is thermometric conductivity of the soil.

The boundary conditions are

$$\frac{dT_1}{dt} = 0 \quad (4)$$

$$\left(\frac{\partial T}{\partial Z} \right)_G = \frac{1}{(\rho c)_G k} \left[S_4 (1 - A) - F_4 - C_4 \right] \quad (5)$$

$$\frac{dM}{dt} = 0, \text{ when } M = 0 \text{ and } T_G > T_s \text{ or} \quad (6)$$

$$\frac{dM}{dt} = \frac{1}{L} \left[F_4 + C_4 - S_4 (1 - A) + (\rho c)_G k \left(\frac{\partial T}{\partial Z} \right)_G \right] \quad (7)$$

$$T_G = T_s, \quad \text{when } M \neq 0 \quad (8)$$

where A is the visible albedo of the ground, T_s is the equilibrium temperature of CO₂ between solid and vapor state, M is the mass of CO₂ per unit area condensed on the Martian surface, L is the latent heat of CO₂, and $(\rho c)_G$ is the volume heat capacity of the soil.

The methods of integration of equations (1) through (3), and (5) through (8) have been treated by Leovy [9]. Since the flux of solar radiation reaching a point at the outer limit of the Martian atmosphere at a given time is

$$S_0 = S_{00} \left(\frac{R_m}{R} \right)^2 \text{Cos } \phi U(\text{Cos } \phi)$$

where S_{00} is the solar constant, R_m and R are, respectively, the mean and actual distance of Mars from the Sun, ϕ is the zenith angle of the Sun, and $U(\text{Cos } \phi)$ is the unit step function which has the value of either one (when $0 < \text{Cos } \phi < 1$) or zero (when $\text{Cos } \phi < 0$). If scattering is neglected and the absorption in the atmosphere is properly assumed, the terms $(S_0 - S_3)$ and $(S_3 - S_4)$ appearing in equations (1) and (2) can be calculated based on the method discussed by Houghton [19]. The net upward radiative energy flux at a level can be estimated by making use of the Schwarzschild equation. A typical method for calculating the radiative energy flux has been shown by Leovy [9], where in our model, the emission at zero optical depth is a constant, because $T_0 (= T_1)$ is always 85°K. The thermometric conductivity and the convection parameters used by Leovy were estimated from the observed diurnal ground temperature variations of Sinton and Strong [20]. The variation of the specific heat of CO₂ at constant pressure was also estimated as a function of temperature only.

Since the amount of solar radiation received by the Martian surface per unit area at a given time differs from one place to another, the incident solar radiation flux is dependent on the zenith angle of the Sun. By means of vector analysis, the cosine of the zenith angle of the Sun with respect to a point on the Martian surface of longitude, λ , and latitude, ϕ , can be shown to be

$$\text{Cos } \phi = \text{Cos } \phi_s \text{ Cos } D_s \text{ Cos } \lambda \text{ Cos } LSS + \text{Cos } \phi_s \text{ Cos } D_s \text{ Sin } \lambda \text{ Sin } LSS + \text{Sin } \phi_s \text{ Sin } D_s \quad (10)$$

where D_s and LSS are respectively, the Martian latitude and longitude of the subsolar point. A method for calculating the subsolar point has been developed by Deshpande [21] and the actual distance from Mars to the Sun appearing in equation (9) can be found from the American Ephemeris and Nautical Almanac [22].

III. CALCULATIONS OF TEMPERATURE AND OTHER ATMOSPHERIC PARAMETERS

The immediate application of the model as described in Section II is to calculate the surface and atmospheric temperatures of Mars, T_G , T_a , and T_b (see Figure 1), at a given time over a grid of points laid out on the Martian surface. These grid points are equally spaced, an interval of 5 to 10 degrees of latitude and longitude being sufficient for large-scale meteorological analysis.

In calculating the temperature, the Martian surface is assumed to be a smooth uniform sphere with constant thermometric conductivity; the initial condition of the atmosphere is assumed to be steady state; and atmospheric water-vapor content is considered negligible.

The acceleration of gravity at latitude ϕ is defined by the following relationship:

$$g = \frac{GM}{d^2} \left[1 - 3J_2 \left(\frac{d_E}{d} \right)^2 P_2^\circ \right] \quad (11)$$

where $GM = 0.429778 \times 10^5 \text{ km}^3/\text{sec}^2$, d_E is the radius of Mars (3381 km), d is the distance in kilometers from the center of Mars to the point of interest, and the constant J_2 is a measure of the flattening of the Martian surface which has the value of 0.1947×10^{-2} , and $P_2^\circ = \frac{3}{2} \sin^2 \phi - \frac{1}{2}$.

All calculations are to be made at constant pressure levels. The values of pressure assumed for the model were listed in Table 1. Experience has shown that any reasonable estimate of temperature at the initial time, $t=0$, will suffice if the initial time is sufficiently ahead of the time period for which a solution is desired. In other words, the governing equations must be integrated until the equilibrium state is reached.

In practice, a computer program can be established based on the equations described in Section II. Once T_G , T_a , and T_b are calculated, the following atmospheric properties can be obtained as well.

From the hydrostatic equation and equation of state, the temperatures T_2 , T_3 , and T_4 in the layer of constant lapse rate atmosphere (from level 4 to level 2 in Figure 1) can be calculated according to the relationship

$$T_{h+1} = T_h \left(\frac{P_{h+1}}{P_h} \right)^{\frac{R^* \gamma}{g \bar{m}}} \quad (12)$$

where the subscripts h and $h+1$ represent levels at $Z=h$ and $Z=h+1$, respectively, R^* is the universal gas constant, \bar{m} is the mean molecular weight in the layer $Z=h$ to $Z=h+1$, and γ is the actual lapse rate of the layer which is determined by the calculated values of T_a and T_b .

The geometric height of each level can be obtained as

$$Z_{h+1} = Z_h + \frac{R^*}{g\bar{m}} \bar{T} \ln \frac{P_h}{P_{h+1}} \quad (13)$$

where \bar{T} is the mean temperature of the layer from Z_h to Z_{h+1} .

The density at each level is given by

$$\rho_{h+1} = \rho_h \left(\frac{T_{h+1}}{T_h} \right)^{\left(\frac{g\bar{m}}{R^* \gamma} + 1 \right)} \quad (14)$$

At surface $h=0$, the density $\rho_{h=0}$ can be solved from the equation of state

$$\rho_{h=0} = \frac{P_{h=0}}{R^* T_{h=0}} \quad (15)$$

The number density can be calculated as

$$\eta_h = \frac{\rho_h R^*}{m_h K} \quad (16)$$

where K is Boltzmann's constant.

The columnar mass of the atmosphere is

$$M_h = \frac{P_h}{g_h} \quad (17)$$

The geometric pressure scale height is

$$H_h = \frac{R^* T_h}{m_{h=0} g_h} \quad (18)$$

The potential pressure scale height is

$$H'_h = \frac{R^* T_h}{m_{h=0} g_{h=0}} \quad (19)$$

The potential density scale height is

$$H'_{\rho h} = \frac{T_h}{\frac{m_{h=0} g_{h=0}}{R^*} + \frac{dT}{dh}} \quad (20)$$

and, finally, the geometric density scale height is given by

$$H_{\rho h} = \frac{g_{h=0}}{g_h} H'_{\rho h} \quad (21)$$

IV. METEOROLOGICAL ANALYSIS AND APPLICATION

Based on the results obtained from Section III, the synoptic maps of isotherms and contours at constant pressure levels can be analyzed over a specific region of interest or over the whole hemisphere on Mars. The standard meteorological analysis technique can be applied for this purpose, wherein a hemispheric map based on Mercator's projection is prepared for plotting and analysis. These synoptic maps provide not only the picture of three-dimensional structure of the Martian atmosphere but also the source of data which can be used to obtain some other atmospheric properties. A few applications of these synoptic maps are discussed as follows.

A. Equilibrium Motion

Because Mars and Earth have many similar physical properties such as nearly equal rotational rate, nearly equal axial tilts, etc., the two planets can be usefully compared. When Le Chatelier's principle applies to geophysical phenomena, various possible equilibrium motions result. Based on Earth analogy, the Geodynamic Paradox also can be applied on Mars, which states that on the rotating Mars a particle subject to a constant force does not move parallel to the force with constant acceleration as expected, but ultimately will move perpendicular to the force with constant speed. The final state will be one in which the net acceleration is zero, the motion is horizontal, and the only forces present are those owing to pressure gradient, gravity, and Mars rotation. The horizontal equations of motion will then yield the geostrophic wind components

$$\begin{aligned}u &= -\frac{g}{f} \left(\frac{\partial Z}{\partial y} \right) p \\v &= \frac{g}{f} \left(\frac{\partial Z}{\partial x} \right) p\end{aligned}\tag{22}$$

where f is the Coriolis parameter, $2\Omega_0 \sin \phi$, and Ω_0 is the angular velocity of rotation of Mars.

Equation (22) can be solved by finite difference analog using the contour map obtained earlier.

The direction of geostrophic wind is parallel to the contours with low values on the left in the northern hemisphere, and on the right in the southern hemisphere. Caution must be taken that the geostrophic approximation is not applied in equatorial regions, since f vanishes as ϕ approaches zero.

On the other hand, friction must be taken into account at or near the Martian surface. If we assume that the friction acts exactly opposite to the direction of motion and proportional to the speed of motion, the horizontal equations of motion become

$$\begin{aligned}\text{and} \quad 0 &= fv - k_0 u \\0 &= -fu - k_0 v - \frac{1}{\rho} \frac{\partial p}{\partial y}\end{aligned}\tag{23}$$

where the isobars have been oriented in the East-West direction, and k_0 is a positive constant. By elimination we obtain

$$u = - \frac{f}{f^2 + k_0^2} \left(\frac{1}{\rho} \frac{\partial p}{\partial y} \right) \quad (24)$$

$$v = - \frac{k_0}{f^2 + k_0^2} \left(\frac{1}{\rho} \frac{\partial p}{\partial y} \right)$$

The total wind speed

$$V_f = \sqrt{u^2 + v^2} = \frac{1}{\sqrt{f^2 + k_0^2}} \left(\frac{1}{\rho} \frac{\partial p}{\partial y} \right) \quad (25)$$

which, when friction is present, is below the geostrophic value. The direction of the wind can be obtained by

$$\tan \alpha = \frac{v}{u} = \frac{k_0}{f} \quad (26)$$

Further application can be made using the thermal wind equation. The vertical shear of the geostrophic wind is given by

$$\frac{\partial u}{\partial z} = - \frac{g}{fT} \left(\frac{\partial T}{\partial y} \right)_p \quad (27)$$

$$\frac{\partial v}{\partial z} = \frac{g}{fT} \left(\frac{\partial T}{\partial x} \right)_p$$

Thus, for u to increase with height, temperature must increase to the South, and for v to increase with height, temperature must increase to the East, in the northern hemisphere.

Since the vertical shear of the geostrophic wind is a vector which lies parallel to the isotherms on a level surface with low temperature on the left in the northern hemisphere, the properties of the thermal wind may be used to show the relationship between the turning of wind with elevation and horizontal temperature gradient. Thus, the wind turns clockwise with height whenever there is a wind component from warm towards cold air, and turns counterclockwise with height whenever there is a wind component from cold towards warm air.

One special case is when the thermal wind equations equal zero. In this case the atmosphere is said to be barotropic in which case the absolute vorticity is conserved, and the motion is simply two-dimensional.

Another approach to calculate the thermal wind is from the thickness chart. Since the thickness of two pressure surfaces can be drawn quickly by superposing the two contour maps in question and subtracting graphically, the speed of the thermal wind, V_T , is given by

$$V_T = - \frac{g}{f} \frac{\Delta Th}{\Delta H} \quad (28)$$

where ΔTh is the height interval of the thickness lines and ΔH is the distance apart of the thickness lines. The direction of the thermal wind is parallel to the thickness lines with lower thickness to the left in the northern hemisphere. Thus, the thermal wind is related to the thickness lines exactly as the geostrophic wind is related to the contour lines of an isobaric surface.

Because of the fact that the thermal wind is the shear along the vertical of the geostrophic wind, the geostrophic wind at lower level, V_L , and upper level, V_U , are related to the thermal wind, V_T , in the following way:

$$V_U = V_L + V_T \quad (29)$$

This relationship provides a qualitative method of estimating the geostrophic wind at a higher level or vice versa.

B. Vertical Motion

Although the motion in the Martian atmosphere is believed to be predominantly horizontal, it does not mean that the vertical motion is absent, but that its magnitude is probably much smaller than the horizontal motion. Furthermore, the vertical motion of the air plays an important role in the evaluation of the flow patterns; therefore, it is of great interest to estimate the vertical velocity.

As on Earth, several methods can be used to compute vertical velocity, among which the adiabatic method is considered to be preferable in synoptic calculation. Since the potential temperature, θ , is conserved by the individual unit of air in the adiabatic process, the vertical velocity in P-system is given by

$$\omega^* = - \frac{\frac{\partial \theta}{\partial t} + V_H \frac{\partial \theta}{\partial s}}{\frac{\partial \theta}{\partial p}} \quad (30)$$

where $\omega^* \equiv \frac{dp}{dt}$, $\frac{\partial \theta}{\partial t}$ is the local rate of change of θ in an isobaric surface, V_H the horizontal speed of wind, and $\frac{\partial \theta}{\partial s}$ the variation of θ per unit distance along the streamlines.

If the vertical velocity is expressed with height as the vertical coordinate, one readily obtains from Poisson's equation and the hydrostatic equation,

$$w = - \frac{\frac{\partial T}{\partial t} + V_H \frac{\partial T}{\partial s}}{\Gamma_d - \gamma} \quad (31)$$

where $w \equiv \frac{dz}{dt}$, Γ_d and γ are dry-adiabatic and actual lapse rate, respectively.

In equation (31), the temperature tendency, $\frac{\partial T}{\partial t}$, can be obtained from two consecutive synoptic maps. The actual horizontal speed of the wind is V_H , but the geostrophic value may be used in the calculation, except in the very shallow frictional layer near the Martian surface, and $\frac{\partial T}{\partial s}$ can be obtained by the finite difference method. Thus, the vertical velocity at a given point on Mars can be numerically calculated.

V. CONCLUSIONS

The model is capable of predicting the surface and atmospheric temperatures at a given point on Mars in terms of Earth dates as they would occur in the absence of circulation. Isothermal and contour maps can be used to derive the horizontal and vertical motions of the Martian atmosphere, and the diurnal and seasonal variabilities of temperature also may be analyzed over a certain period of time. It is likely that the results obtained from the model will yield the approximate Martian atmospheric structure. The assumption of steady state may not be realistic, in which case any scale of circulation would probably modify the temperature distribution. However, there is reason to believe that the modification of temperature due to circulation may be small in the Martian atmosphere because the atmosphere is thin and acts as an efficient radiator.

The calculated temperatures should be compared with those obtained from previous investigations, such as the radiometric and spectroscopic measurements, Mariner IV occultation data, etc. Obviously, once winds are introduced, heat will be transported from one place to another and thus smooth out the temperature gradient. As a consequence, the calculated temperature gradient should be stronger than those observed.

The basic approach of predicting temperature, as discussed in this study, could be applied to any model atmosphere such as Manabe's and Strickler's [7] eighteen-layer model. Prabhakara's and Hogan's [8] fifty-layer model, or any others. Furthermore, better temperature distribution is expected by using a model with many layers if the final goal of treating the problem is based on a purely thermodynamic point of view.

Since no computation has been made, the validity of the model itself and the flexibility of the technical approach require justification. It is believed that further improvement can be made by using this model as a basis for a dynamic model from which a more realistic Martian atmosphere structure will result.

REFERENCES

1. Gowan, E.H., "The Effect of Ozone on the Temperature of the Upper Atmosphere," Proc. Roy. Soc., A, 120, 1928, pp. 655-669.
2. Goody, R.M., "The Thermal Equilibrium at the Tropopause and the Temperature of the Lower Stratosphere," Proc. Roy. Soc., A 197, 1949, pp. 487-505.
3. King, J.I.F., "Line Absorption and Radiative Equilibrium," J. Meteor., 9, 1952, pp. 311-321.
4. King, J.I.F., "Radiative Equilibrium of a Line-Absorbing Atmosphere II," Astrophys. J., 124, 1956, pp. 272-297
5. Yamamoto, G., "Radiative Equilibrium of the Earth's Atmosphere II. The Use of Rosseland's and Chandrasekher's means in the Line Absorbing Case," Sci. Rep. of the Tohoku Univ., Series 5,6, 1955, pp. 127-136.

6. Moller, f., and Manabe, S., "Uber das Strahlungsgleichgewicht in der Atmosphere," Z. F. Meteor., 15, 1961, pp. 3-8.
7. Manabe, S., and Strickler, R.F., "Thermal Equilibrium of the Atmosphere with a Convective Adjustment," J. Atmosphere Science, Vol. 21, July 1964, pp. 361-385.
8. Prabhakara, C., and Hogan, J.S., Jr., "Ozone and Carbon Dioxide Heating in the Martian Atmosphere," J. Atmospheric Sciences, Vol. 22, No. 2, March 1965, pp. 97-109.
9. Leovy, C., "Radiative-Convective Equilibrium Calculations for a Two-Layer Mars Atmosphere," Rand Memo. RM-5017, 1966.
10. Johnson, F.S., "Atmosphere of Mars," Science Vol. 150, 10 December 1965, pp. 1445-1448.
11. Chamberlain, J.W., and McElroy, M.B., "Martian Atmosphere: The Mariner Occultation Experiment," Science, Vol. 152, No. 3718, 1 April 1966, pp. 21-25.
12. Fjeldbo, G., Fjeldbo, W.C., and Eshleman, V.R., "Models for the Atmosphere of Mars Based on the Mariner IV Occultation Experiment," J. Geophys. Res., Vol. 71, No. 9, 1 May 1966, pp. 2307-2316.
13. Smith, N., and Beutler, A., "A Model Martian Atmosphere and Ionosphere," Report 66-3, University of Michigan, Ann Arbor, Michigan, March 1966.
14. Fjeldbo, G., Fjeldbo, W.C., and Eshleman, V.R., "Atmosphere of Mars: Mariner IV Models Compared," Science, Vol. 153, 23 September 1966, pp. 1518-1523.
15. Ohring, G., "A Theoretical Estimate of the Average Vertical Distribution of Temperature in the Martian Atmosphere," Icarus, 1, 1963, pp. 328-333.
16. Neubauer, F.M., "Thermal Convection in the Martian Atmosphere," J. Geophys. Res., Vol. 71, No. 10, 15 May 1966, pp. 2419-2426.
17. Mintz, Y., "The General Circulation of Planetary Atmospheres," National Academy of Sciences - National Research Council, Publication 944, 1962, pp. 107-146.
18. Weidner, D.K., and Hasseltine, C.L., "Natural Environment Design Criteria Guidelines for MSFC Voyager Spacecraft For Mars 1973 Mission," NASA TM X-53616, Goerge C. Marshall Space Flight Center, Huntsville, Alabama, June 8, 1967.
19. Houghton, J.T., "The Absorption of Solar Infrared Radiation by the Lower Stratosphere," Quart. J. Roy. Meteor. Soc., 89, 1963, pp. 319-331.
20. Sinton, W.M., and Strong, J., "Radiometric Observations of Mars," Astrophys. J., 131, 1960, pp. 459-469.

21. Deshpande, P.B., "Determination of the Subsolar Point of Mars and Prediction of Martian Seasons in Terms of Earth Dates," Informal Memorandum, Northrop Space Laboratories, Huntsville, Alabama, 1967.
22. The American Ephemeris and Nautical Almanac, U.S. Government Printing Office, Washington, D.C.

PREDICTION OF MARTIAN SURFACE TEMPERATURE*

by

F. B. Tatom
P. B. Deshpande
F. T. Hung

Nortronics-Huntsville
Huntsville, Alabama

N 68-18840

SUMMARY

An analytical model for predicting the surface temperature of Mars has been developed. Based on the analytical model, a digital computer program was written which locates the subsolar point on Mars, calculates the shape factor of a specific point on the Martian surface with respect to the Sun, and then solves the governing radiation and conduction heat transfer equations to establish the surface temperature, as well as the radial temperature profile beneath the surface. In developing the model, Mars was considered to be a smooth sphere with a uniform outer coating and a homogeneous interior. The atmosphere was not included in the model. The model is self-sufficient in that it can be used to predict the temperature at a specific planetographic latitude and longitude in terms of Earth time without use of astronomical tables.

The predicted values of the latitude of the subsolar point are in good agreement with the published values. The predicted temperature profiles using a two-layer model of powdery limonite over solid basalt are in general agreement with the observed temperatures, especially in the brightlands. Predicted nocturnal temperatures are slightly lower than observed surface temperatures, due to the absorptive and radiative characteristics of the atmosphere which are not considered in the model.

I. INTRODUCTION

The thermal environment of Mars has been the subject of a number of studies [1-8]. These studies generally fall into one of two categories. The first category involves astronomical observations such as those reported in [1, 2, 3], with a limited explanation of the thermal phenomena observed. The second category, such as reported in [4-8], involves the formulation of analytical models which produce temperature-time histories, isothermal contour maps, and thermophysical property values. The temperatures predicted by such models are surface temperatures, atmospheric temperatures, or both. Such analytical treatments generally are based on Martian local time and involve a spatial coordinate system which is not clearly defined or related to the

*Prepared for NASA/MSFC under Contract under NAS8-20082.

Martian surface. In the past, no practical means has been available for determining the thermal environment of a specific region on the Martian surface, during a specific Earth time period, without first referring to astronomical tables and then performing a number of calculations based on these tabulated astronomical data.

An analytical model in the form of a digital computer program has been developed for predicting the surface temperature of Mars at a specified plane-tographic position at a specified Earth time without reference to the astro-nomical tables. Subsequent portions of this paper describe the initial efforts involved in the development of this engineering tool. For the sake of sim-plicity in these initial efforts, the Martian atmosphere has not been taken into account.

II. TECHNICAL DISCUSSION

Because of the eccentricity of the Martian orbit, Mars receives 43 per-cent more solar energy at perihelion than at aphelion. Therefore, the amount of heat and light received by the two hemispheres during like seasons is quite different. The inclination of the equator of Mars to its orbit is $24^{\circ}.94$, which is within 1-1/2 degrees of the corresponding inclination of Earth. The eccentricity of the orbit, period of rotation, and equatorial inclination influence the diurnal and seasonal temperature variations on Mars.

The prediction of the diurnal variations of the Martian surface temper-ature has been carried out in three phases. The first phase was devoted to the calculation of the subsolar point on Mars. In the second, heat transfer equations were developed for the calculation of Martian surface and subsurface temperatures. During the third phase, the results obtained were compared with existing temperature measurements.

A. Calculation of Subsolar Point on Mars

In carrying out a radiation analysis of Mars with the view of pre-dicting the surface temperature, it is necessary to calculate the related shape factor between Mars and the Sun. By definition, the shape factor repre-sents that fraction of the total solar energy which is incident on a given surface on Mars. The shape factor is a function of the solar zenith angle*, in turn, depends on the location of the subsolar point on Mars. The Martian subsolar point represents the interception of the Martian surface with a vector drawn from the center of Mars to the center of the Sun. For an observer standing at the point of interception, the Sun will be directly over-head. Based on the information obtained from [9-13], the necessary equations for calculating the latitude and longitude of the subsolar point have been developed as provided in the paragraphs which follow. A more detailed develop-ment is provided in [14].

* Solar zenith angle is defined as the angle between the normal to a specific point on Mars and the line-of-sight from the point to the Sun.

The Julian day interval from the Epoch (January 1900, 0.5 E.T. *) can be calculated as

$$d = 365 X + \frac{X-1}{4} + p - 0.5 + \frac{h}{24} \quad (1)$$

where

X = Y - 1900

Y = calendar year of interest

p = number of days from the beginning of the year to date

h = Greenwich mean time.

The right ascension, α_0 , and the declination, δ_0 , of the point on the celestial sphere toward which the axis of rotation of Mars is directed are given by

$$\alpha_0 = 21^h 11^m 10^s.42 + 1^s.565(Y-1950) \quad (2)$$

$$\delta_0 = 54^\circ 39' 27'' + 12''.60(Y-1950) \quad (3)$$

where

$$\begin{aligned} 1^h &= 15^\circ \\ 1^m &= 15' \\ 1^s &= 15''. \end{aligned}$$

The mean obliquity of the ecliptic, ϵ , is given by

$$\epsilon = 23^\circ.452294 - 0^\circ.0130125t - 0^\circ.00000164t^2 + 0^\circ.000000503t^3 \quad (4)$$

where $t = d/36525$.

*Universal Time (U.T.) is the Greenwich mean time beginning at midnight. Ephemeris Time (E.T.) is the uniform time system used in computations. E.T. is not affected by the variable rotation of the Earth, hence it is ahead of U.T. by a small amount, $\Delta\tau$, which is determined by observations

$$E.T. = U.T. + \Delta\tau$$

For the year 1961, $\Delta\tau$ was 34 seconds. The effect of $\Delta\tau$ is usually small and is neglected in the present study.

The orbit of Mars can be defined by six elements:

- (1) The inclination of the orbit to the ecliptic
- (2) The longitude of the ascending node of the orbit on the ecliptic
- (3) The longitude of the perihelion
- (4) The true anomaly
- (5) The eccentricity
- (6) The true orbital longitude of the planet.

These elements are referred to the mean equinox and ecliptic of date.

The inclination of the orbit to the ecliptic, as corrected by Ross, is

$$i = 1^{\circ}51'01''.20 - 2''.430t + 0''.0454t^2. \quad (5)$$

The longitude of the ascending node of the orbit on the ecliptic, measured from the equinox, is

$$\bar{\Omega} = 48^{\circ}47'11''.19 + 2775''.57t - 0''.005t^2 - 0''.0192t^3. \quad (6)$$

The longitude of the perihelion, measured from the equinox along the ecliptic to the node and then along the orbit from node to perihelion, is given by

$$\bar{\omega} = 334^{\circ}13'05''.53 + 6626''.73t + 0''.4675t^2 - 0''.0043t^3. \quad (7)$$

The eccentricity is given by

$$e = 0.09331290 + 0.000092064t + 0.000000077t^2. \quad (8)$$

The true anomaly, F, is given as

$$F = M + \left(2e - \frac{1}{4}e^3\right) \sin(M) + \frac{1}{4}e^2 \sin(2M) + \frac{13}{12}e^3 \sin(3M) \quad (9)$$

where the mean anomaly, M, is

$$M = 319^{\circ}.529425 + 0^{\circ}.524020766d + 0^{\circ}.000013553D^2 + 0^{\circ}.000000025D^3 \quad (10)$$

with

$$D = d/10000.$$

Although equation (9) is a series approximation, the accuracy obtainable by using the first four terms is quite sufficient for the present study. The orbital longitude of the planet is

$$L = F + \bar{\omega}. \quad (11)$$

Figures 1 and 2 are provided to indicate the location of the subsolar point with respect to various astronomical quantities. In Figure 1, the subsolar point has been located with respect to the vernal equinox. In Figure 2, the quantities required to calculate the planetographic longitude and latitude of the subsolar point are shown.

I = Inclination of the equator to the orbit.

L_s = Planetocentric longitude of the Sun.

D_s = Latitude of the subsolar point.

A_s = Planetocentric right ascension of the Sun.

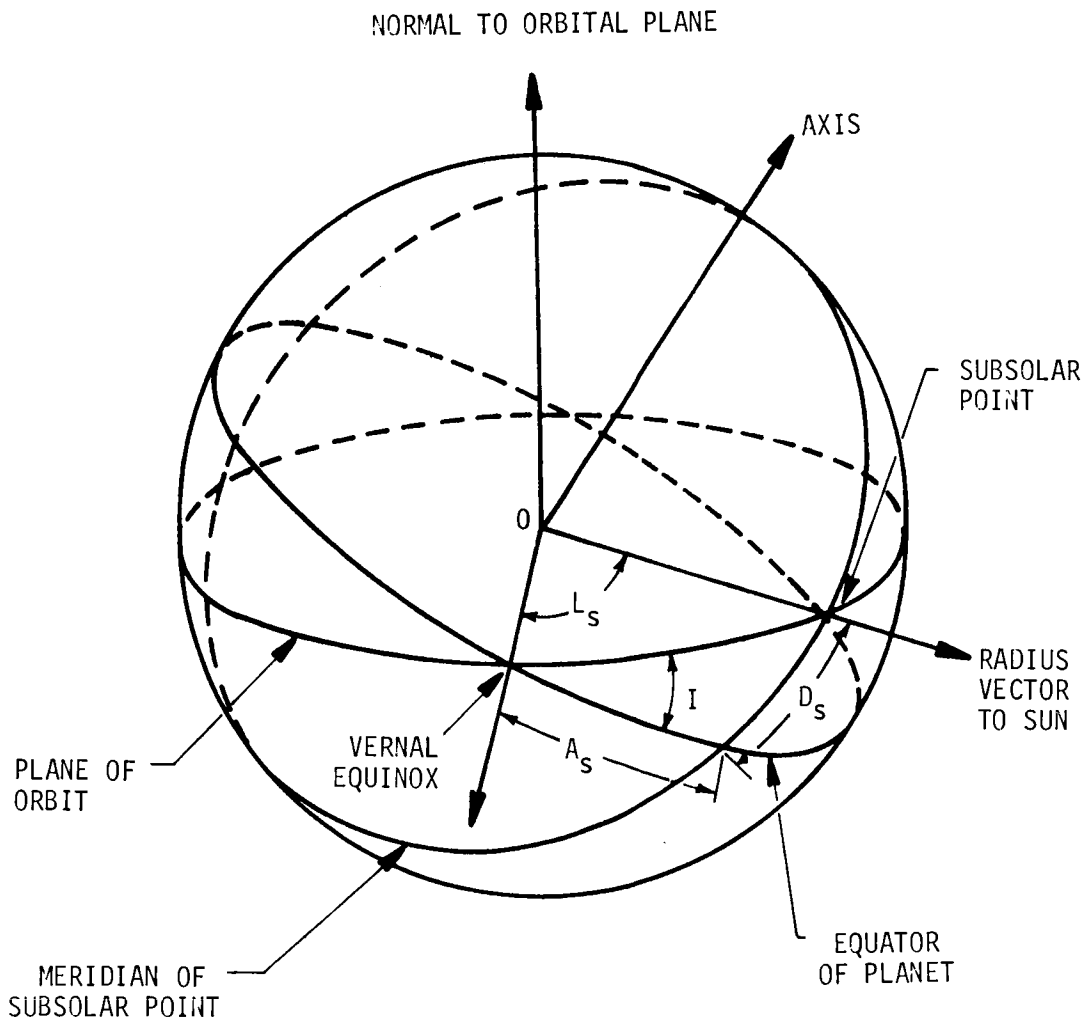


Figure 1. LOCATION OF SUBSOLAR POINT ON THE PLANET MARS

- A = North Pole of rotation of Mars.
- N = North Celestial Pole.
- S = Heliocentric position of the planet.
- i = Inclination of the orbit to the ecliptic.
- τ = First point of Aries.
- I = Inclination of the equator to the orbit.

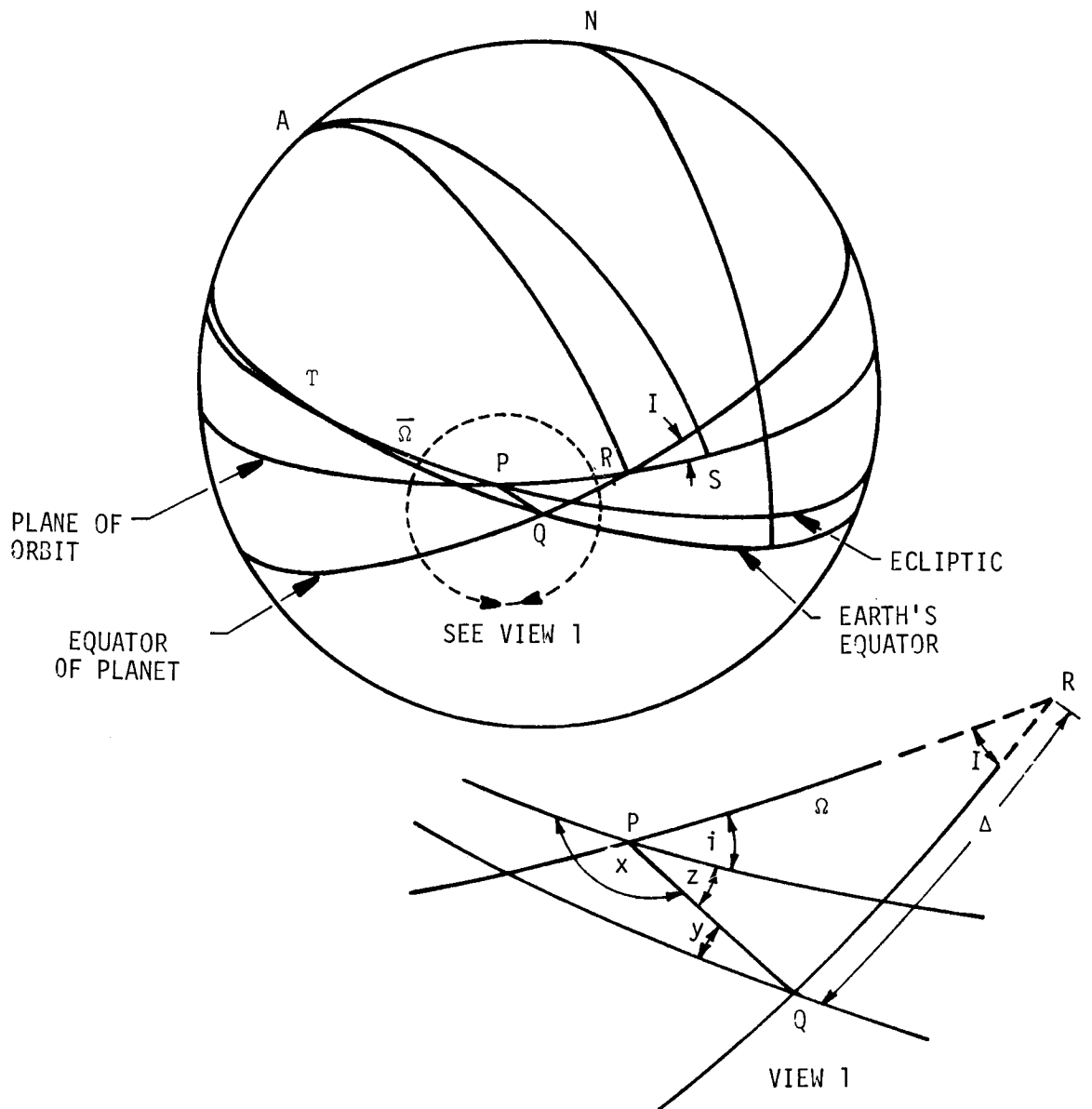


Figure 2. THE PLANETOCENTRIC SPHERE FOR MARS

From the triangle PQT in Figure 2, the angles x, y, and z may be determined as follows:

$$z = \arccos(\cos \epsilon \sin \bar{\Omega} \cos \alpha_0 - \cos \bar{\Omega} \sin \alpha_0) \quad (12)$$

$$x = \arccos[(-\cos \epsilon \cos \bar{\Omega} \cos \alpha_0 - \sin \bar{\Omega} \sin \alpha_0) / \sin z] \quad (13)$$

$$y = \arccos[(\cos \epsilon \sin \bar{\Omega} \sin \alpha_0 + \cos \bar{\Omega} \cos \alpha_0) / \sin z]. \quad (14)$$

From the triangle PQR, in which the angles are I, $180+(i-x)$ and $90+(\delta_0 - y)$, the angle I and the arcs Δ and $\bar{\Omega}$ are given by

$$I = \arccos [\cos(x-i)\sin(y-\delta_0) + \sin(x-i)\cos(y-\delta_0)\cos z] \quad (15)$$

$$\bar{\Omega} = \arccos\{[\sin(x-i)\sin(y-\delta_0) - \cos(x-i)\cos(y-\delta_0)\cos z] / \sin I\} \quad (16)$$

$$\Delta = \arccos\{[-\cos(x-i)\cos(y-\delta_0) + \sin(x-i)\sin(y-\delta_0)\cos z] / \sin I\} \quad (17)$$

Planetocentric longitude of the Sun, L_s , measured in the plane of the orbit of Mars from vernal equinox, is

$$L_s = L - (\Omega + \bar{\Omega}). \quad (18)$$

The latitude of the subsolar point, b_s , equals the declination of the Sun, D_s . This quantity, along with the planetocentric right ascension of the Sun, A_s , can be calculated from the right spherical triangle formed by L_s , D_s , and A_s in Figure 1 as follows:

$$\begin{aligned} D_s &= \arcsin(\sin L_s \sin I) \\ &= b_s \end{aligned} \quad (19)$$

$$\begin{aligned} A_s &= \arccos(\cos L_s / \cos D_s) \\ &= \arcsin(\sin L_s \cos I / \cos D_s). \end{aligned} \quad (20)$$

The Martian hour angle, V, of the vernal equinox of Mars measured westward from the prime meridian in the adopted system of elements (with reference to the Epoch of January 15, 1909 GMAT*) for any Earth date is

$$V = 145^{\circ}.845 + 350^{\circ}.891962(d - 2418322). \quad (21)$$

The longitude of the subsolar point is then given by

$$\ell_s = V - A_s. \quad (22)$$

After calculating the longitude and latitude of the subsolar point, the cosine of the zenith angle, Z, of the Sun with respect to a point on the Martian surface of planetographic longitude ℓ and latitude b is calculated as

$$\begin{aligned} \cos Z &= \cos b \cos(b_s) \cos \ell \cos(\ell_s) + \sin b \sin(b_s) \\ &\quad + \cos b \cos(b_s) \sin \ell \sin(\ell_s) \end{aligned} \quad (23)$$

* Greenwich Mean Astronomical Time (GMAT) is Greenwich mean time beginning at Noon. It was used before 1 January 1925.

Then, the shape factor between a specific point on the Martian surface and the Sun can be shown to be [15]:

$$F_{ms} = \cos Z \left(\frac{R_s}{r} \right)^2 U(\cos Z) \quad (24)$$

where

R_s = radius of the Sun

r = radial distance between the Sun and Mars at a given time

$$= \frac{a(1-e^2)}{1+e \cos F}$$

a = mean distance between Mars and the Sun

$U(\cos Z)$ = unit step function.

B. Development of the Heat Transfer Equations

Mars receives its energy almost entirely from the Sun. Part of the incident radiation is reflected and the rest absorbed. Part of the absorbed energy is conducted into the deeper layers and stored as thermal energy, the rest is lost to space in the form of emitted radiation. In the present analysis, Mars is assumed to consist of an inner homogeneous sphere covered by a thin coating (of thickness D_1) of a material with a low thermal conductivity. The atmosphere is not included in the model. It has been assumed that no significant temperature variations occur within the inner sphere below a certain depth, D_2 , except for the case of internal heat flow. Denoting the top-layer temperatures with a subscript "1" and the inner-layer temperatures with a subscript "2", the governing heat transfer equations in spherical coordinates are

$$\frac{\partial^2 T_1}{\partial R^2} + \frac{2}{R} \frac{\partial T_1}{\partial R} = \frac{1}{a_1} \frac{\partial T_1}{\partial \tau} \quad (R_m - D_1 \leq R \leq R_m) \quad (25)$$

and

$$\frac{\partial^2 T_2}{\partial R^2} + \frac{2}{R} \frac{\partial T_2}{\partial R} = \frac{1}{a_2} \frac{\partial T_2}{\partial \tau} \quad (R_m - (D_1 + D_2) \leq R \leq R_m - D_1) \quad (26)$$

Equations (25) and (26) are based on the assumption that the angular temperature variations are negligible. The corresponding initial conditions and boundary conditions are

$$T_1 = T_1(R) \quad (R_m - D_1 \leq R \leq R_m) @ \tau = 0 \quad (27)$$

$$T_2 = T_2(R) \quad (R_m - (D_1 + D_2) \leq R \leq R_m - D_1) @ \tau = 0 \quad (28)$$

$$T_{1,i+1,j} = T_{1,i,j} + \frac{a_1 \Delta\tau}{(\Delta R_1)^2} (T_{1,i,j+1} + T_{1,i,j-1} - 2T_{1,i,j}) \quad (34)$$

with $j = 0, 1, \dots, L$

$$T_{2,i+1,j} = T_{2,i,j} + \frac{a_2 \Delta\tau}{(\Delta R_2)^2} (T_{2,i,j+1} + T_{2,i,j-1} - 2T_{2,i,j}) \quad (35)$$

with $j = 0, 1, \dots, M$

$$T_{1,0,j} = T_1(j) \quad (j = 0, 1, \dots, L) \quad (36)$$

$$T_{2,0,j} = T_2(j) \quad (j = 0, 1, \dots, M) \quad (37)$$

$$T_{1,1,-1} = T_{1,i,+1} - 2 \frac{\sigma \Delta R_1}{K_1} \left[\epsilon T_{1,i,0}^4 - \alpha_s F_{ms} T_s^4 \right] \quad (38)$$

$$T_{1,i,L} = T_{2,i,0} \quad (39)$$

$$T_{1,i,L+1} = \frac{1}{a_1 K_2 \Delta R_2 + a_2 K_1 \Delta R_1} \left[T_{1,i,L} \left(2a_1 K_2 \Delta R_2 - 2a_2 K_2 \Delta R_1 \frac{\Delta R_1}{\Delta R_2} \right) + 2a_2 K_2 \Delta R_1 \frac{\Delta R_1}{\Delta R_2} T_{2,i,1} - (a_1 K_2 \Delta R_2 - a_2 K_1 \Delta R_1) T_{1,i,L-1} \right] \quad (40)$$

and

$$T_{2,i,M+1} = T_{2,i,M-1} + 2 \Delta R_2 q_c'' / K_2 \quad (41)$$

For a given set of reasonable initial conditions, the preceding finite difference equations can be solved to yield surface and subsurface temperatures. Theoretically, any set of initial conditions will suffice, but if unrealistic initial conditions are assumed, considerable computation time is required for the solution to converge to the right values. Therefore, an intelligent guess for the initial temperatures is desirable. When the temperature profiles for two or three diurnal cycles show little or no change, a solution has been reached.

In problems involving numerical solutions, the question of stability arises. Because of the nonlinear boundary condition at the Martian surface as

and

$$\frac{\partial T_1}{\partial R} = - \frac{\sigma}{K_1} (\epsilon T^4 - \alpha_s F_{ms} T_s^4) \quad @ R = R_m \quad (29)$$

$$T_1 = T_2 \quad @ R = R_m - D_1 \quad (30)$$

$$K_1 \frac{\partial T_1}{\partial R} = K_2 \frac{\partial T_2}{\partial R}$$

$$- K_2 \frac{\partial T_2}{\partial R} = q_c'' \quad @ R = R_m - (D_1 + D_2) \quad (31)$$

where

- T = Martian temperature
- R = radial distance
- R_m = radius of Mars
- τ = time
- a = thermal diffusivity
- σ = Stefan-Boltzmann constant
- T_s = effective temperature of the Sun
- K^s = thermal conductivity
- ε = emissivity of the Martian surface
- α_s = solar absorptivity of the Martian surface
- q_c'' = flow of heat from the interior of the planet.

Since R is very large in the present study, equations (25) and (26) may be simplified to:

$$\frac{\partial^2 T_1}{\partial R^2} = \frac{1}{a_1} \frac{\partial T_1}{\partial \tau} \quad (R_m - D_1 \leq R \leq R_m) \quad (32)$$

and

$$\frac{\partial^2 T_2}{\partial R^2} = \frac{1}{a_2} \frac{\partial T_2}{\partial \tau} \quad (R_m - (D_1 + D_2) \leq R \leq R_m - D_1) \quad (33)$$

A finite difference approach has been chosen for solving the heat transfer equations. If the subscripts "i" and "j" refer to time and space, respectively, equations (27) through (33) can be expressed in finite difference form as follows:

indicated by equation (38), the standard criteria for stability, used in ordinary heat conduction problems, are not applicable. For the current problem, based on [16], the following criteria was established for stability:

$$\frac{a_1 \Delta \tau}{(\Delta R_1)^2} \left(1 + \frac{\Delta R_1 \epsilon \sigma T_{1,i,o}^3}{K_1} \right) < 0.5. \quad (42)$$

III. DISCUSSION OF RESULTS

The subsolar point calculations and the finite difference equations have been incorporated into a digital computer program. The program is capable of predicting the Martian surface and subsurface temperatures as a function of Earth time.

The predictions of the latitude of the subsolar point on Mars were made for specific dates on which comparison with published values of latitude [4 and 7] was possible. As indicated in Table 1, the predicted values of the subsolar point latitudes generally agree with the published values. The published subsolar point latitudes are not given for a specific hour (Earth time), but instead for a time period of two or more days. The predicted latitudes, however, are given for a specific hour, as indicated in the table. In addition, the subsolar point latitudes published by Opik in [4] appear to have been rounded off to the nearest degree. These facts explain the differences between the published and predicted values. Since no published values of Martian subsolar point longitude were found, a comparison in terms of longitude could not be made.

Table 1. LATITUDE OF SUBSOLAR POINT OF MARS

REFER- ENCE	DATE OF PUBLISHED DATA	PUBLISHED LATITUDE	DATE AND TIME OF PREDICTION	PREDICTED LATITUDE
7	July 20-24, 1954	$8^{\circ}2 \pm 0.5$	1200 GMT July 22, 1954	$8^{\circ}24$
4	November 21-22, 1958	-12°	1200 GMT November 22, 1958	$-12^{\circ}47$
4	December 7-8, 1958	-9°	1200 GMT December 8, 1958	$-9^{\circ}43$

Information concerning the thermophysical properties of the Martian surface is essential to the prediction of the surface temperature. Thermophysical property data are summarized in Table 2 for three materials which are considered probable constituents of the Martian surface [17]. As indicated in this table, the property values for powdery limonite and goethite are similar. For solid basalt, the property values for density and specific

heat resemble those values for the other two materials. The thermal conductivity and thermal inertia parameter of basalt, however, are quite different from their counterparts. Therefore, since powdery limonite and goethite display such similar properties only the former along with solid basalt were used in the present study.

Table 2. THERMOPHYSICAL PROPERTIES OF THE MARTIAN SURFACE

MATERIAL	THERMAL CONDUCTIVITY	SPECIFIC HEAT	DENSITY	THERMAL INERTIA PARAMETER
	K (cal/cm-sec- $^{\circ}K$)	c_p (cal/gm- $^{\circ}K$)	ρ (gm/cm 3)	$(\frac{\rho c_p K}{2})^{-1/2}$ (cm 2 sec $^{1/2}$ $^{\circ}K$ /cal)
Basalt (solid)	0.0052	0.185	2.95	18.80
Limonite (powdery)	0.20×10^{-4}	0.15	2.0	409.0
Goethite	0.33×10^{-4}	0.173	2.7	255.0

The Martian surface temperature-time histories observed by Sinton and Strong [1] and Gifford [2] are summarized in Table 3. Sinton and Strong's temperature data were selected for comparison with the predicted temperatures because such data appeared to be better defined with regard to location and time period. The darklands and brightlands were both assumed to have an emissivity of 0.95. The albedo was assumed to be 0.17 for the darklands and 0.34 for the brightlands. Two types of surfaces were selected for the study of the diurnal temperature variations. The first type consists of a one-layer, homogeneous model of solid basalt and the second consists of a thin layer of powdery limonite over a homogeneous layer of solid basalt. To determine the effect of layer depth on the surface temperature prediction, two different limonite layer thicknesses (3.048 and 30.48 cm) were considered. The Martian surface temperature-time histories, which were predicted with these surface models for the latitude and time of the observations from [1], are presented in Figures 3 through 6. Observed temperature values of Sinton and Strong also are presented in these figures.

For the darklands, as indicated by curve A in Figures 3 and 4, the predicted diurnal temperatures based on the one-layer model are generally lower than those observed. For the two-layer model of the darklands (curves B and C in Figures 3 and 4), the predicted daylight temperatures are generally higher ($\sim 25^{\circ}K$) than the corresponding observed values. The two-layer model with the thicker limonite layer produced lower nocturnal temperatures than the model with the thinner limonite layer. Also, the predicted temperature profiles during daylight hours for the former lag behind the corresponding profiles for the latter. In general, the two-layer darklands model of limonite over basalt produced higher daylight and lower nocturnal temperatures than produced by the one-layer basalt model.

Table 3. OBSERVED MARTIAN SURFACE TEMPERATURE ($^{\circ}$ K) AS A FUNCTION OF MARTIAN LOCAL TIME

REFERENCE	DATE	PLANETO- GRAPHIC LATITUDE ($^{\circ}$)	MARTIAN LOCAL TIME								COMMENTS
			0700	0800	0900	1000	1100	1200	1300	1400	
1	7/20/54	-2	209	241	257	272	289	295	295	280	Bright & dark areas mixed
1	7/20/54	10	209	232	254	271	286	299	301	288	Almost all in bright areas
1	7/21/54	8	219	238	262	271	291	299	296	293	Almost all in bright areas
1	7/23/54	14	195	227	252	273	283	289	287	281	Bright & dark areas mixed
1	7/23/54	-12	231	241	267	281	291	291	291	281	All in dark areas
1	7/23/54	-8	218	234	263	282	292	293	293	287	All in dark areas
2	10/25/26 & 12/10/28	0	---	240	252	261	269	275	279	279	Bright & dark areas mixed & averaged for two dates

A = ONE-LAYER MODEL
 B = TWO-LAYER MODEL DEPTH OF TOP LAYER = 3.048 CM
 C = TWO-LAYER MODEL DEPTH OF TOP LAYER = 30.48 CM
 Δ = OBSERVED TEMPERATURES FROM REF. 1

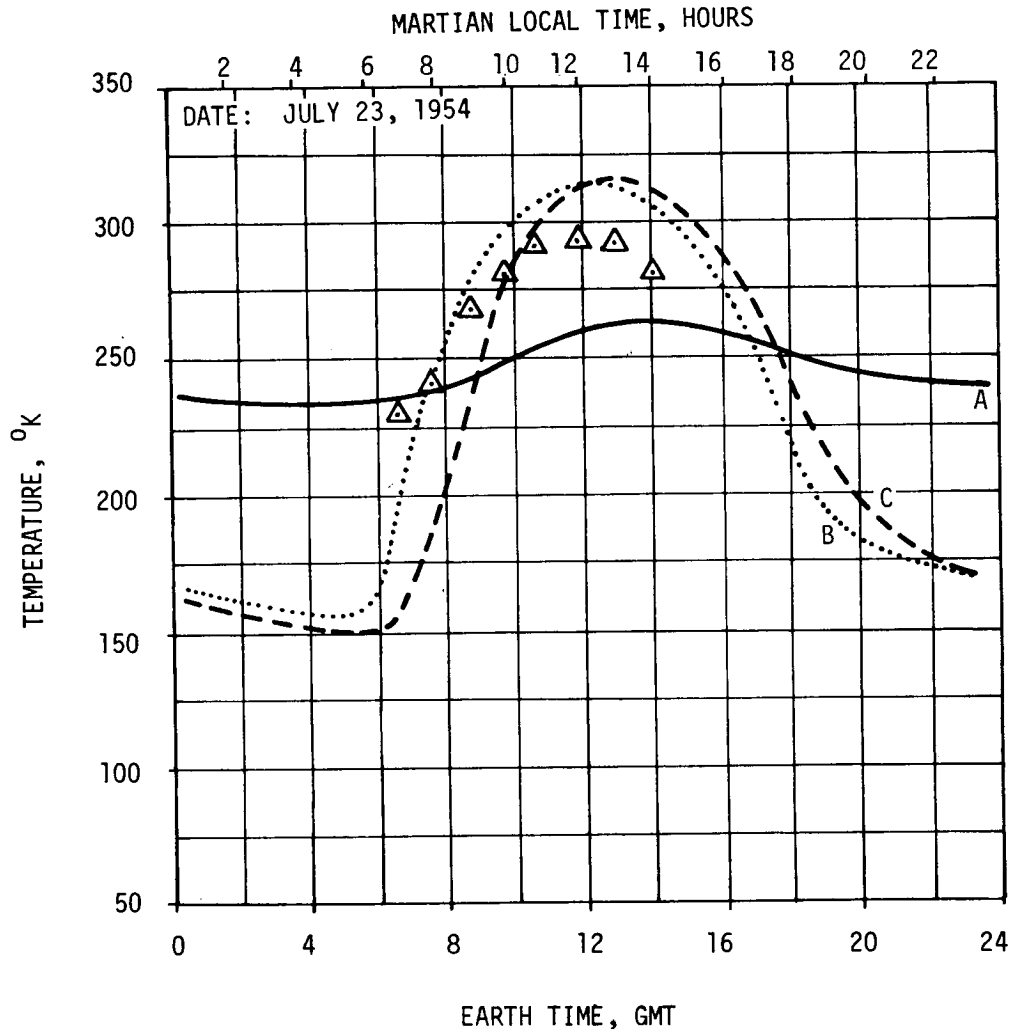


Figure 3. MARTIAN DARKLAND SURFACE TEMPERATURE-TIME HISTORY FOR A LATITUDE OF -12°

A = ONE-LAYER MODEL
 B = TWO-LAYER MODEL DEPTH OF TOP LAYER = 3.048 CM
 C = TWO-LAYER MODEL DEPTH OF TOP LAYER = 30.48 CM
 Δ = OBSERVED TEMPERATURES FROM REF. 1

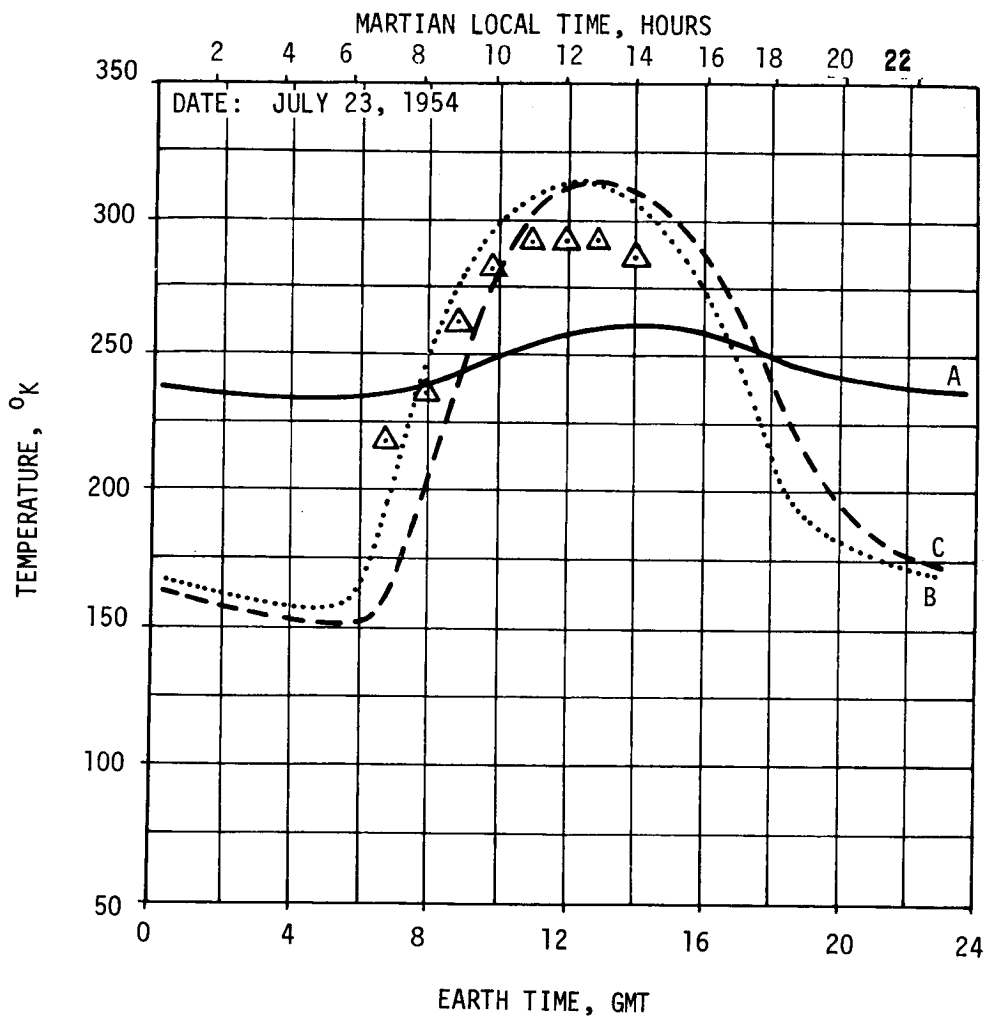


Figure 4. MARTIAN DARKLAND SURFACE TEMPERATURE-TIME HISTORY FOR A LATITUDE OF -8°

For the brightlands, curves A of Figures 5 and 6 indicate that the one-layer model produced daylight temperature profiles which are, in general, lower than the corresponding observed profiles. The predicted daylight temperatures, based on the two-layer model (curves B and C of Figures 5 and 6), appear in good agreement with the observed temperatures. As was the case with the darklands, the brightlands model with thicker limonite layer produced temperature profiles that are lower at night, and during the day lag behind the corresponding profiles generated by the model with the thinner limonite layer.

The two-layer brightlands model of limonite over basalt produced lower temperatures at night and higher temperatures during the day than produced by the one-layer basalt model. The two-layer model with the thinner limonite layer produced daylight temperature profiles which are in closest agreement with the observed profiles for the brightlands.

For both the brightlands and darklands, the two-layer model generally proved more satisfactory. Thus, this model appears most suitable for establishing the effect of the Martian atmosphere on the surface temperature.

Although no nocturnal temperature observations are available, extrapolation of the temperature observations during the morning indicates that the Martian nocturnal surface temperature should be $\sim 200^{\circ}\text{K}$ near the equator. This is 40 to 50°K above the nocturnal temperatures predicted by the two-layer model for either the brightlands or darklands. This temperature difference indicates that the Martian atmosphere has a strong "greenhouse" effect on the Martian nocturnal temperature. As already noted, based on the two-layer model, the predicted daylight temperatures for the darklands were $\sim 25^{\circ}\text{K}$ above the observed, while, for the brightlands, good agreement between observation and prediction was obtained. Based on an understanding of the underlying thermodynamic considerations, these results would indicate that the atmospheric effects on the surface temperatures are not as strong during the day as during the night. In addition, the atmosphere possibly has a stronger influence on the temperature of the darklands than the brightlands.

IV. CONCLUSIONS

The feasibility of an analytical model for locating the Martian subsolar point and predicting the temperature-time history of the Martian surface with reasonable accuracy in terms of Earth time has been demonstrated. The current model can accurately locate the subsolar point and can produce reasonable diurnal temperature predictions based on the two-layer concept. During the Martian night, using the two-layer model, the predicted temperatures appear considerably lower than the actual values. Atmospheric effects appears to be the cause for such a difference.

The present analytical model, modified to take into account atmospheric effects, should be capable of predicting the Martian surface temperature-time histories with a significant improvement in accuracy. Such a modified analytical model could then be used, in a manner similar to that described in [18], to predict the thermal environment which a spacecraft on or near the Martian surface would experience.

A = ONE-LAYER MODEL
 B = TWO-LAYER MODEL DEPTH OF TOP LAYER = 3.048 CM
 C = TWO-LAYER MODEL DEPTH OF TOP LAYER = 30.48 CM
 Δ = OBSERVED TEMPERATURES FROM REF. 1

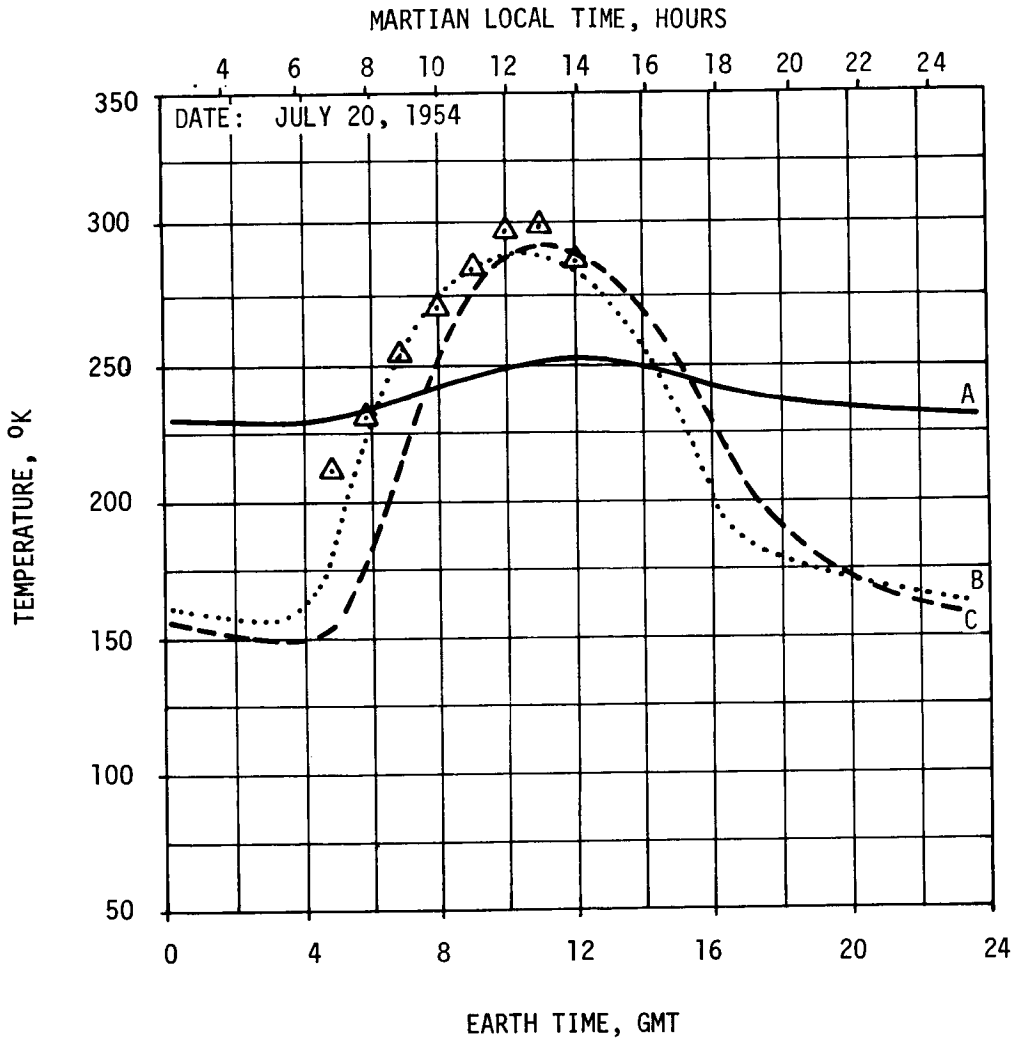


Figure 5. MARTIAN BRIGHTLAND SURFACE TEMPERATURE-TIME HISTORY FOR A LATITUDE OF + 10°

A = ONE-LAYER MODEL
 B = TWO-LAYER MODEL DEPTH OF TOP LAYER = 3.048 CM
 C = TWO-LAYER MODEL DEPTH OF TOP LAYER = 30.48 CM
 Δ = OBSERVED TEMPERATURES FROM REF. 1

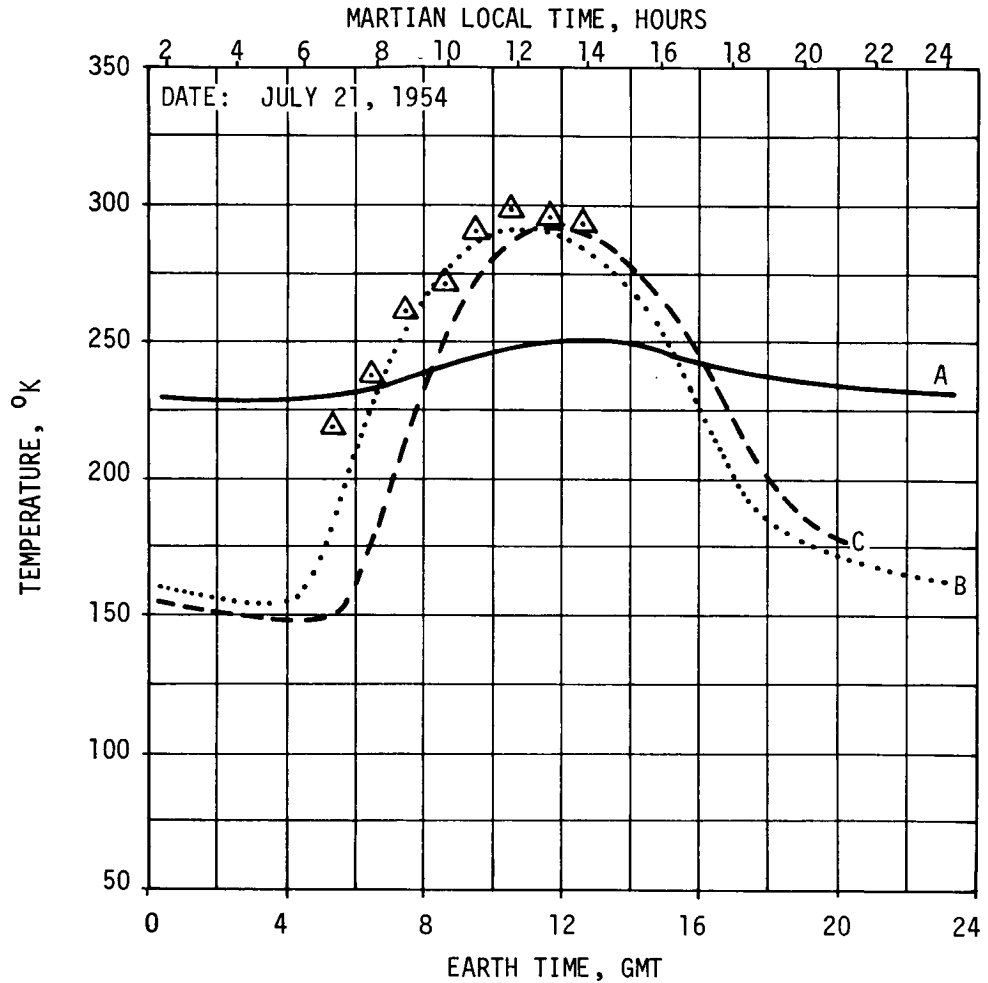


Figure 6. MARTIAN BRIGHTLAND SURFACE TEMPERATURE-TIME HISTORY FOR A LATITUDE OF +8°

REFERENCES

1. Sinton, W. M. and Strong, J. S., "Radiometric Observations of Mars," Astrophysics Journal, Vol. 131, 1960, pp. 459-469.
2. Gifford, Frank, "The Surface-Temperature Climate of Mars," The Astrophysical Journal, Vol. 123, January-May 1956, p. 154.
3. Giordmaine, J. A., et al., "Observations of Jupiter and Mars at 3-CM Wavelength," The Astronomical Journal, Vol. 64, No. 1273, p. 332.
4. Öpik, Ernst, "The Martian Surface," Science, Vol. 153, No. 3733, July 1966, p. 255.
5. Leovy, C. B., "Radiative-Convective Equilibrium Calculations for a Two-Layer Mars Atmosphere," The Rand Corporation, Memorandum No. RM-S017, May 1966.
6. Leighton, R. B. and Murray, B. C., "Behavior of Carbon Dioxide and Other Volatiles on Mars," Science, Vol. 153, pp. 136-144.
7. Kachur, V., "Thermology of the Martian Surface," AIAA Paper No. 66-436, AIAA 4th Aerospace Sciences Meeting, Los Angeles, California, June 27-29, 1966.
8. Leovy, C., "Note on Thermal Properties of Mars," Icarus, Vol. 5, 1966, pp. 1-6.
9. The Handbook of the British Astronomical Association for the Year 1960, British Astronomical Association, Sussex, England, November 1959.
10. Explanatory Supplement to the Ephemeris, Her Majesty's Stationery Office, London, 1960.
11. The American Ephemeris and Nautical Almanac for the Year 1954, U. S. Government Printing Office, Washington, D. C., 1963.
12. Blance, V. M. and McCuskey, S. W., Basic Physics of the Solar System, Addison-Wesley Publishing Company, Inc., Reading, Massachusetts, 1961.
13. Smart, W. M., Text-Book on Spherical Astronomy, Fourth Edition, Cambridge University Press, London, 1960.
14. Deshpande, P. B., "Determination of the Subsolar Point on Mars and Prediction of Martian Seasons in Terms of Earth Dates," Nortronics-Huntsville Technical Report No. TR-792-7-242, Huntsville, Alabama, September 1967.
15. Tatom, F. B., Ramakrishna, K. B., and Vaughan, O. H., "Prediction of the Lunar Thermal Environment," Session I, Paper No. 4, American Astronautical Society Southeastern Symposium on Missiles and Aerospace Vehicles Sciences, 4-7 December 1966, Huntsville, Alabama.

16. Dusenberre, G. M., Heat Transfer Calculations by Finite Differences, International Textbook Company, Scranton, Pennsylvania, 1961.
17. Blair, J. T., Lucas, W. C., Stanley, J. T., and Tatom, F. B., "Analytical Model of the Martian Surface," Northrop Huntsville Technical Report, March 1967.
18. Tatom, F. B., Ramakrishna, K. V., and Vaughan, Otha H., "Study of the Lunar Thermal Environment," Paper No. EN-6, American Astronautical Society 1967 National Symposium, 'Saturn V/Apollo and Beyond,' Huntsville, Alabama, 11-14 June 1967.

THE MSFC PLANETARY ATMOSPHERE COMPUTER PROGRAM

by

John Chambers¹ and Ed Seely²

SUMMARY

N68-18841

The MSFC Planetary Atmosphere Computer Program contains the exact equations and most refined techniques necessary to the development of planetary atmospheric models. All of the atmospheric parameters that are essential to spacecraft design studies and aerospace operations are output in tabular form from the surface to an altitude where the planetary atmosphere may be taken to be the same as interplanetary space. This program is on file in the MSFC Computation Laboratory.

I. INTRODUCTION

Accuracy and versatility have been emphasized in the development of the MSFC Planetary Atmosphere Computer Program. Atmospheric pressures are computed from the exact hydrostatic equation without constant molecular weight or isothermal temperature assumptions. A high degree of versatility in the application of the computer program is maintained by inputting all constants that are descriptive of an individual planet. The program may be used in the development of an atmospheric model for any planet, including the earth.

The program, written in the Extended ALGOL programming language for the Burrough's B-5500 computer, will process multiple cases of data with output on printer and SC 4020 plotter. The printing increment may be varied at the discretion of the operator.

¹Computer Sciences Corp., Huntsville, Alabama.

²Computation Laboratory, MSFC, Huntsville, Alabama.

II. DEFINITION OF SYMBOLS

<u>Symbol</u>	<u>Definition</u>
C_s	speed of sound
CF	collision frequency
CV	coefficient of viscosity
G	gravity
H	geopotential height
J	= dM/dH , molecular weight vertical gradient
K	Boltzman's constant
L_K	= dT_K/dH , kinetic temperature lapse rate
L_M	= dT_M/dH , molecular temperature lapse rate
M	molecular weight
MFP	mean atmospheric free path
N	Avogadro's number
ND	number density
P	atmospheric pressure
PS_P	most probable air-particle speed
PS_M	mean air-particle speed
R	radius of planet
R^*	universal gas constant
SH_P	pressure scale height
SH_d	density scale height
T_K	kinetic temperature

<u>Symbol</u>	<u>Definition</u>
T_M	molecular temperature
Z	geometric altitude
ρ	atmospheric density
β, S	Sutherland's constants
σ	effective collision diameter of mean air particle
γ	ratio of specific heats

Subscripts

n	denotes an input level
i	denotes a level of geometric altitude
j	denotes a level of geopotential height

III. COMPUTATIONAL PROCEDURE

This section outlines the computational procedure¹ used in developing the computer program and provides the analytical equations.

A. Input Data

1. Kinetic temperature at geopotential height levels.
2. Molecular weight at geopotential height levels.
3. Surface pressure.

¹The computational procedure used in the development of the computer program was taken from R-AERO-IN-5-67, "A Preliminary Summary of the MSFC Planetary Atmosphere Computer Program," by Don K. Weidner.

4. Surface kinetic temperature.
5. Surface molecular weight.
6. Surface gravity.
7. Planet radius.
8. Universal gas constant.
9. Sutherland's constant.
10. Boltzman's constant.
11. Avogadro's number.
12. Effective collision diameter of mean air particle.
13. Ratio of specific heats.

B. Computations at Geopotential Height Levels

1. Kinetic Temperature Lapse Rates

$$L_K = \frac{dT_K}{dH} = \frac{(T_K)_n - (T_K)_{n+1}}{H_{n+1} - H_n} \quad (1)$$

where n = input levels in geop. km.

2. Molecular Weight Lapse Rates

$$J = \frac{dM}{dH} = \frac{M_n - M_{n+1}}{H_{n+1} - H_n} \quad (2)$$

where n = input levels in geop. km.

3. Kinetic Temperatures

Kinetic temperatures are computed for each km from 1 to 1000 km geopotential height from the surface temperature (T_0) and the computed lapse rate (L_K).

4. Molecular Weight

Molecular weight values are computed for each km from 1 to 1000 km geopotential height from the surface molecular weight (M_0) and computed molecular weight lapse rate (J).

5. Molecular Temperatures

Molecular temperatures are computed for each km from 0 to 1000 km geopotential height.

$$(T_M)_j = \frac{(T_K)_j M_0}{M_j} \quad (3)$$

6. Molecular Temperature Lapse Rate

$$(L_M)_{j-1 \text{ to } j} = \frac{(T_M)_{j-1} - (T_M)_j}{H_j - H_{j-1}} \quad (4)$$

$$j = 1, 2, 3, \dots, 999, 1000$$

$$(T_M)_{j-1} = (T_M)_0 \text{ for first computation.}$$

7. Atmospheric Pressure (see Appendix)

a. If $L_M \neq 0$,

$$P_j = P_{j-1} \left[\frac{(T_M)_{j-1}}{(T_M)_j} \right]^{\frac{M_0 G_0}{R^* (L_M)_{j-1 \text{ to } j}}} \quad (5)$$

where $P_{j-1} = P_0$ for first computation.

b. If $L_M = 0$,

$$P_j = P_{j-1} \exp \left[\frac{-M_0 G_0 (H_j - H_{j-1})}{R^* (T_M)_j} \right] \quad (6)$$

C. Computations for Each Km from 0 to 1000 Km Geometric Altitude

1. Geometric Altitude

$$Z_i = \frac{RH_i}{R - H_i} \quad (7)$$

2. Atmospheric Pressure

Using pressure values (P_j) computed at geopotential height levels by equations (5) and (6), atmospheric pressures are interpolated logarithmically for each kilometer of geometric altitude and denoted as $(P)_i$.

3. Kinetic Temperature

Using kinetic temperatures $(T_K)_j$ computed at geopotential height levels, kinetic temperatures are interpolated for each km of geometric altitude and denoted as $(T_K)_i$.

4. Molecular Weight

Molecular weight values are similarly interpolated for each km of geometric altitude and denoted by M_i .

5. Molecular Temperature

$$(T_M)_i = \frac{(T_K)_i M_o}{M_i} \quad (8)$$

6. Atmospheric Density

$$\rho_i = \frac{M_o P_i}{R^* (T_M)_i} \quad (9)$$

7. Gravity

$$G_i = G_o \left[\frac{R}{R + (Z)_i} \right]^2 \quad (10)$$

8. Pressure Scale Height

$$SH_P = \frac{R^*(T_M)_i}{M_o G_i} . \quad (11)$$

9. Density Scale Height

$$SH_d = \frac{(SH_P)_i}{1 + \frac{R^*}{M_o G_i} (dT_M/dZ)_i} \quad (12)$$

where

$$(dT_M/dZ)_i = \frac{(T_M)_{i-1} - (T_M)_{i+1}}{Z_{i+1} - Z_{i-1}} . \quad (13)$$

10. Number Density

$$(ND)_i = \frac{M_o N P_i}{R^* M_i (T_M)_i} . \quad (14)$$

11. Most Probable Air-Particle Speed

$$PS_P = \left[2 \frac{R^*}{M_o} (T_M)_i \right]^{1/2} . \quad (15)$$

12. Mean Air-Particle Speed

$$PS_M = \left[\frac{8}{\pi} \frac{R^*}{M_o} (T_M)_i \right]^{1/2} . \quad (16)$$

13. Atmospheric Mean Free Path

$$(\text{MFP})_i = \frac{R^*(M)_i (T_M)_i}{\sqrt{2} \pi N \sigma^2 M_O (P)_i} \quad (17)$$

14. Collision Frequency

$$(\text{CF})_i = \frac{(PS_M)_i}{(\text{MFP})_i} \quad (18)$$

15. Speed of Sound

$$(C_s)_i = \left[\gamma \frac{R^*}{M_O} (T_M)_i \right]^{1/2} \quad (19)$$

16. Coefficient of Viscosity

$$(\text{CV})_i = \frac{(T_K)_i^{3/2}}{(T_K)_i + S} \quad (20)$$

IV. PROGRAM DESCRIPTION

After the input data are read into the program, they are printed out in such a form that it may be checked for possible key punch errors. Once the data are printed, the lapse rates of kinetic temperature and molecular weight are computed from the first two end points of kinetic temperature and molecular weight. In the atmospheric layer described by the lapse rates just calculated, the various atmospheric parameters are computed at the geopotential height increments

specified in the input data. Once the top of this atmospheric layer is reached, lapse rates of kinetic temperature and molecular weight are calculated for the next higher layer, and the various parameters are computed in that layer. This process continues until the top of the atmosphere, as specified by the last end point of kinetic temperature and molecular weight, is reached. When this occurs, the results are printed in increments specified in the input data set.

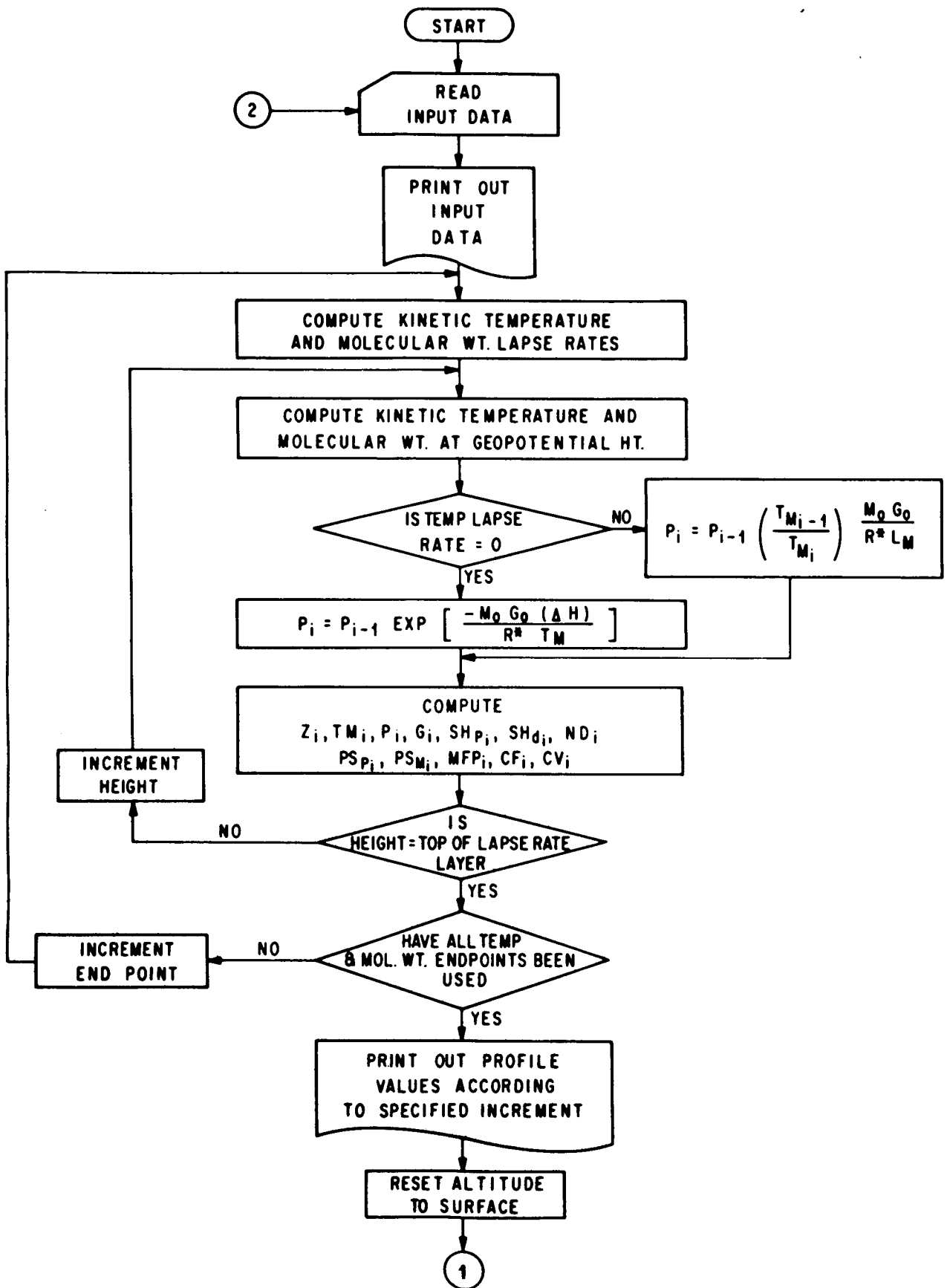
After the atmospheric parameters at geopotential height levels are printed, values of kinetic temperature, molecular weight and the natural logarithm of pressure are interpolated for geometric altitude from their corresponding values at geopotential heights. The remaining atmospheric parameters are calculated from these interpolated pressure, kinetic temperature, and molecular weight values.

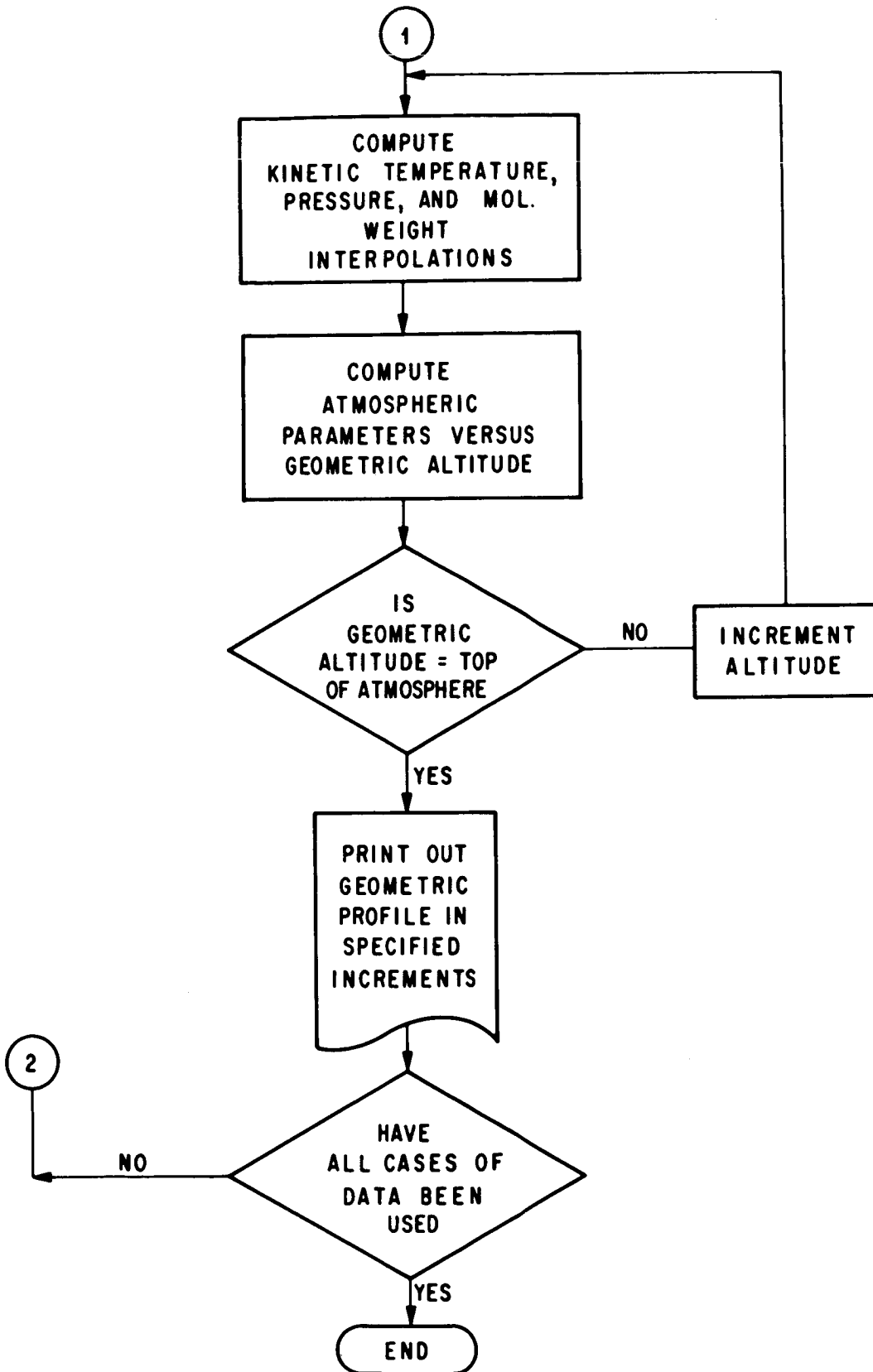
After the atmospheric parameters at geometric altitude increments are calculated to the top of the atmosphere, they are printed in the specified altitude increments.

At this point one case of data has been processed. If more cases of data are to be processed, then the entire calculation and printing procedure begins again at the start of the program until all cases of data have been processed.

V. PROGRAM FLOW DIAGRAM

The following generalized diagram depicts the order in which the program computes and prints the various atmospheric parameters.





FLOW CHART (Continued)

MARTIAN ATMOSPHERIC MODELS

by

Don K. Weidner

Aerospace Environment Division
Aero-Astroynamics Laboratory
George C. Marshall Space Flight Center
Huntsville, Alabama

N68-18842

SUMMARY

This paper presents a mean model of the Martian atmosphere and an envelope of extreme atmospheric density that have been developed for use in the design of spacecraft and planning of future Mars missions. The models are based upon the results of various theoretical studies and available literature.

I. INTRODUCTION

A model of the mean Martian atmosphere and an envelope which represents the extreme variability of the Martian atmospheric density have been developed for the design of spacecraft and planning of future Mars missions. In developing this model and extreme envelope, an extensive literature search was made for information related to the Mars atmosphere, and detailed parametric studies were conducted to establish the sensitivity of atmospheric density computations to the various input parameters such as atmospheric temperature and molecular weight and surface pressure. Additional studies were made concerning (1) the various interpretations of Mariner IV data, (2) the diffusion and possible escape of the Martian exospheric constituents, (3) the relationship of temperature and exospheric constituent distribution, (4) the probability of space plasma and Martian exospheric mixing and (5) the dependency of exospheric temperature on solar flux and sunspot cycle.

II. BASIC DATA

Results of these studies and information obtained from the literature search were used to idealize the temperature and molecular weight, versus geopotential height, profiles illustrated in figures 1 and 2, respectively.

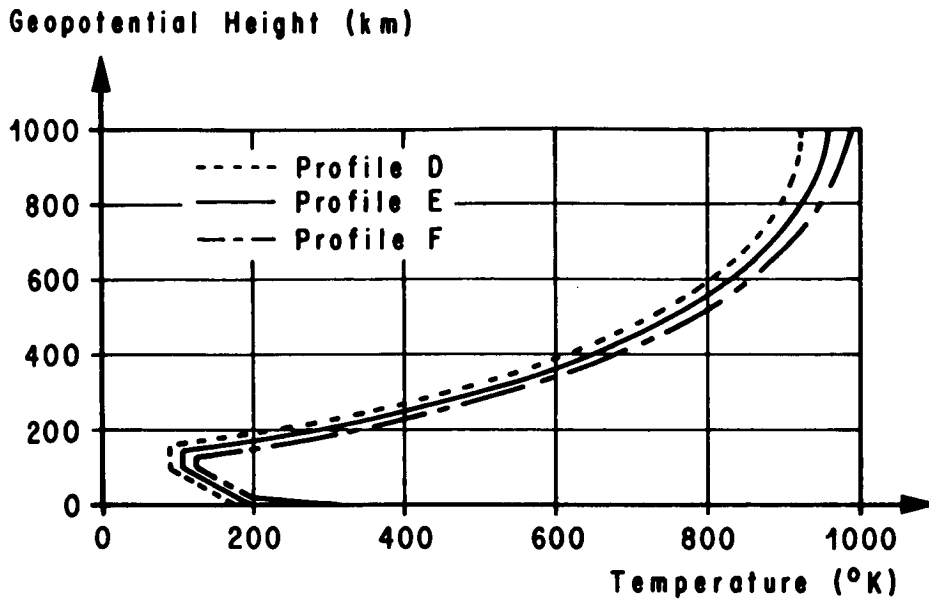


Figure 1. Idealized Martian Atmospheric Temperature Profiles

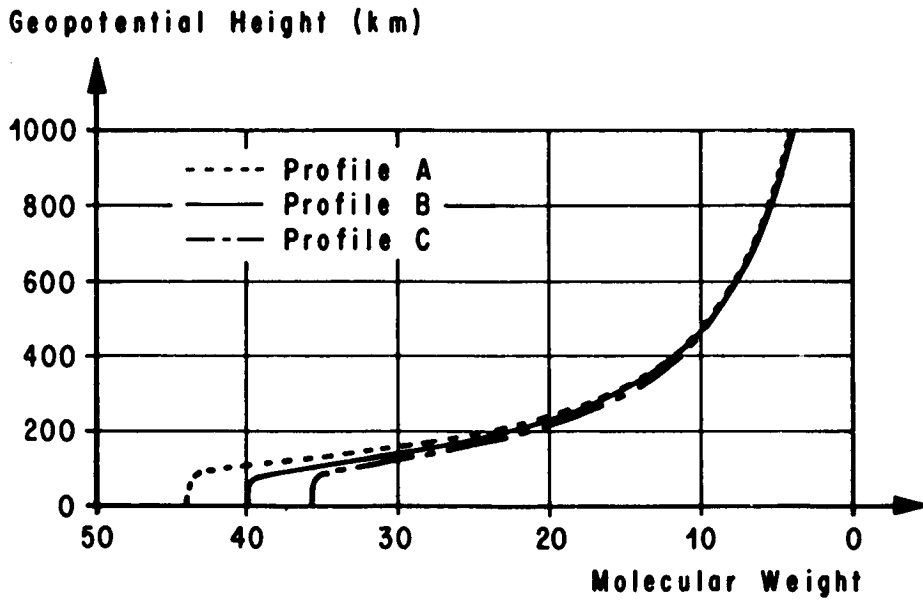


Figure 2. Idealized Martian Atmospheric Molecular Weight Profiles

The lower atmospheric temperatures are very similar to those of Fjeldbo, et al. [1] and Johnson [2] and are characteristic of an F₂ type ionospheric layer. This favoritism toward the F₂ type over Chamberlain's [3] E type ionospheric layer is due to the unreasonably high effective recombination coefficient necessary for the E type. However, information concerning the dissociative and recombination rates of the Martian atmospheric constituents is so limited that any concept of the Martian ionosphere must be considered speculative.

The Mariner IV occultation experiment and spectroscopic measurements have indicated the Martian atmosphere to be composed almost entirely of carbon dioxide. For the three models of this report, the composition has been taken to be 100 percent CO₂, 75 percent CO₂ and 25 percent N₂, and 48.8 percent CO₂ and 51.2 percent N₂ so that the extreme range of variability would be defined. A range of surface pressure values was likewise taken so that it would be representative of the total pressure variability.

III. ATMOSPHERIC MODELS

The atmospheric models given in this paper were generated by utilization of the MSFC Planetary Atmosphere Computer Program. This program, which is on file in the MSFC Computation Laboratory, contains the exact equations and most refined techniques necessary for the development of planetary atmospheric models.

A detailed parametric study revealed that the envelope of extreme density is greatest when the input parameters are combined in the following manner:

Mean Model

1. Temperature - Profile E (Figure 1)
2. Molecular weight - Profile B (Figure 2)
3. Surface pressure - 8.0 mb

Extreme Envelope

(Minimum model)

1. Temperature - Profile D (Figure 1)
2. Molecular weight - Profile A (Figure 2)
3. Surface pressure - 4.0 mb

(Maximum model)

1. Temperature - Profile F (Figure 1)
2. Molecular weight - Profile C (Figure 2)
3. Surface pressure - 10.0 mb

Atmospheric density profiles derived from these three sets of input data are illustrated in Figure 3. The mean density profile is thought to be representative of the mean Martian atmosphere, and it is anticipated that there is a 99 percent probability that any actual Martian atmospheric density profile would fall within the envelope defined by the maximum and minimum profiles.

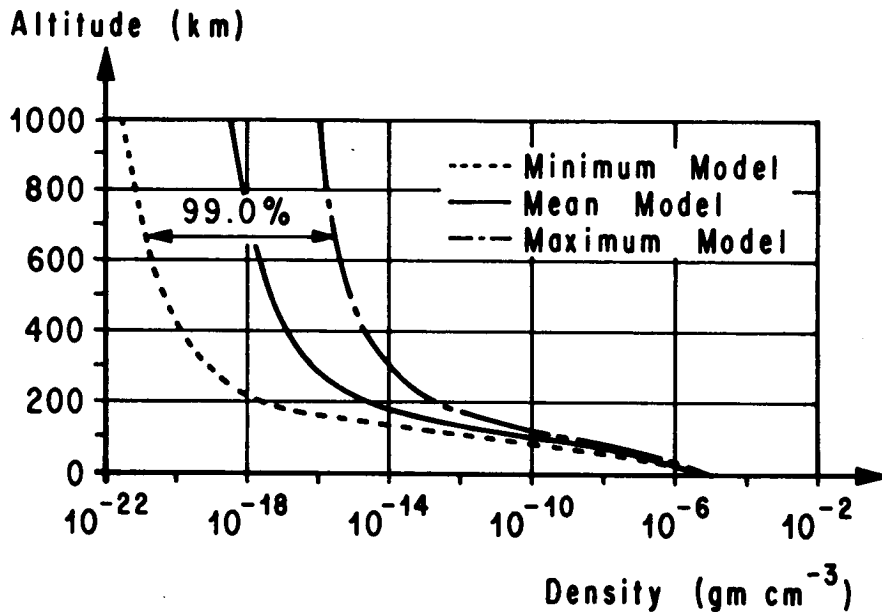


Figure 3. Martian Atmospheric Density

Because of a lack of information concerning chemical kinetics in the upper Martian atmosphere, a model of the atmospheric constituent distribution has not been established. However, using the mean number density profile and the idealized mean molecular weight profile, a plausible constituent distribution may be obtained as illustrated in Figure 4.

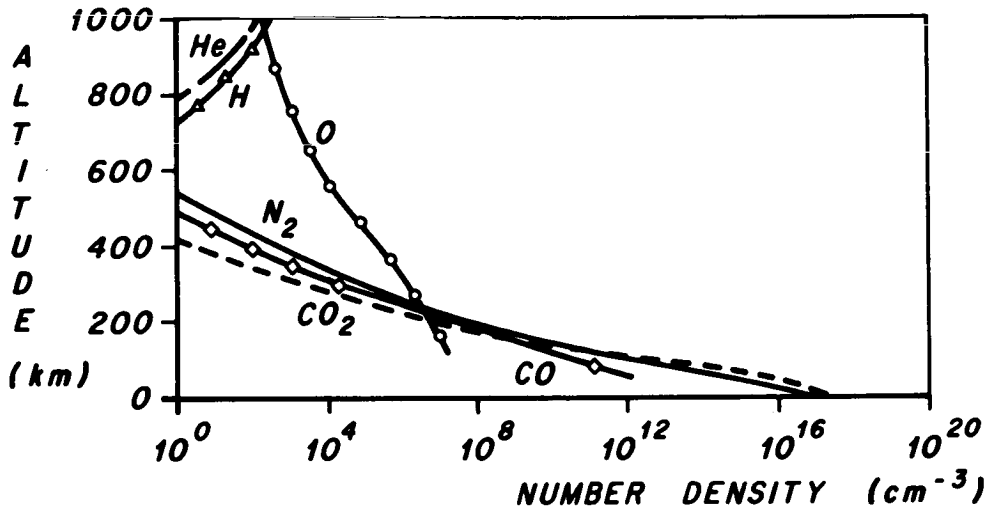


Figure 4. Martian Atmospheric Constituent Distribution

This distribution agrees very well with the models of Donahue [4] and Smith and Beutler [5] from 0 to 300 km altitude. The total number density also agrees with Donahue's model, but decreases much more rapidly than the model of Smith and Beutler above 100 km altitude.

IV. CONCLUSIONS

The models presented in this report must be classified as semi-empirical as they are based upon idealized temperature and molecular weight profiles. They are, however, thought to be the most accurate representations that can be established at this time.

More information concerning the Mars atmosphere is needed before highly reliable models may be established. Of particular interest would be information related to the Martian atmospheric processes, time constants for CO₂ sublimation, and dissociative and recombination rates for the Martian atmospheric constituents. Much of this information could be obtained from Martian atmospheric simulation experiments.

REFERENCES

1. Fjeldbo, G., W. C. Fjeldbo, and Von R. Eshleman, Atmosphere of Mars: Mariner IV Models Compared, Science, Vol. 153, 1518, September 1966.
2. Johnson, F. S., Atmosphere of Mars, Science, Vol. 150, 1445, December 1965.
3. Chamberlain, J. W. and M. B. McElroy, Martian Atmosphere: The Mariner IV Occultation Experiment, Science, Vol. 152, 21, April 1966
4. Donahue, T. M., Upper Atmosphere and Ionosphere of Mars, Science, Vol. 152, 763, 1966.
5. Smith, N., and A. Beutler, A Model Martian Atmosphere and Ionosphere, Report 66-3, University of Michigan, Ann Arbor, Michigan, March 1966.

OUTER ATMOSPHERE STRUCTURE OF MARS

By

Don Vachon and K. Lichtenfeld*

SUMMARY

N68-18843

Based on the Mariner IV ionospheric experiment data, the base of the thermosphere may be as low as 105 km. The thermal gradient is expected to range in value from 0.5 to 3.0 °K/km during periods of low to high solar activity, respectively. The MSFC maximum density envelope compares favorably with the maximum density profile from the VM3 extension, the MSFC density at 1000 km being less than one order of magnitude below the VM3 extended model value. The MSFC mean density profile compares favorably with the older GE Voyager reference atmosphere. The MSFC mean density profile and associated confidence envelopes were found to be consistent with most models presently available.

Estimates of the variations of the atmospheric structure as a function of solar activity were prepared and indicate:

- (a) The density at altitudes of about 1,000 kilometers is likely to exhibit a diurnal (day-night) variation of an order of magnitude.
- (b) The atmospheric density at 1,000 kilometers during a period of high solar activity is likely to be three orders of magnitude greater than it is during a period of low solar activity.
- (c) Solar cyclic variations of the atmosphere's density at 1,000 kilometers of five and six orders of magnitude are expected to result more from uncertainties in the models than from probable variations of the atmosphere itself.
- (d) The MSFC mean-to-maximum density profiles appear reasonable for periods of high solar activity.

*The authors are associated with the General Electric Corp., Missile and Space Division, Valley Forge, Pa. This paper was prepared for MSFC under contract number NAS8-22603.

- (e) The MSFC mean-to-minimum density profiles appear adequate to define the density likely to be encountered during a period of moderate to low solar activity.

I. INTRODUCTION

The orbital lifetime of a body placed in orbit around Mars can be calculated by considering the atmospheric density likely to be experienced at orbital altitudes. Defining the density profile is somewhat of a problem, however, since it can be expected that the structure of the outer atmosphere will be greatly influenced by solar variations in much the same manner as the Earth's atmosphere. It is expected that the density at orbital altitudes will be greatest during periods of high solar activity, as is the case in the Earth's upper atmosphere. Thus, an estimate of the probable solar cyclic related variation of the upper atmosphere of Mars can be of assistance in reducing the uncertainty range of density variation likely to be experienced in any given year. In addition, such an estimate would provide a means of relating derived density profiles from fly-by experiments made at different periods of time.

This paper (1) provides a brief discussion of the probable time-space variations of the outer atmosphere of Mars, (2) presents several models of the outer atmosphere which have been developed, and (3) develops, by empirical means, a method of reducing density uncertainties associated with a given model by allowing for solar cyclic variations.

II. PREDICTED SOLAR FLUX

Before discussing the probable solar cyclic variations of the upper atmosphere of Mars, the probable variation of solar activity should be estimated. Of particular interest is the time variation of the 10.7 cm radiation flux for the years 1964, 1969, 1971, 1973, and 1975.

The predicted mean and extreme values of the 10.7 cm flux [3], together with the observed mean and extreme values for 1964, are given in table I.

From the values given in table I, it is seen that the Mariner IV fly-by occurred during a period of low solar activity, while the Mars '69 fly-by should occur during a period of high solar activity. Consequently, if the upper atmosphere of Mars behaves in a manner similar to the Earth's atmosphere, then the derived densities from the Mars '69 fly-by experiments should be considerably greater than those derived from the Mariner IV experiments.

TABLE I

Predicted Values of the 10.7 cm Flux
(in units of 10^{-22} watts/cm²)

<u>Year</u>	<u>Mean</u>	<u>Extreme</u>
1964	70	75 - 85
1969	205 - 225	280 - 310
1971	150 - 160	205 - 225
1973	110 - 135	140 - 175
1975	70 - 80	85 - 110

A period of relatively low solar activity is expected in 1973 with a minimum of activity occurring in 1976. Thus, it is likely that the atmospheric density encountered at orbital altitudes by the Voyager spacecraft in 1973 will be closer to that derived from the Mariner IV experiments than to that derived from the Mars '69 experiments. Significantly, the atmospheric densities derived from the Mars '69 experiments should provide a close estimate of the maximum density likely to be encountered in the upper atmosphere of Mars.

III. EXOSPHERE

A. Temperature Variation

The empirical relation between the exospheric temperature and solar activity [1] was found to be consistent with the temperature values derived from the Mariner IV data [12]. On the basis of this agreement, the empirical relation appears acceptable at this time. Data from the Mars '69 fly-by may provide an opportunity to check the relative validity of the relation for periods of high solar activity. For the present, it is assumed that the empirical relation will provide a reasonable estimate of the exospheric temperature variation as a function of solar activity.

The temperature minima (T_n) are taken to occur at 0400 while the maxima (T_x) occur at 1400 for any value of the 10.7 cm solar flux (S). The minima and maxima are obtained by the following formulation:

$$T_n = 1.94S + 275$$

$$T_x = 3.05S + 372,$$

where T_n and T_x are in degrees Kelvin, and the 10.7 cm solar flux is in units of 10^{-22} watts/m²-cps. The values of exospheric temperatures as a function of solar activity are given in Table II.

TABLE II

Martian Exospheric Temperature (°K) as a Function of the 10.7 cm Solar Flux (S)

T(°K)	Solar Flux (S)				
	70	100	150	200	250
Minima	411	469	566	663	760
Maxima	586	677	829	982	1134

B. Altitude of Exosphere Base

The base of the exosphere (i.e., top of the thermosphere) was initially proposed as a variable, dependent on the thermosphere thermal gradient and the exosphere temperature. More recent evaluations indicate that, for all practical purposes, the altitude of the base of the exosphere may be relatively constant in time, although intimately related to the selected values of the thermosphere thermal gradient. The Harris and Priester [5] temperature values at 420 kilometers are compared with the temperature value at 2000 kilometers, well within the Earth's exosphere, in Table III. It thus appears that the base of the exosphere is relatively insensitive to variations in solar activity. The base altitude of the Martian exosphere is intuitively expected to be lower than it is in the Earth's atmosphere. The upper atmosphere models presented by Hess and Pounder [6] would suggest an exosphere base altitude of 250 km. Similarly, the model of Smith and Beutler [9] would suggest an exosphere base altitude of about 340 kilometers.

TABLE III

Comparison of the Harris and Priester Model Temperatures
at 2000 km and 420 km

T(°K)	Solar Flux (S)				
	250	200	150	100	70
Minima					
2000 km	1392	1163	944	737	612
420 km	1383	1155	938	732	609
Maxima					
2000 km	2121	1768	1409	1046	827
420 km	2068	1739	1394	1039	822

The empirically derived base altitude of the exosphere will be discussed in Section IV since, as mentioned above, it is expected to be related to the selected values of the thermosphere thermal gradient.

IV. THERMOSPHERE

A. Altitude of Base

The atmosphere of Mars at high altitudes is expected to exhibit a region of temperature increase because of recombination heating. The altitude at which this heat source occurs has recently been estimated at about 90 kilometers, Gross, et al. [4], 100 km, Donahue [2], and < 140 km, Chamberlain and McElroy [1]. Based on our own evaluations of the Mariner IV data, Vachon [12], the base of the thermosphere was evaluated at about 103 kilometers. For our purposes, the base of the thermosphere is taken as being at an altitude of 100 kilometers. To simplify further calculations, it is assumed that conditions at 100 kilometers remain constant in time and space. Thus, we introduce a fixed boundary condition at 100 km, which contains all of the inherent limitations contained in the same assumption made in regard to the Earth's upper atmosphere; e.g., the density at the boundary altitude is held constant in time and space, although it is known to vary substantially. In the Harris and Priester model [5], it is found that a fixed boundary exists at an altitude of

120 kilometers. Considering that the Harris and Priester model provides a reasonable fit to the observed conditions at altitudes in excess of 200 kilometers, the assumption of a fixed boundary condition appears permissible as a means of developing models of the atmospheric structure above 200 kilometers for use in orbit decay evaluations.

B. Thermal Gradient

The thermal gradient in the thermosphere would be expected to be greatest near the base and to diminish with altitude. The magnitude of the gradient itself is dependent upon the chemical kinetics of the atmosphere. Although it is doubtful that one can use the thermal gradients of the Earth's atmosphere to derive the probable gradients in the Mars thermosphere, it would be interesting to compare such empirically derived values with those from existing models of the Mars upper atmosphere.

The intensity of solar radiation at the Mars orbital distance is about half that incident at the Earth's distance. Since the thermosphere is a byproduct of photodissociation or recombination, it will be assumed that the Mars thermosphere thermal gradients are equal to half the value of the Earth's thermosphere thermal gradients. This is an admittedly crude assumption for it totally neglects the differences in the chemical kinetics of the two atmospheres. The thermal gradients for three selected altitude intervals, as well as the equivalent over the three intervals, are given in Table IV for the Earth, and in Table V for Mars as a function of solar activity.

The values presented in Table V show that the estimates of the altitude variation of the Mars thermal gradients, based on values for the Earth's atmosphere, decrease much more rapidly than those used in Mars atmosphere models. However, based on our own evaluation of the Mariner IV data, Vachon [12], the thermal gradient over the altitude range of 105 to 138 kilometers, during a period of low solar activity, was found to lie within the limits of 1 ± 0.5 °K/km.

From the viewpoint of establishing empirical relationships, it would appear more prudent at this time to use only the integrated gradient values between 400 and 100 kilometers. Since the integrated thermal gradients obtained from evaluations of the chemical kinetics, Smith and Beutler [9], are in reasonable agreement with the empirically derived values, the latter may then provide a relatively reasonable means of relating variations of the thermal gradients as a function of solar activity.

TABLE IV

Altitude Variation of the Thermal Gradient ($^{\circ}\text{K}/\text{km}$)
in the Earth's Thermosphere as a Function of Solar Activity

Altitude (km)	Solar Flux (S)				
	250	200	150	100	70
220 - 120					
Minima	8.72	6.83	4.94	3.13	2.06
Maxima	12.65	10.58	8.28	5.70	3.99
320 - 220					
Minima	1.32	0.98	0.74	0.53	0.40
Maxima	3.52	2.64	1.76	0.97	0.58
420 - 320					
Minima	0.24	0.19	0.15	0.11	0.08
Maxima	0.96	0.65	0.35	0.17	0.10
420 - 120					
Minima	3.42	2.67	1.94	1.26	0.85
Maxima	5.70	4.61	3.46	2.28	1.56

TABLE V

Altitude Variation of the Thermal Gradient ($^{\circ}\text{K}/\text{km}$)
in the Martian Thermosphere as a Function of Solar Activity

Altitude (km)	Solar Flux (S)						
	250	200	150	100	70	Smith/ Beutler [9]	Weidner/ Hasselstine [15]
200 - 100							
Minima	4.36	3.42	2.47	1.56	1.03	2.40	2.84*
Maxima	6.33	5.29	4.14	2.85	2.00	2.40	2.84*
300 - 200							
Minima	0.66	0.49	0.37	0.27	0.20	1.06	1.02
Maxima	1.76	1.32	0.88	0.49	0.29	1.06	1.02
400 - 300							
Minima	0.12	0.09	0.07	0.06	0.04	0.28	1.36
Maxima	0.48	0.31	0.17	0.09	0.05	0.28	1.36
400 - 100							
Minima	1.71	1.33	0.97	0.63	0.42	1.27	1.63
Maxima	2.85	2.30	1.73	1.14	0.78	1.27	1.63

* Gradient value given is for an altitude interval of 200-150 km.

C. Altitude of Top of Thermosphere

As mentioned in section III, the altitude of the top of the thermosphere (i.e., base of the exosphere) is expected to be relatively constant. However, if one uses the integrated thermal gradients of section IV, together with the exospheric temperature values of section III and a fixed boundary at the base of the thermosphere, then it is found that the altitude of the base of the exosphere must vary. Thus, it is found that either the altitude of the top of the thermosphere must be made variable or the integrated thermal gradients must be changed to fit the condition of a fixed base altitude for the exosphere. Since the thermal gradients are dependent upon the chemical kinetics of the atmosphere, which were largely ignored, it is felt that modifying the gradient values would be better than introducing a variable exosphere base altitude. Using the integrated gradient values from Table V, together with the exosphere temperature from Table II, the lowest altitude of the exosphere (460 km) was found to be associated with the highest integrated thermal gradient ($2.85 \text{ }^\circ\text{K/km}$), and the highest exosphere temperature ($1134 \text{ }^\circ\text{K}$). Since it is doubtful that the exosphere temperature could be this high, and that the integrated thermal gradient is itself much higher than the Smith and Beutler [9] value based on evaluation of the chemical kinetics, it was decided to reject this condition as the basis for scaling. The next lowest altitude of the exosphere (482 km) was found to be associated with an integrated thermal gradient of $1.7 \text{ }^\circ\text{K/km}$, and an exosphere temperature of $760 \text{ }^\circ\text{K}$. The relative agreement between the integrated gradient of this case and the model of Weidner and Hasseltine [15] was taken as a favorable aspect, since their model is based in part on an evaluation of the chemical kinetics. Further, the exosphere temperature value of $760 \text{ }^\circ\text{K}$ is now out of accord with most studies of the chemical kinetics of the Mars upper atmosphere. Although intuitively the top of the thermosphere is expected to be lower than it is in the Earth's atmosphere, for the present it is assumed that the top of the thermosphere on Mars is at an altitude of 482 kilometers.

The introduction of a fixed altitude for the top of the thermosphere, with a fixed boundary at 100 kilometers and for the given exospheric temperatures, requires a change in the integrated thermal gradient values. The integrated thermal gradient values for a variable exosphere altitude and for a fixed exosphere altitude are given in table VI.

TABLE VI

Integrated Thermal Gradients ($^{\circ}\text{K}/\text{km}$) in the
Martian Thermosphere as a Function of Solar Activity

T($^{\circ}\text{K}$)	Solar Flux (S)				
	250	200	150	100	70
Variable Exosphere					
Minima	1.71	1.33	0.97	0.63	0.42
Maxima	2.85	2.30	1.73	1.14	0.78
Fixed Exosphere					
Minima	1.71	1.46	1.20	0.95	0.80
Maxima	2.69	2.29	1.89	1.49	1.26

V. OUTER ATMOSPHERE MODELS

Several models of the outer atmosphere of Mars have been developed in the past year and used in orbital lifetime and planetary quarantine studies. The first of these, identified as the VM-3 extension, is an empirical model intended as an estimate of the maximum density likely to be encountered at orbital altitudes. The second, identified as the GE Voyager reference atmosphere, is based on a theoretical model which represented the mean atmospheric structure consistent with the Mariner IV fly-by results. The third, identified as the MSFC model, is a semi-empirical model which provides a preliminary estimate of the mean density profile and associated confidence envelopes.

A. VM-3 Model Extension

The probable characteristics of the thermosphere and exosphere of Mars were used in extending the VM-3 model atmosphere, Vachon [12]. Because the main purpose of the model was to provide an estimate of the maximum density likely at orbital altitudes, the VM-3 model atmosphere was selected for extension, since it provided the highest density at altitudes of 100 kilometers.

The VM-3 atmosphere density profile was extended as follows:

1. The altitude of the base of the thermosphere was taken as equal to 103 kilometers.
2. The solar flux index was taken as 250 units.
3. The thermal gradient in the thermosphere was taken as 1°K/km for the night side and 1.5 °K/km for the day side.
4. The exosphere temperature was taken as 760 °K on the night side and 1134 °K on the day side.
5. The molecular weight was assumed constant with altitude. In testing the influence of molecular weight variations, the molecular weight above 103 kilometers was assumed to decrease by one-half its value below 103 kilometers. This latter condition resulted in a four-order-of-magnitude increase in the density at 1,000 kilometers.
6. The density of interplanetary space during high solar activity was assumed to be on the order of 10^{-21} to 10^{-22} gms/cc.
7. To simplify the calculations, the geopotential altitude concept was used; this resulted in reducing the thermal gradients cited above.

The density in the thermosphere was calculated by use of the following formula:

$$\rho = \rho_0 \left(\frac{T}{T_0} \right)^{- \left(1 + \frac{M_0 g_0}{R \, dT/dh} \right)}$$

The density in the exosphere was calculated by use of the more common exponential decay formula:

$$\rho = \rho_0 \exp \left[\left(- \frac{M_0 g_0}{RT} \right) h - h_0 \right]$$

The density at 1000 kilometers during a period of high solar activity was thus calculated as ranging from a diurnal minimum of 9×10^{-18} g/cc to a diurnal maximum of 3×10^{-15} g/cc. On the basis of the theoretical studies being performed at JPL, Newburn [8], the maximum density profile

appeared quite conservative. Indeed, the maximum exosphere temperature consistent with Gunn's model (of JPL) is 700 °K as compared with our empirically derived value of 760 to 1134°K for periods of high solar activity.

Thus, the VM-3 model extension, daytime density profile, is expected to represent what should prove to be a very conservative density profile.

B. GE Voyager Reference Atmosphere

The description of the Martian upper atmosphere recently provided by Hess and Pounder [6] was used as the basis for a proposed Voyager Mars reference atmosphere [13]. The reference atmosphere was intended not as an extreme atmosphere model, but rather as a probable mean.

To provide a complete profile of the atmospheric structure up to 900 kilometers, the upper limit of figure 9 in Hess and Pounder [6], it was necessary to extrapolate the data downward below 100 kilometers. The assumptions made in extrapolating the JPL model downward were discussed with D. Spencer of JPL [10] and are considered reasonable. The following approach was used in extrapolating the JPL model downward.

The atmospheric structure between 100 and 900 kilometers is given in graphical form by Hess and Pounder [6] who provide (a) the number density of the various constituents, (b) the kinetic temperature up to 300 kilometers, and (c) the free electron concentration up to about 200 kilometers. The constituent number densities were obtained from figure 9 of reference 6 (Hess and Pounder) for altitude increments of 50 kilometers up to 300 kilometers, and thereafter at 100 kilometer intervals. The molecular weight and mass density were then calculated from the extracted values of number density. These latter values were in turn replotted and curve-fitted to obtain smooth profiles.

The temperature values were extracted from figure 9 of reference 6 for a number of altitude values required to closely fit the profile given.

The atmospheric structure below 100 kilometers consistent with the definition of the structure above 100 kilometers was quickly found not to fit any of the VM atmosphere models. Thus, in order to obtain a self-consistent model, it was necessary to extrapolate the atmosphere downward. The conditions at 100 kilometers obtained from figure 9 of reference 6 are

$$T = 150 \text{ }^\circ\text{K}; \quad \rho = 1.9 \times 10^{-10} \text{ g/cc}$$

$$M = 43 \text{ or } 44; \quad p = 5.4 \times 10^{-5} \text{ millibars.}$$

Assuming the surface temperature to be 275 °K (which corresponds to the value used in VM-1, 3, 5, 7, and 9) and the troposphere temperature gradient equal to the adiabatic, then for a CO₂ rich atmosphere with M = 44, dT/dZ equals to -5.39 °K/km. The tropopause is assumed to occur at an altitude where the temperature reaches a value of 150 °K (equal to the value at 100 km). The tropopause altitude is thus obtained as 23.2 kilometers. Using this temperature profile, extrapolating the pressure downward yields a surface pressure of 7.5 millibars.

The density values above 100 kilometers selected for this reference atmosphere are those which correspond to the model developed using an eddy diffusivity value of 10⁻³ km²/sec. This latter value corresponds to a diffusion time on the order of a few hours. This model was selected since it contains the higher densities of the two models given.

The vertical structure of this reference atmosphere is provided in figure 1 and includes the density values obtained directly from figure 9 of reference 6 (Hess and Pounder). The computer printout and associated automatic plots for the model are provided in milestone report VOY-D4-TM-4 by Vachon [13].

Comparing the density at 1000 kilometers obtained from this model ($\approx 2 \times 10^{-20}$ g/cc) with that obtained in the VM-3 extension (9×10^{-18} to 3×10^{-15} g/cc) shows that the VM-3 extension is indeed very conservative. However, since the reference model is not necessarily intended as

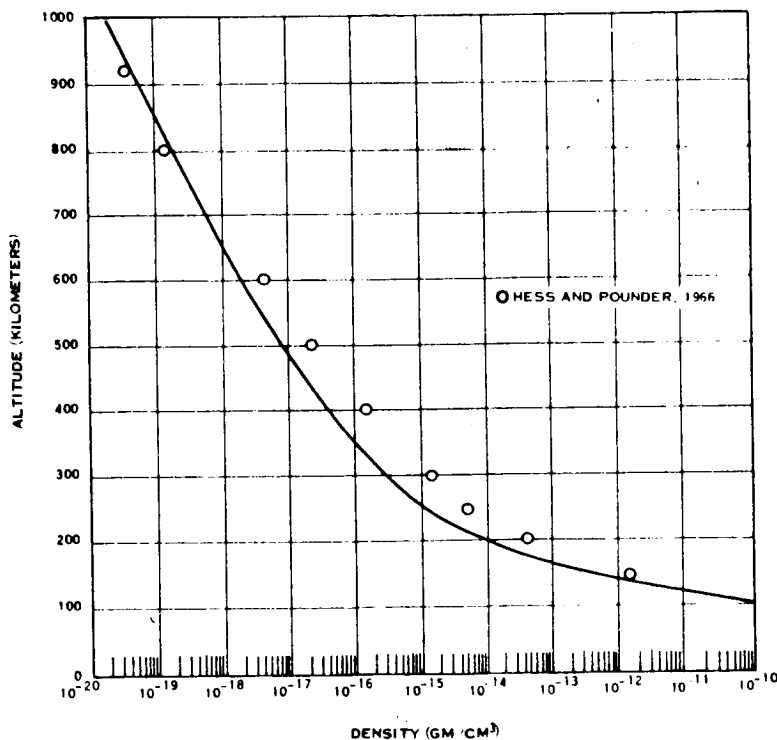


Figure 1. GE Voyage Reference Atmosphere Density Profile

a mean during periods of high solar activity, while the VM-3 extension is restricted to that period, comparisons between the two models require a degree of latitude.

C. MSFC Atmosphere Model

The MSFC mean model and 99 percent confidence envelopes for the Mars atmosphere, recently prepared by Weidner [4], contain the attractive feature of having a molecular weight variation with altitude (figure 2) which does not asymptote at 16 as in models based on the chemical kinetics of the Mars atmosphere. Although the minimum, mean, and maximum density models (figure 3) are semi-empirical, they appear reasonable at this time, pending further studies of the chemical kinetics of the upper atmosphere.

The mean atmosphere parameter values from Weidner [14] and from the GE Voyager reference atmosphere [13] are compared in table VII.

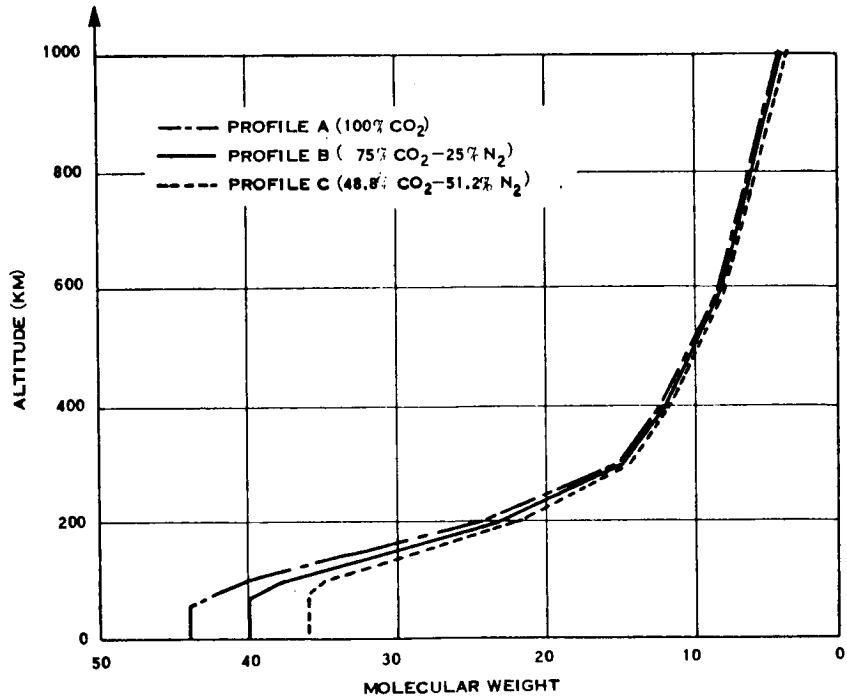


Figure 2. Idealized Martian Molecular Weight Profiles (from Weidner [14])

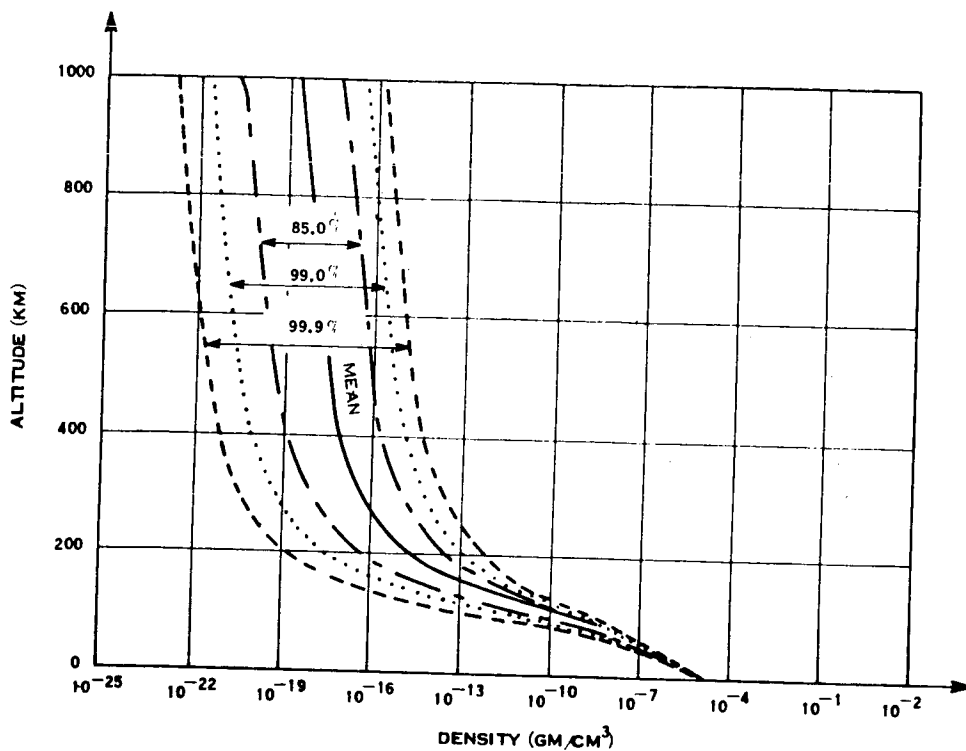


Figure 3. Preliminary Mean Profile and Confidence Envelopes for Martian Atmospheric Density (from Weidner [14])

TABLE VII

Comparison of Mean Atmosphere Parameter Values at 1000 Kilometers

Parameter	Weidner	GE Reference Atmosphere
Kinetic temperature (°K)	914	412
Pressure (dynes/cm ²)	7.7×10^{-9}	4.6×10^{-9}
Density (g/cc)	6×10^{-19}	2×10^{-20}
Molecular weight	5.9	16

The comparison of the parameter values indicates that, while the density values do not differ appreciably, there exists considerable conflict in the temperature and molecular weight values. Based on the theoretical studies of Gunn at JPL, it is unlikely that the kinetic temperature will exceed 700°K. On the other hand, it is intuitively unlikely that the molecular weight will asymptote at 16. Future studies of the chemical kinetics of the upper atmosphere which includes the probable concentrations of hydrogen and helium may well resolve this quandary. For the present, the mean density model of Weidner [14] is preferred, since associated with this mean density model are a family of density profiles representing various confidence levels which include the GE reference atmosphere profile.

The maximum density given by Weidner [14] for 1000 kilometers (1×10^{-16} g/cc) compares favorably with the maximum from the VM-3 extension (3×10^{-15} g/cc). Recalling that the latter was thought to be quite conservative, the difference between the two values is perhaps to be expected. In addition, since the VM-3 extension totally neglects variations of molecular weight with altitude, while the MSFC maximum density model accounts for such variations, the latter appears to be reasonable.

From the viewpoint of providing a common reference atmosphere and associated extremes, the preliminary models of Weidner [14] should be utilized. Tabulations of the minimum, mean, and maximum density models were included in milestone report VOY-D4-TM-4, Vachon [13], and are also available in the recent report by Weidner and Hasseltine [15].

VI. VARIATION OF ATMOSPHERIC DENSITY

A. Diurnal Variation

The atmospheric density in the Earth's upper atmosphere at 1000 kilometers varies by about one order of magnitude from a minimum at 0400 hours to a maximum at 1400 hours during maximum solar activity periods. Although the magnitude of the diurnal variation of density is about a factor of 3 during periods of low solar activity, occasionally larger variations are encountered even during these periods.

In regard to the Mars atmosphere, it is likely that diurnal variations of density of an order of magnitude are likely to be encountered at orbital altitudes around 1000 kilometers. In a previous estimate of the variation of density on Mars, Vachon [12], diurnal variations of about two orders of magnitude were suggested as being probable during periods of high solar activity. However, based on more recent evaluations of the probable density variations as a function of solar activity,

which are discussed in the following section, it appears that this earlier estimate was overly pessimistic. Indeed, from the density values given in Table IX (presented in section VI-B), it is seen that the diurnal density variation is about one order of magnitude.

B. Solar Cyclic Variations

The range of density values at 1000 kilometers given by Weidner and Hasseltine [15] is expected to reflect the range of variation likely to be experienced over the full solar cycle. The full range of the Mars density variations at 1000 kilometers is about 3×10^5 , according to the models of Weidner and Hasseltine.

To relate the probable distribution of density as a function of solar activity within this range, the Harris and Priester models of the Earth's atmosphere [5] are again considered. The range of density variation at 1000 kilometers from a period of low solar activity ($S = 70$) to a period of high solar activity ($S = 250$) is found to be about three orders of magnitude. The distribution of density at 1000 kilometers in models of the terrestrial and Mars atmospheres is given in table VIII.

TABLE VIII

Distribution of Density at 1000 Kilometers in Models of the Terrestrial and Martian Atmospheres

S	Density (g/cc)	Range	Remarks
200 to 250	3×10^{-18} to 1.3×10^{-16}	$\sim 10^2$	Priester and Harris Models of the Earth's atmosphere at 1000 km
70 to 100	2×10^{-19} to 1.7×10^{-18}	$\sim 10^1$	
70 to 250	2×10^{-19} to 1.3×10^{-16}	$\sim 10^3$	
Mean to Maximum	5.97×10^{-19} to 1.4×10^{-16}	$\sim 2-3 \times 10^2$	Weidner and Hasseltine models of Mars atmosphere at 1000 km
Minimum to Mean	5.03×10^{-22} to 5.97×10^{-19}	$\sim 10^3$	
Minimum to Maximum	5.03×10^{-22} to 1.4×10^{-16}	$\sim 3 \times 10^5$	

From a comparison of the density values and the range of variation given in table VIII, several possibilities are suggested. First, the range of density variation in the Mars mean-to-maximum model agrees closely with that expected during a period of high solar activity. Second, the range of density variation in the Mars minimum-to-mean model is much greater than would be expected during a period of low solar activity. Third, the full range of density variation in the Mars atmosphere models is almost twice as large as that expected in the Earth's atmosphere. On the basis of the above comparisons, it would appear reasonable to assume the mean-to-maximum density models to be representative of periods of high solar activity. On the other hand, assuming the minimum-to-mean density models to be representative of periods of low solar activity would appear to introduce a greater range of variation than would be encountered by analogy with the Harris and Priester models [5].

In order to provide an estimate of the probable variation of the atmospheric structure as a function of solar activity, the mean atmosphere model of Weidner and Hasseltine [15] was modified. The modification consisted of altering the thermal structure above 100 kilometers by substitution of the thermosphere thermal gradient values given in table VI, together with the exosphere temperature values given in table II. This rather simple modification provides a means of estimating the probable variation of the atmosphere as a function of solar activity for any given model. In the case of the Weidner and Hasseltine mean model, the resulting range of density variation as a function of solar activity (table IX) was found to closely agree with that obtained from the Harris and Priester models [5].

TABLE IX

Variation of the Mars Atmospheric Density at 700 Kilometers
as a Function of Solar Activity

	Solar Flux (S)				
	250	200	150	100	70
Minima	5×10^{-17}	2.2×10^{-17}	7×10^{-18}	1.8×10^{-18}	6.2×10^{-19}
Maxima	4.2×10^{-16}	2.2×10^{-16}	8×10^{-17}	2.4×10^{-17}	8.2×10^{-18}

From the values in table IX, it is seen that the density at 700 kilometers during a period of high solar activity is likely to be almost three orders of magnitude greater than during a period of low solar activity. At an altitude of 1000 kilometers, the calculated density variations indicate a three-orders-of-magnitude spread over the full solar cycle. The diurnal variation of density seen from table IX to amount to about one order of magnitude.

Based on the calculated values for the modified Weidner and Hasseltine mean model [15], as well as similar calculations using other models, it appears unlikely that the density at 1000 kilometers will vary by much more than three orders of magnitude over the full solar cycle. However, since the composition of the upper atmosphere is uncertain, the range of density variations must be increased to allow for this uncertainty. As mentioned previously, the Weidner maximum density profile was in reasonable agreement with the expected highly conservative VM-3 model extension. Thus, if the uncertainty in the composition is to produce an increase in the range of density values at any given altitude, then the range should be increased to include less dense atmospheres.

MSFC's (Weidner and Hasseltine models) mean-to-maximum density profiles thus provide a reasonable range of density values for periods of high solar activity. The MSFC mean-to-minimum density profiles would, by the same token, provide a reasonable range of density values for periods of moderate to low solar activity.

VII. CONCLUSIONS

Based on the Mariner IV ionospheric experiment data, the base of the thermosphere may be as low as 105 km. The thermal gradient is expected to range in value for 0.5° to 3.0°K/km during periods of low to high solar activity, respectively. The MSFC maximum density envelope compares favorably with the maximum density profile from the VM3 extension (the MSFC density at 1000 kms being less than 1 order of magnitude below the VM3 extended model value). The MSFC mean density profile compares favorably with the older GE Voyager reference atmosphere. The MSFC mean density value at 1000 kms is approximately 1 order of magnitude greater than that obtained from the GE Voyager reference model. The MSFC mean density profile and associated confidence envelopes were found to be consistent with most models presently available.

Estimates of the variations of the atmospheric structure as a function of solar activity indicate:

(a) The density at altitudes of about 1000 kilometers is likely to exhibit a diurnal (day-night) variation of an order of magnitude.

(b) The atmospheric density at 1000 kilometers during a period of high solar activity is likely to be three orders of magnitude greater than it is during a period of low solar activity.

(c) Solar cyclic variations of the atmosphere's density at 1000 kilometers of five and six orders of magnitude are expected to result more from uncertainties in the models than from probable variations of the atmosphere itself.

(d) The MSFC mean-to-maximum density profiles appear reasonable for periods of high solar activity.

(e) The MSFC mean-to-minimum density profiles appear adequate to define the density likely to be encountered during a period of moderate to low solar activity.

REFERENCES

1. Chamberlain, J. W. and M. B. McElroy, "Martian Atmosphere: The Mariner Occultation Experiment," *Science*, 152, No. 3718, April 1, 1966.
2. Donahue, T. M., "Upper Atmosphere and Ionosphere of Mars," *Science*, 152, May 6, 1966.
3. Galbraith, T. L., Personal Communication, GE-MSD, August 22, 1967.
4. Gross, S. H., W. E. McGovern, and S. I. Rasool, "Mars: Upper Atmosphere," *Science*, 151, March 11, 1966.
5. Harris, I. and W. Priester, "Theoretical Models for the Solar-Cycle Variation of the Upper Atmosphere," NASA TN D-1444, August 1962.
6. Hess, D. S. and E. Pounder, "Voyager Environmental Predictions Document," SE-003-BB001-1B28, NASA-JPL, October 1966.
7. Johnson, F. S., "Atmosphere of Mars," *Science*, 150, 1965.

REFERENCES (Continued)

8. Newburn, R., personal communications, NASA-JPL, July 7, 1966.
9. Smith, N. and A. E. Beutler, "A Model Martian Atmosphere and Ionosphere," University of Michigan, draft copy of paper, April 1967.
10. Spencer, D., personal communication, NASA-JPL, February 8, 1967.
11. Vachon, D. N. and R. J. Homsey, "Design Environments for Missions to Mars and Venus," GE-TIS-63SD344, December 1963.
12. Vachon, D. N., "On the Distribution of Density at Orbital Altitudes in the Martian Atmosphere," GE-TM-8126-5, June 1966.
13. Vachon, D. N., "Proposed Voyager Mars Reference Atmosphere for Planetary Quarantine Studies," GE-PIR-8126-196, February 1967.
14. Weidner, D. K., "Preliminary Models and Confidence Envelopes for the Mars Atmosphere," presented at the Planetary Mission Board Meeting, June 16, 1967 and at the Voyager Science Panel Meeting, June 21, 1967, NASA-MSFC, 1967.
15. Weidner, D. K. and C. L. Hasseltine, "Natural Environment Design Criteria Guidelines for MSFC Voyager Spacecraft for Mars 1973 Mission," NASA-MSFC, TM X-53616, June 8, 1967.

MODEL ATMOSPHERES OF MERCURY

By

Otha H. Vaughan, Jr.

George C. Marshall Space Flight Center

N 68-18844

SUMMARY

Atmospheric models for both the sunlit and dark sides of the planet Mercury based on latest environmental data for this planet have been developed for engineering use and for preliminary design criteria guidelines. The models are considered by the author to be as realistic as available data will permit; however, as more data are obtained, they will probably need to be refined.

INTRODUCTION

Although the planet Mercury has not yet been seriously considered in the United States space exploration program, in view of the information obtained from the Ranger, Orbiter, Surveyor, and the Mariner programs, Mercury will probably become an object of interest as more progress is made. Any effort at the present time to design a suitable spacecraft either for flyby missions or for landing on Mercury is restricted to a set of environmental criteria obtained from earth-based measurements and observations only. This paper presents the results of an in-house effort to develop atmospheric models for use in preliminary design studies for a spacecraft to probe the environment of Mercury.

ASTRONOMICAL AND GEOPHYSICAL DATA

Mercury, the smallest of the major planets, has a diameter of only $4,880 \text{ km} \pm 15 \text{ km}$, according to de Vaucouleurs [31], and is the innermost planet of the solar system. According to Ray [17], its mean distance from the sun is 0.3871 A.U. (about 57,900,000 km). Mercury's orbit around the sun has a perihelion of 45,980,000 km and an aphelion of 69,780,000 km, its orbital eccentricity (0.2056) being greater than any other planet in the solar system excluding that of Pluto. Mercury's orbital path and location with respect to the sun make this planet very difficult to observe since at its most favorable elongation it recedes

only 28 degrees from the sun in the plane of the ecliptic. However, Mercury has been observed by astronomers for two thousand years, dating back to at least 265 B.C. Several volumes have been written about the techniques of observing and obtaining environmental data for the planets of our solar system. References 1, 2, and 3 provide probably the most comprehensive source of this type of data. Geophysical and astronomical data for Mercury are summarized in table I.

DISCUSSION

For a long time, it was generally agreed that Mercury had no atmosphere because of the low escape velocity and because it was believed to be in captured rotation which would cause large temperature extremes between the sunlit and dark sides of the planet. This hypothesis was further supported by the apparent absence of any significant diffusion or reflection of light. The sharply defined appearance of Mercury as it crosses the face of the sun also suggests that there is little if any atmosphere. Early estimates for the temperature extremes for this planet were 690 °K for the sunlit side at the sub-solar point and 5 °K for the dark side at the anti-solar point, considering that the planet was not rotating. In 1936, Pettit and Nicholson (see Kuiper [2] and Kiess [6]) made infrared measurements over a number of phase angles, obtaining a temperature at the sub-solar point of 610 °K. Walker in 1961 [22] calculated the mean sub-solar temperature to be 621 °K and the dark-side temperature to be 28 °K by assuming that (1) the planet did not rotate, (2) the interior was in thermal steady state, (3) the specific rate of radioactive heat production was equal to that of chondritic meteorites ($1.33 \text{ cal deg}^{-1} \text{ cm}^{-1} \text{ m}^{-1}$), and (4) the planet was at a mean orbital distance. Because of the orbital eccentricities, the sub-solar temperature as determined by Pettit (see Kuiper [2]) can be as high as 688°K at perihelion and 588 °K at aphelion by assuming that the sub-solar temperature is 613 °K when the planet is at its mean distance from the sun.

Evidence for an atmosphere of Mercury has been based mainly on polarization studies [5,8], spectrographic data [2,9,15,16,13], and thermal data [14,26,27]. Early polarization studies by Lyot (see Dollfus [8]) and later by Dollfus [8] provided the first evidence for an atmosphere. Dollfus [8] examined the distribution of polarized light from different parts of the planet. At small phase angles, there appeared to be no difference in polarization for the bright or dark regions. However, as the phase angle increased, the polarization became stronger at the tips than at the center of the crescent. Since the moon does not exhibit this phenomenon and since the surfaces of Mercury and the moon are considered similar, Dollfus concluded that this excess polarization was the result of a weak atmosphere.

In 1963 N. Kozyrev [10,13] obtained 20 spectrograms of the planet and of its near vicinity. For comparison, spectrograms of the sun were also taken at the same position where Mercury would be when the spectrograms of the planet and vicinity were programmed to be taken. This technique enabled Kozyrev to make a direct comparison using both kinds of data samples. Analysis of the data revealed some hydrogen lines which appeared to have shifted toward the violet region while other hydrogen lines appeared to have shifted toward the red region of the spectrum. Because the ultraviolet radiation of the sun, in ionizing hydrogen, is not sufficient to produce these effects, the data implied that hydrogen was present as a genuine dense atmosphere rather than an ionosphere. Kozyrev believed that since Mercury is the nearest planet to the sun, a tenuous hydrogen atmosphere might be maintained by fluxes of protons from the sun. Obscuration of surface features as noted by Antoniadi (see Sandner, [4]) and others, as well as Futschek and Severinski [see Sandner [4]], who claimed to have detected an aureole surrounding the planet, are also evidence for an atmosphere. According to Spinrad and Hodge [15,16] the spectrographic, polarization and radio observations lead to the conclusion that the planet does have a tenuous atmosphere and that it may be time variable. Field [14] in his analysis of microwave emission (3 cm wavelength) data obtained by Howard, Barrett and Haddock [25] observed a systematic tendency of the brightness temperature data to lie above the theoretical curve of brightness temperature with respect to phase assuming a back-side temperature of 0 °K. Field [14] suggested that an atmosphere is responsible for the transport of heat to the back side.

In addition Barrett [23], after analysis of data from reference 25, postulated that the dark-side temperatures as predicted by Walker [22] were not as low as 28 °K but could be close to 270 °K.

By means of microwave equipment (1.53 cm wavelength), Welch and Thornton in September 1964 [24] obtained brightness measurements of Jupiter Saturn, and Mercury while Mercury's average illumination was about 25 percent. When these data were analyzed, they obtained a mean disk temperature of $465 \text{ °K} \pm 115 \text{ °K}$ for Mercury. By assuming a subsolar temperature of 620°K and a pole-darkening proportional to $\cos^{1/2}\theta$, Welch and Thornton postulated that the contribution of temperature from the unilluminated part of the disk was about 100 °K. Also, by assuming that the properties of the surface materials of Mercury are similar to the moon, as indicated by polarization studies, Welch and Thornton theorized that the large dark-side contribution to the disk temperature is a result of internal radioactive heat sources. Although the thermal data tended to imply that Mercury has an atmosphere, additional information was required to support or disprove its existence. Before 1965, Mercury was considered to be in synchronous rotation, and the high back-side temperature could be explained if there was an atmosphere to transport the heat to the dark side. Recent radar probe measurements by Pettengill and his associates [18] at Arecibo,

Puerto Rico, during the 1965 inferior conjunction of Mercury, indicated that the rotational period was different from the orbital period. The rotation of the planet is now considered to be direct with a sidereal period of 59 ± 5 days. Although the direction of the pole is not well determined from these limited data, the authors of reference 18 agree that it is approximately normal to the planetary orbit. Analysis of these data by Peale and Gold [20] indicated that (1) the rotation rate was between 56.6 and 88 days, (2) Mercury has little permanent rigidity, and (3) the nonsynchronous rotation may be explained in terms of solar tidal effects. Analysis of the same data by Colombo and Shapiro [29,30] suggests that the rotational period is 58.65 days ($2/3$ of the orbital period) and that the rigidity of the planet is higher than that permitted by Peale and Gold. McGovern, Rasool and Gross [21] in their analysis of 50 drawings of Mercury produced from visual observations by Antoniadi, Lyot and Dollfus, and Baum concluded that, in addition to the previously accepted 88 days, there exists, based on 6 pairs of these drawings, at least three possible values for the rotation rate: 50.1, 58.4, and 70.2 days. Recently, McGovern, Rasool, and Gross [11] have indicated that a period of rotation of 43.6 days could also be possible. However, the 58.4 ± 0.4 days represent the best value for the rotational rate, at the present time, since it is consistent with both the radar and observational data. Since the planet has been found not to be in synchronous rotation, the case against an atmosphere becomes somewhat stronger.

In April 1965, Epstein and his associates [26,27], in making brightness measurements in the 3.4 mm band, obtained a value of 220 ± 35 °K for the dark-side temperature. The most significant result was that there appeared to be no dependence of temperature on variation in phase. These data seemed to be in disagreement since other measurements [27] at 8 mm indicated that a large variation with phase should occur at the smaller wavelength of 3 mm if the surface materials of Mercury were like that of the moon. Recent radio thermal measurements at 1.9 mm by Kaftan-Kassim and Kellermann [28] of the National Radio Astronomy Observatory during February and March 1966 revealed that Mercury's day-to-night range in brightness temperature is about 75 °K centered on a mean value of 288 °K. Later, using his 3.4 mm data, Epstein [28] reported that he also found these day-to-night variations. Since the thermal emission originates a few wavelengths below the surface, the temperature a few decimeters below the surface may remain constant at 270 °K at least. Since the planet is rotating, the entire surface is being exposed to solar radiation. Therefore, the high dark-side temperature now seems realistic. Since there has been no actual surface temperature measurements for the dark side (anti-solar point) of Mercury, the possibility of a meager atmosphere consisting of heavy gases, however, still exists. If a 5 mb atmosphere of carbon dioxide is present, then atmospheric circulation could be an efficient means to transport the heat from the day to the night side.

Recently, Rasool, Gross, and McGovern [11] have interpreted the spectrographic, polarization, and thermal data to indicate that Mercury has an atmosphere with a probable surface pressure of 0.01 to 10 mb. Thus, at the present time, it is very difficult to either prove or disprove the existence of an atmosphere or its composition. Using the data of Rasool, Gross and McGovern [11] as a starting point for an inhouse study by the author, several atmospheric models for this planet were developed to provide the spacecraft design engineer with preliminary environmental criteria for use in spacecraft design studies. In the development of each model, it has been assumed that the atmosphere is not in circulation and that the atmosphere is stable against gravitational escape and solar wind effects. The input data assumptions for the model atmospheres are presented in table II.

Figures 1 and 2 illustrate profiles of the sunlit side pressure and density data, while figures 3 and 4 illustrate similar profiles of the dark side. Other atmospheric data are presented in tables III through VIII. Figure 5 illustrates a typical atmospheric density operations envelope for the maximum density model.

CONCLUDING REMARKS

Atmospheric models for the planet Mercury have been based on the latest data. Because these models are only as good as the input information, they must be considered as rough approximations. However, the author believes that this information is realistic enough for use as preliminary design criteria guidelines at least for the present time. As more data become available, more realistic atmospheric models will be constructed.

TABLE I

Planetary Geophysical and Astronomical Data for Mercury
[5,6,7,11,17,32]

Mean distance (Earth = 1 A.U.)	0.387099 A.U.
Orbital velocity	47.87 km/sec
Sidereal period	87.969 days
Inclination to ecliptic	7.00399°
Eccentricity	0.205627
Equatorial radius	2,422 km
Flattening	-
Mass of planet to mass of earth	0.056
Mean density	5.13 gm/cm ³
Velocity of escape	4.2 km/sec
Rotation period	58.4 ± 0.4 days
Inclination of equator to orbit	0°
Gravitational parameter	21,685.53 km ³ /sec ²
Visual albedo	0.056
Mass of sun to mass of planet	6,120,000
Theoretical temperature	
Spherical black body (rapidly rotating)	441 °K
Hemispherical black body (slowly rotating)	525 °K
Sub-solar black body (mean measured value)	624 °K

TABLE II

MERCURY ATMOSPHERIC MODELS
INPUT DATA SUMMARY

MODEL	SURFACE PRESSURE	SURFACE TEMPERATURE	CONSTITUENTS	HEIGHT OF MESOPAUSE
<u>Minimum Density</u> Sun-lit Side Dark Side	1,000 dynes/cm ² 500 dynes/cm ²	520°K 270°K	100% CO ₂	145KM
<u>Mean Density</u> Sun-lit Side Dark Side	5,000 dynes/cm ² 3,000 dynes/cm ²	520°K 270°K	50% CO ₂ 50% Argon	200KM
<u>Maximum Density</u> Sun-lit Side Dark Side	5,000 dynes/cm ² 3,000 dynes/cm ²	520°K 270°K	60% CO ₂ 25% Ne 15% N ₂	280KM

TABLE III
MINIUM DENSITY MODEL
SUNLIT SIDE

GEOMETRIC ALTITUDE (KM)	KINETIC TEMPERATURE (DEG K)	PRESSURE (MB)	DENSITY (GM/CM3)	SPEED OF SOUND (M/SEC2)	MOL. WT.	DENSITY SCALE HEIGHT (KM)	NUMBER DENSITY (/CM)	MEAN FREE PATH (M)	COEFFICIENT OF VISCOSITY (KG/M-SEC)
0.0	520.00	1.0003+00	1.0183-06	370.90	44.0	34.03	1.3933+16	1.2133-03	2.7423-05
1.0	513.75	9.6303-01	9.8813-07	369.38	44.0	33.79	1.3533+16	1.2493-03	2.7273-05
2.0	511.51	9.2713-01	9.5923-07	367.86	44.0	33.54	1.3133+16	1.2873-03	2.7123-05
3.0	507.27	8.9233-01	9.3093-07	366.33	44.0	33.29	1.2743+16	1.3263-03	2.6973-05
4.0	503.03	8.5863-01	9.0333-07	364.80	44.0	33.03	1.2373+16	1.3663-03	2.6823-05
5.0	498.79	8.2593-01	8.7623-07	363.26	44.0	32.78	1.2003+16	1.4093-03	2.6663-05
6.0	494.56	7.9423-01	8.4983-07	361.71	44.0	32.53	1.1633+16	1.4523-03	2.6513-05
7.0	490.34	7.6333-01	8.2403-07	360.16	44.0	32.28	1.1283+16	1.4983-03	2.6353-05
8.0	486.11	7.3373-01	7.9873-07	358.61	44.0	32.03	1.0943+16	1.5453-03	2.6203-05
9.0	481.89	7.0493-01	7.7413-07	357.05	44.0	31.78	1.0603+16	1.5943-03	2.6043-05
10.0	477.67	6.7703-01	7.5003-07	355.48	44.0	31.53	1.0273+16	1.6463-03	2.5883-05
11.0	473.46	6.5003-01	7.2653-07	353.91	44.0	31.27	9.9463+15	1.6993-03	2.5733-05
12.0	469.25	6.2393-01	7.0363-07	352.33	44.0	31.02	9.6323+15	1.7543-03	2.5573-05
13.0	465.05	5.9863-01	6.8113-07	350.75	44.0	30.77	9.3253+15	1.8123-03	2.5413-05
14.0	460.84	5.7413-01	6.5933-07	349.16	44.0	30.51	9.0263+15	1.8723-03	2.5253-05
15.0	456.64	5.5033-01	6.3793-07	347.57	44.0	30.26	8.7343+15	1.9353-03	2.5093-05
16.0	452.45	5.2763-01	6.1713-07	345.97	44.0	30.01	8.4483+15	2.0003-03	2.4933-05
17.0	448.25	5.0553-01	5.9683-07	344.36	44.0	29.75	8.1703+15	2.0683-03	2.4773-05
18.0	444.06	4.8423-01	5.7703-07	342.75	44.0	29.50	7.8993+15	2.1393-03	2.4613-05
19.0	439.88	4.6333-01	5.5773-07	341.13	44.0	29.25	7.6353+15	2.2133-03	2.4443-05
20.0	435.70	4.4363-01	5.3883-07	339.50	44.0	27.92	7.3773+15	2.2913-03	2.4283-05
21.0	433.13	4.2443-01	5.1863-07	338.50	44.0	25.80	7.1003+15	2.3803-03	2.4183-05
22.0	430.89	4.0603-01	4.9873-07	337.62	44.0	25.44	6.8273+15	2.4753-03	2.4093-05
23.0	428.65	3.8833-01	4.7943-07	336.75	44.0	25.33	6.5633+15	2.5753-03	2.4003-05
24.0	426.41	3.7133-01	4.6083-07	335.87	44.0	25.22	6.3083+15	2.6793-03	2.3923-05
25.0	424.17	3.5493-01	4.4283-07	334.98	44.0	25.11	6.0633+15	2.7873-03	2.3833-05
50.0	368.83	1.0733-01	1.5403-07	312.37	44.0	22.28	2.1093+15	8.0143-03	2.1553-05
75.0	314.60	2.7533-02	4.6323-08	288.49	44.0	19.39	6.3413+14	2.6653-02	1.9143-05
100.0	261.44	5.6523-03	1.1443-08	262.99	44.0	16.44	1.5663+14	1.0793-01	1.6583-05
125.0	222.29	8.6473-04	2.0163-09	245.03	43.1	12.66	2.7603+13	5.9963-01	1.4783-05
150.0	213.45	1.2963-04	2.9323-10	248.76	40.2	13.28	4.0143+12	3.8423+00	1.5153-05
175.0	210.00	2.1513-05	4.6423-11	254.71	37.7	13.97	6.3553+11	2.2773+01	1.5743-05
200.0	210.00	4.0663-06	8.2723-12	262.31	35.5	15.05	1.1333+11	1.2053+02	1.6513-05
300.0	373.99	4.9863-08	4.5223-14	392.91	28.2	29.31	6.1913+08	1.7493+04	2.9623-05
400.0	561.09	7.8773-09	3.6443-15	550.13	21.6	53.34	4.9883+07	1.6613+05	4.4973-05
500.0	735.36	3.1613-09	7.9663-16	745.16	15.4	79.72	1.0913+07	5.4273+05	6.3463-05
600.0	898.14	2.0003-09	2.5873-16	1040.44	9.7	94.51	3.5423+06	1.0473+06	9.0823-05
700.0	960.07	1.5773-09	1.4963-16	1215.06	7.6	320.47	2.0483+06	1.4203+06	1.0683-04
800.0	980.48	1.2993-09	1.1133-16	1278.12	7.0	357.46	1.5243+06	1.7613+06	1.1263-04
900.0	999.66	1.1013-09	8.5323-17	1344.37	6.4	395.08	1.1683+06	2.1173+06	1.1863-04
1000.0	1017.72	9.5723-10	6.6993-17	1414.33	5.9	432.65	9.1723+05	2.4803+06	1.2503-04

TABLE IV
MINIUM DENSITY MODEL
DARK SIDE

GEOMETRIC ALTITUDE (KM)	KINETIC TEMPERATURE (DEG K)	PRESSURE (MB)	DENSITY (GM/CM3)	SPEED OF SOUND (M/SEC2)	MOL. WT.	DENSITY SCALE HEIGHT (KM)	NUMBER DENSITY (/CM)	MEAN FREE PATH (M)	COEFFICIENT OF VISCOSITY (KG/M-SEC)
0.0	270.00	5.0007-01	9.8007-07	267.26	44.0	14.19	1.3427+16	1.2597-03	1.7007-05
1.0	269.50	4.6517-01	9.1337-07	267.01	44.0	14.18	1.2507+16	1.3517-03	1.6987-05
2.0	269.00	4.3267-01	8.5107-07	266.77	44.0	14.16	1.1657+16	1.4507-03	1.6957-05
3.0	268.50	4.0237-01	7.9307-07	266.52	44.0	14.15	1.0867+16	1.5577-03	1.6937-05
4.0	268.00	3.7427-01	7.3887-07	266.27	44.0	14.13	1.0127+16	1.6717-03	1.6907-05
5.0	267.51	3.4797-01	6.8837-07	266.02	44.0	14.12	9.4247+15	1.7937-03	1.6887-05
6.0	267.01	3.2357-01	6.4127-07	265.78	44.0	14.10	8.7797+15	1.9257-03	1.6867-05
7.0	266.51	3.0087-01	5.9737-07	265.53	44.0	14.09	8.1787+15	2.0667-03	1.6837-05
8.0	266.01	2.7977-01	5.5647-07	265.28	44.0	14.07	7.6177+15	2.2187-03	1.6817-05
9.0	265.52	2.6007-01	5.1827-07	265.03	44.0	14.06	7.0947+15	2.3827-03	1.6787-05
10.0	265.02	2.4177-01	4.8267-07	264.78	44.0	14.04	6.6077+15	2.5587-03	1.6767-05
11.0	264.52	2.2467-01	4.4947-07	264.54	44.0	14.03	6.1577+15	2.7467-03	1.6737-05
12.0	264.03	2.0887-01	4.1857-07	264.29	44.0	14.01	5.7297+15	2.9507-03	1.6717-05
13.0	263.53	1.9407-01	3.8967-07	264.04	44.0	14.00	5.3347+15	3.1687-03	1.6687-05
14.0	263.04	1.8037-01	3.6287-07	263.79	44.0	13.98	4.9667+15	3.4027-03	1.6667-05
15.0	262.55	1.6757-01	3.3777-07	263.55	44.0	13.97	4.6237+15	3.6557-03	1.6637-05
16.0	262.05	1.5577-01	3.1447-07	263.30	44.0	13.95	4.3047+15	3.9267-03	1.6617-05
17.0	261.56	1.4467-01	2.9267-07	263.05	44.0	13.94	4.0067+15	4.2187-03	1.6587-05
18.0	261.07	1.3447-01	2.7247-07	262.80	44.0	13.93	3.7297+15	4.5327-03	1.6567-05
19.0	260.57	1.2487-01	2.5357-07	262.55	44.0	13.91	3.4707+15	4.8707-03	1.6537-05
20.0	260.08	1.1597-01	2.3597-07	262.31	44.0	13.86	3.2297+15	5.2337-03	1.6517-05
21.0	259.69	1.0777-01	2.1947-07	262.11	44.0	13.81	3.0047+15	5.6257-03	1.6497-05
22.0	259.31	1.0007-01	2.0417-07	261.92	44.0	13.79	2.7947+15	6.0487-03	1.6477-05
23.0	258.94	9.2877-02	1.8987-07	261.73	44.0	13.78	2.5987+15	6.5037-03	1.6457-05
24.0	258.57	8.6247-02	1.7657-07	261.54	44.0	13.77	2.4167+15	6.9937-03	1.6437-05
25.0	258.20	8.0087-02	1.6417-07	261.35	44.0	13.76	2.2477+15	7.5207-03	1.6417-05
50.0	248.97	1.2387-02	2.6317-08	256.64	44.0	13.55	3.6027+14	6.9937-03	1.6437-05
75.0	239.93	1.8557-03	4.0927-09	251.94	44.0	13.32	5.6027+13	3.0177-01	1.5477-05
100.0	231.07	2.6907-04	6.1607-10	247.25	44.0	13.09	8.4337+12	2.0047+00	1.5007-05
125.0	222.29	3.7877-05	8.8317-11	245.03	43.1	12.67	1.2097+12	1.3697+01	1.4787-05
150.0	213.46	5.6777-06	1.2847-11	248.76	40.2	13.28	1.7587+11	8.7707+01	1.5157-05
175.0	210.00	9.4247-07	2.0347-12	254.70	37.7	13.97	2.7847+10	5.1977+02	1.5747-05
200.0	210.00	1.7827-07	3.6257-13	262.31	35.5	15.05	4.9637+09	2.7497+03	1.6517-05
300.0	373.93	2.1857-09	1.9827-13	592.87	28.2	29.31	2.7137+07	3.9927+05	2.9617-05
400.0	560.99	3.4517-10	1.5977-16	550.04	21.6	53.34	2.1867+06	3.7917+06	4.4977-05
500.0	735.24	1.3857-10	3.4927-17	744.99	15.4	79.75	4.7817+05	1.2397+07	6.3447-05
600.0	897.95	6.7617-11	1.1347-17	1039.96	9.7	94.55	1.5337+05	2.3917+07	9.0777-05
700.0	960.03	6.9087-11	6.5527-18	1214.95	7.6	320.56	8.9707+04	3.2417+07	1.0687-04
800.0	980.43	5.6697-11	4.8777-18	1277.98	7.0	337.58	6.6767+04	4.0197+07	1.1257-04
900.0	999.61	4.8247-11	3.7367-18	1344.19	6.4	395.22	5.1187+04	4.8337+07	1.1867-04
1000.0	1017.66	4.1937-11	2.9357-18	1414.08	5.9	432.90	4.0197+04	5.6617+07	1.2497-04

TABLE V
MEAN DENSITY MODEL
SUNLIT SIDE

GEOMETRIC ALTITUDE (KM)	KINETIC TEMPERATURE (DEG K)	PRESSURE (MB)	DENSITY (GM/CM3)	SPEED OF SOUND (M/SEC2)	MOL. WT.	DENSITY SCALE HEIGHT (KM)	NUMBER DENSITY (/CM)	MEAN FREE PATH (M)	COEFFICIENT OF VISCOSITY (KG/M-SEC)
0.0	520.00	5.0000+00	4.8578-06	379.63	42.0	39.01	6.9667+16	2.4267-05	2.7423-05
1.0	514.69	4.8233+00	4.7347-06	377.68	42.0	38.65	6.7997+16	2.4897-05	2.7243-05
2.0	509.38	4.6518+00	4.6128-06	375.73	42.0	38.28	6.6157+16	2.5543-05	2.7043-05
3.0	504.08	4.4837+00	4.4937-06	373.77	42.0	37.92	6.4447+16	2.6223-05	2.6853-05
4.0	498.79	4.3203+00	4.3757-06	371.80	42.0	37.55	6.2757+16	2.6937-05	2.6663-05
5.0	493.49	4.1617+00	4.2607-06	369.82	42.0	37.18	6.1097+16	2.7667-05	2.6477-05
6.0	488.20	4.0077+00	4.1467-06	367.84	42.0	36.81	5.9467+16	2.8427-05	2.6277-05
7.0	482.92	3.8577+00	4.0347-06	365.84	42.0	36.44	5.7863+16	2.9207-05	2.6087-05
8.0	477.64	3.7117+00	3.9237-06	363.84	42.0	36.08	5.6297+16	3.0027-05	2.5897-05
9.0	472.36	3.5697+00	3.8177-06	361.82	42.0	35.71	5.4747+16	3.0877-05	2.5697-05
10.0	467.09	3.4317+00	3.7117-06	359.80	42.0	35.34	5.3227+16	3.1757-05	2.5497-05
11.0	461.83	3.2977+00	3.6077-06	357.76	42.0	34.97	5.1737+16	3.2677-05	2.5297-05
12.0	456.56	3.1687+00	3.5037-06	355.72	42.0	34.60	5.0267+16	3.3627-05	2.5097-05
13.0	451.31	3.0417+00	3.4047-06	353.66	42.0	34.23	4.8827+16	3.4617-05	2.4897-05
14.0	446.05	2.9197+00	3.3067-06	351.60	42.0	33.86	4.7417+16	3.5647-05	2.4687-05
15.0	440.80	2.8007+00	3.2097-06	349.52	42.0	33.49	4.6027+16	3.6727-05	2.4487-05
16.0	435.56	2.6857+00	3.1147-06	347.44	42.0	29.27	4.4667+16	3.7847-05	2.4287-05
17.0	433.78	2.5747+00	2.9977-06	346.73	42.0	25.81	4.2997+16	3.9317-05	2.4217-05
18.0	432.41	2.4677+00	2.8827-06	346.18	42.0	25.44	4.1337+16	4.0887-05	2.4137-05
19.0	431.04	2.3647+00	2.7717-06	345.63	42.0	25.38	3.9747+16	4.2537-05	2.4107-05
20.0	429.68	2.2657+00	2.6637-06	345.09	42.0	25.32	3.8207+16	4.4247-05	2.4047-05
21.0	428.32	2.1717+00	2.5607-06	344.54	42.0	25.26	3.6727+16	4.6027-05	2.3997-05
22.0	426.95	2.0807+00	2.4617-06	343.99	42.0	25.20	3.5297+16	4.7887-05	2.3947-05
23.0	425.59	1.9927+00	2.3657-06	343.44	42.0	25.14	3.3927+16	4.9827-05	2.3887-05
24.0	424.23	1.9087+00	2.2727-06	342.89	42.0	25.08	3.2597+16	5.1857-05	2.3837-05
25.0	422.87	1.8287+00	2.1847-06	342.34	42.0	25.02	3.1327+16	5.3967-05	2.3787-05
30.0	389.24	6.0037-01	7.7907-07	328.45	42.0	23.50	1.1177+16	1.5127-04	2.2417-05
50.0	356.29	1.8287-01	2.5927-07	314.24	42.0	21.95	3.7187+15	4.5457-04	2.1017-05
75.0	323.99	5.0987-02	7.9487-08	299.65	42.0	20.36	1.1407+15	1.4827-03	1.9577-05
100.0	292.32	1.2807-02	2.2117-08	284.63	42.0	18.74	3.7277+14	5.3287-03	1.8097-05
125.0	261.27	2.8297-03	5.4707-09	269.09	42.0	17.08	7.8467+13	2.1547-02	1.6577-05
150.0	230.81	5.3507-04	1.1717-09	252.92	42.0	14.85	1.6797+13	1.0067-01	1.4987-05
175.0	209.88	9.1077-05	2.0697-10	248.23	39.6	14.31	2.9687+12	5.3757-01	1.4537-05
200.0	245.81	1.4527-07	2.2257-13	302.32	31.3	17.56	3.1917+09	3.9477+02	1.9847-05
300.0	474.91	9.5187-09	5.7437-15	483.27	23.7	41.56	8.2377+07	1.1567+04	3.7427-05
400.0	668.33	3.1387-09	9.0777-16	695.67	16.6	69.06	1.3027+07	5.1177+04	5.7307-05
500.0	887.62	1.8977-09	2.5487-16	1020.94	9.9	84.51	3.6557+06	1.0917+05	8.6867-05
600.0	980.07	1.4937-09	1.4167-16	1215.06	7.6	320.47	2.0317+06	1.4997+05	1.0437-04
700.0	980.46	1.2307-09	1.0547-16	1278.12	7.0	357.46	1.5127+06	1.8597+05	1.0997-04
800.0	999.66	1.0437-09	8.0797-17	1344.37	6.4	395.08	1.1597+06	2.2367+05	1.1587-04
1000.0	1017.72	9.0647-10	6.3447-17	1414.33	5.9	432.65	9.0987+05	2.6197+05	1.2207-04

TABLE VI
MEAN DENSITY MODEL
DARK SIDE

GEOMETRIC ALTITUDE (KM)	KINETIC TEMPERATURE (DEG K)	PRESSURE (MB)	DENSITY (GM/CM3)	SPEED OF SOUND (M/SEC2)	MOL. WT.	DENSITY SCALE HEIGHT (KM)	NUMBER DENSITY (/CM)	MEAN FREE PATH (M)	COEFFICIENT OF VISCOSITY (KG/M-SEC)
0.0	270.00	3.0007+00	5.6137-06	273.55	42.0	14.68	8.0307+16	2.0997-04	1.7007-05
1.0	269.75	2.8007+00	5.2437-06	273.42	42.0	14.68	7.5207+16	2.2477-04	1.6997-05
2.0	269.50	2.6137+00	4.8987-06	273.30	42.0	14.68	7.0237+16	2.4067-04	1.6987-05
3.0	269.25	2.4397+00	4.5757-06	273.17	42.0	14.68	6.5627+16	2.5757-04	1.6977-05
4.0	269.00	2.2767+00	4.2747-06	273.04	42.0	14.68	6.1307+16	2.7577-04	1.6957-05
5.0	268.75	2.1247+00	3.9927-06	272.92	42.0	14.67	5.7267+16	2.9517-04	1.6947-05
6.0	268.50	1.9827+00	3.7297-06	272.79	42.0	14.67	5.3497+16	3.1597-04	1.6937-05
7.0	268.25	1.8507+00	3.4847-06	272.66	42.0	14.67	4.9967+16	3.3827-04	1.6927-05
8.0	268.01	1.7267+00	3.2547-06	272.54	42.0	14.67	4.6677+16	3.6217-04	1.6917-05
9.0	267.76	1.6117+00	3.0407-06	272.41	42.0	14.67	4.3607+16	3.8767-04	1.6907-05
10.0	267.51	1.5047+00	2.8397-06	272.29	42.0	14.67	4.0727+16	4.1497-04	1.6897-05
11.0	267.26	1.4037+00	2.6527-06	272.16	42.0	14.67	3.8047+16	4.4427-04	1.6887-05
12.0	267.01	1.3107+00	2.4777-06	272.03	42.0	14.66	3.5537+16	4.7567-04	1.6877-05
13.0	266.77	1.2227+00	2.3147-06	271.91	42.0	14.66	3.3197+16	5.0917-04	1.6847-05
14.0	266.52	1.1407+00	2.1627-06	271.78	42.0	14.66	3.1007+16	5.4517-04	1.6837-05
15.0	266.27	1.0647+00	2.0197-06	271.66	42.0	14.66	2.8967+16	5.8367-04	1.6827-05
16.0	266.03	9.9317-01	1.8867-06	271.53	42.0	14.65	2.7057+16	6.2487-04	1.6817-05
17.0	265.79	9.2687-01	1.7617-06	271.41	42.0	14.65	2.5267+16	6.6897-04	1.6797-05
18.0	265.56	8.6497-01	1.6457-06	271.29	42.0	14.65	2.3607+16	7.1627-04	1.6787-05
19.0	265.32	8.0717-01	1.5377-06	271.17	42.0	14.65	2.2047+16	7.6687-04	1.6777-05
20.0	265.09	7.5317-01	1.4357-06	271.05	42.0	14.64	2.0587+16	8.2107-04	1.6767-05
21.0	264.85	7.0267-01	1.3407-06	270.93	42.0	14.64	1.9227+16	8.7907-04	1.6757-05
22.0	264.62	6.5567-01	1.2527-06	270.81	42.0	14.64	1.7967+16	9.4117-04	1.6747-05
23.0	264.38	6.1207-01	1.1697-06	270.69	42.0	14.64	1.6777+16	1.0087-03	1.6727-05
24.0	264.15	5.7117-01	1.0927-06	270.57	42.0	14.64	1.5667+16	1.0797-03	1.6717-05
25.0	263.92	5.3297-01	1.0207-06	270.45	42.0	14.64	1.4637+16	1.1557-03	1.6707-05
50.0	258.15	9.4557-02	1.8467-07	267.48	42.0	14.61	2.6487+15	6.3817-03	1.6417-05
75.0	252.49	1.6657-02	3.3317-08	264.53	42.0	14.58	4.7787+14	3.5377-02	1.6127-05
100.0	246.94	2.9277-03	5.9887-09	261.61	42.0	14.55	8.5887+13	1.9687-01	1.5837-05
125.0	241.51	5.1257-04	1.0727-09	258.71	42.0	14.51	1.5377+13	1.0997+00	1.5537-05
150.0	236.18	8.9307-05	1.9107-10	255.84	42.0	14.47	2.7407+12	6.1687+00	1.5277-05
175.0	230.95	1.5487-05	3.5877-11	253.00	42.0	14.50	4.8577+11	3.4797+01	1.4997-05
200.0	229.84	2.6347-06	5.9867-12	248.20	39.6	14.30	8.5867+10	1.6587+02	1.4527-05
300.0	245.81	4.2017-09	6.4357-15	302.32	31.3	17.56	9.2297+07	1.3657+05	1.9847-05
400.0	474.91	2.7717-10	1.6617-16	483.27	23.7	61.56	2.3627+06	3.9977+06	3.7427-05
500.0	688.33	9.0757-11	2.6257-17	695.67	16.6	69.06	1.0577+05	1.7697+07	5.7307-05
600.0	887.62	5.4877-11	7.3707-18	1020.94	9.9	84.51	5.8747+04	3.7737+07	8.6867-05
700.0	960.07	4.3197-11	4.0967-18	1215.06	7.6	320.47	1.0437+04	5.1847+07	1.0437-04
800.0	986.48	3.5577-11	3.0487-18	1278.12	7.0	357.46	4.3727+04	6.4297+07	1.0997-04
900.0	999.66	3.0167-11	2.3367-18	1344.37	6.4	399.50	3.3517+04	7.7307+07	1.1967-04
1000.0	1017.72	2.6217-11	1.8357-18	1414.33	5.9	432.65	2.6317+04	9.0567+07	1.2207-04

TABLE VII
MAXIMUM DENSITY MODEL
SUNLIT SIDE

GEOMETRIC ALTITUDE (KM)	KINETIC TEMPERATURE (DEG K)	PRESSURE (MB)	DENSITY (GM/CMS)	SPEED OF SOUND (M/SEC ²)	MOL. WT.	DENSITY SCALE HEIGHT (KM)	NUMBER DENSITY (/CM)	MEAN FREE PATH (M)	COEFFICIENT OF VISCOSITY (KG/M-SEC)
0.0	520.00	5.0000*00	4.1178-06	412.34	35.6	43.56	6.9667*16	2.4263-04	2.7423-05
1.0	516.14	4.8503*00	4.0233-06	410.81	35.6	43.28	6.8083*16	2.4823-04	2.7293-05
2.0	512.28	4.7033*00	3.9313-06	409.27	35.6	42.99	6.6523*16	2.5403-04	2.7153-05
3.0	508.42	4.5603*00	3.8403-06	407.72	35.6	42.70	6.4983*16	2.6003-04	2.7013-05
4.0	504.57	4.4213*00	3.7513-06	406.18	35.6	42.41	6.3473*16	2.6623-04	2.6873-05
5.0	500.72	4.2843*00	3.6643-06	404.62	35.6	42.12	6.1993*16	2.7263-04	2.6733-05
6.0	496.88	4.1513*00	3.5773-06	403.07	35.6	41.83	6.0533*16	2.7923-04	2.6593-05
7.0	493.03	4.0223*00	3.4923-06	401.51	35.6	41.55	5.9103*16	2.8593-04	2.6453-05
8.0	489.19	3.8953*00	3.4093-06	399.94	35.6	41.26	5.7693*16	2.9293-04	2.6313-05
9.0	485.36	3.7723*00	3.3273-06	398.37	35.6	40.97	5.6303*16	3.0013-04	2.6173-05
10.0	481.52	3.6513*00	3.2473-06	396.79	35.6	40.68	5.4943*16	3.0763-04	2.6033-05
11.0	477.69	3.5343*00	3.1683-06	395.21	35.6	40.39	5.3603*16	3.1533-04	2.5893-05
12.0	473.87	3.4203*00	3.0903-06	393.62	35.6	40.09	5.2283*16	3.2323-04	2.5743-05
13.0	470.04	3.3083*00	3.0133-06	392.03	35.6	39.80	5.0993*16	3.3143-04	2.5603-05
14.0	466.22	3.1993*00	2.9383-06	390.44	35.6	39.51	4.9723*16	3.3993-04	2.5453-05
15.0	462.40	3.0943*00	2.8653-06	388.83	35.6	39.22	4.8473*16	3.4863-04	2.5313-05
16.0	458.59	2.9913*00	2.7923-06	387.23	35.6	38.93	4.7233*16	3.5763-04	2.5163-05
17.0	454.78	2.8903*00	2.7213-06	385.61	35.6	38.64	4.6033*16	3.6683-04	2.5023-05
18.0	450.97	2.7933*00	2.6513-06	384.00	35.6	38.35	4.4863*16	3.7633-04	2.4873-05
19.0	447.16	2.6973*00	2.5833-06	382.37	35.6	38.05	4.3703*16	3.8633-04	2.4733-05
20.0	443.36	2.6033*00	2.5163-06	380.74	35.6	37.76	4.2573*16	3.9703-04	2.4583-05
21.0	439.56	2.5153*00	2.4503-06	379.11	35.6	37.47	4.1433*16	4.0773-04	2.4433-05
22.0	435.77	2.4273*00	2.3853-06	377.47	35.6	34.17	4.0333*16	4.1873-04	2.4283-05
23.0	434.03	2.3423*00	2.3113-06	376.72	35.6	30.93	3.9103*16	4.3223-04	2.4223-05
24.0	432.62	2.2603*00	2.2363-06	376.19	35.6	30.31	3.7833*16	4.4673-04	2.4173-05
25.0	431.62	2.1803*00	2.1633-06	375.67	35.6	30.25	3.6603*16	4.6173-04	2.4123-05
50.0	401.71	8.6923-01	9.2643-07	362.42	35.6	28.75	1.5683*16	1.0783-03	2.2923-05
75.0	372.41	3.2943-01	3.7873-07	348.95	35.6	27.17	6.4083*15	2.6373-03	2.1703-05
100.0	343.69	1.1783-01	1.4683-07	335.23	35.6	25.58	2.4843*15	6.8043-03	2.0463-05
125.0	315.53	3.9413-02	5.3483-08	321.20	35.6	23.96	9.0503*14	1.8673-02	1.9193-05
150.0	287.92	1.2203-02	1.8143-08	306.83	35.6	22.29	3.0683*14	5.5073-02	1.7863-05
175.0	260.84	3.4413-03	5.6483-09	292.04	35.6	20.59	9.5533*13	1.7683-01	1.6553-05
200.0	244.10	8.8833-04	1.5403-09	284.21	35.6	18.60	2.6033*13	6.4093-01	1.5043-05
300.0	206.05	3.6833-06	6.9733-12	271.93	32.4	18.40	1.1803*11	1.3053*02	1.4733-05
400.0	361.30	6.7383-08	5.1343-14	428.67	22.9	31.89	8.6883*08	1.2313*04	2.8893-05
500.0	626.30	1.8393-08	5.6963-15	672.32	16.1	66.55	9.6373*07	7.9443*04	5.0203-05
600.0	873.75	1.0923-08	1.4753-15	1017.85	9.8	82.27	2.4983*07	1.8673*05	7.9313-05
700.0	952.89	8.5863-09	8.2033-16	1210.51	7.6	325.74	1.3883*07	2.5893*05	9.9263-05
800.0	963.58	7.0343-09	6.1513-16	1267.07	7.0	365.68	1.0413*07	3.1863*05	9.9823-05
900.0	973.63	5.9393-09	4.7403-16	1326.76	6.4	402.30	8.0203*06	3.8113*05	1.0483-04
1000.0	983.09	5.1573-09	3.7363-16	1390.06	5.9	438.96	6.3223*06	4.4473*05	1.1003-04

TABLE VIII
MAXIMUM DENSITY MODEL
DARK SIDE

GEOMETRIC ALTITUDE (KM)	KINETIC TEMPERATURE (DEG K)	PRESSURE (MB)	DENSITY (GM/CM3)	SPEED OF SOUND (M/SEC2)	MOL. WT.	DENSITY SCALE HEIGHT (KM)	NUMBER DENSITY (/CM)	MEAN FREE PATH (M)	COEFFICIENT OF VISCOSITY (KG/M-SEC)
0.0	270.00	3.0003+00	4.7573-06	297.12	35.6	17.44	6.0503+16	2.0993-04	1.7007-05
1.0	269.66	2.8293+00	4.4923-06	296.95	35.6	17.43	7.6013+16	2.2233-04	1.6997-05
2.0	269.36	2.6693+00	4.2423-06	296.77	35.6	17.43	7.1703+16	2.3543-04	1.6977-05
3.0	269.05	2.5173+00	4.0033-06	296.60	35.6	17.42	6.7773+16	2.4933-04	1.6963-05
4.0	268.73	2.3743+00	3.7823-06	296.42	35.6	17.42	6.3993+16	2.6413-04	1.6943-05
5.0	268.41	2.2383+00	3.5713-06	296.25	35.6	17.41	6.0423+16	2.7973-04	1.6933-05
6.0	268.10	2.1113+00	3.3713-06	296.07	35.6	17.40	5.7033+16	2.9623-04	1.6913-05
7.0	267.78	1.9913+00	3.1833-06	295.90	35.6	17.40	5.3833+16	3.1373-04	1.6893-05
8.0	267.46	1.8773+00	3.0033-06	295.72	35.6	17.39	5.0833+16	3.3233-04	1.6883-05
9.0	267.15	1.7703+00	2.8373-06	295.55	35.6	17.38	4.8013+16	3.5203-04	1.6863-05
10.0	266.83	1.6693+00	2.6793-06	295.37	35.6	17.38	4.5323+16	3.7283-04	1.6853-05
11.0	266.52	1.5743+00	2.5293-06	295.20	35.6	17.37	4.2793+16	3.9493-04	1.6833-05
12.0	266.20	1.4843+00	2.3873-06	295.02	35.6	17.37	4.0403+16	4.1833-04	1.6813-05
13.0	265.89	1.4003+00	2.2543-06	294.85	35.6	17.36	3.8143+16	4.4313-04	1.6803-05
14.0	265.57	1.3203+00	2.1283-06	294.68	35.6	17.35	3.6033+16	4.6943-04	1.6783-05
15.0	265.26	1.2443+00	2.0083-06	294.50	35.6	17.35	3.3983+16	4.9723-04	1.6773-05
16.0	264.94	1.1733+00	1.8963-06	294.33	35.6	17.34	3.2083+16	5.2683-04	1.6753-05
17.0	264.63	1.1063+00	1.7903-06	294.15	35.6	17.33	3.0283+16	5.5803-04	1.6743-05
18.0	264.32	1.0433+00	1.6933-06	293.98	35.6	17.33	2.8583+16	5.9123-04	1.6723-05
19.0	264.00	9.8323-01	1.5933-06	293.80	35.6	17.32	2.6983+16	6.2633-04	1.6703-05
20.0	263.69	9.2693-01	1.5033-06	293.63	35.6	17.32	2.5473+16	6.6353-04	1.6693-05
21.0	263.38	8.7383-01	1.4213-06	293.46	35.6	17.31	2.4043+16	7.0303-04	1.6673-05
22.0	263.06	8.2383-01	1.3413-06	293.28	35.6	17.29	2.2693+16	7.4483-04	1.6663-05
23.0	262.77	7.7663-01	1.2653-06	293.12	35.6	17.27	2.1413+16	7.8923-04	1.6643-05
24.0	262.48	7.3213-01	1.1943-06	292.96	35.6	17.26	2.0213+16	8.3623-04	1.6633-05
25.0	262.20	6.9013-01	1.1273-06	292.80	35.6	17.26	1.9073+16	8.8613-04	1.6613-05
50.0	255.08	1.5693-01	2.6343-07	288.80	35.6	17.14	4.4573+15	3.7913-03	1.6253-05
75.0	248.11	3.5303-02	6.0913-08	284.83	35.6	17.01	1.0313+15	1.6393-02	1.5893-05
100.0	241.28	7.8483-03	1.3933-08	280.88	35.6	16.87	2.3563+14	7.1713-02	1.5543-05
125.0	234.59	1.7233-03	3.1453-09	276.95	35.6	16.73	5.3223+13	3.1753-01	1.5183-05
150.0	228.02	3.7333-04	7.0133-10	273.05	35.6	16.58	1.1873+13	1.4243+00	1.4833-05
175.0	221.58	7.9823-05	1.5423-10	269.17	35.6	16.43	2.6103+12	6.4743+00	1.4493-05
200.0	216.76	1.6963-05	3.3103-11	267.82	35.2	16.24	5.6003+11	2.9813+01	1.4373-05
300.0	202.30	4.7213-06	9.1033-14	269.44	32.4	17.71	1.5403+09	9.9963+03	1.4513-05
400.0	361.15	8.5583-10	6.5243-16	428.55	22.9	31.88	1.1043+07	9.8433+05	2.8883-05
500.0	626.08	2.3343-10	7.2353-17	672.09	16.1	62.55	1.2243+06	6.2553+06	5.0183-05
600.0	873.46	1.3833-10	1.8743-17	1017.29	9.8	82.29	3.1713+05	1.4713+07	7.9263-05
700.0	952.87	1.0903-10	1.0413-17	1210.41	7.6	329.84	1.7623+05	2.0403+07	9.5253-05
800.0	963.56	8.9523-11	7.8083-18	1266.94	7.0	365.80	1.3213+05	2.3113+07	9.9913-05
900.0	973.60	7.5633-11	6.0173-18	1326.59	6.4	402.45	1.0183+05	3.0023+07	1.0483-04
1000.0	983.06	6.5453-11	4.7443-18	1389.83	5.9	439.22	8.0263+04	3.5033+07	1.1003-04

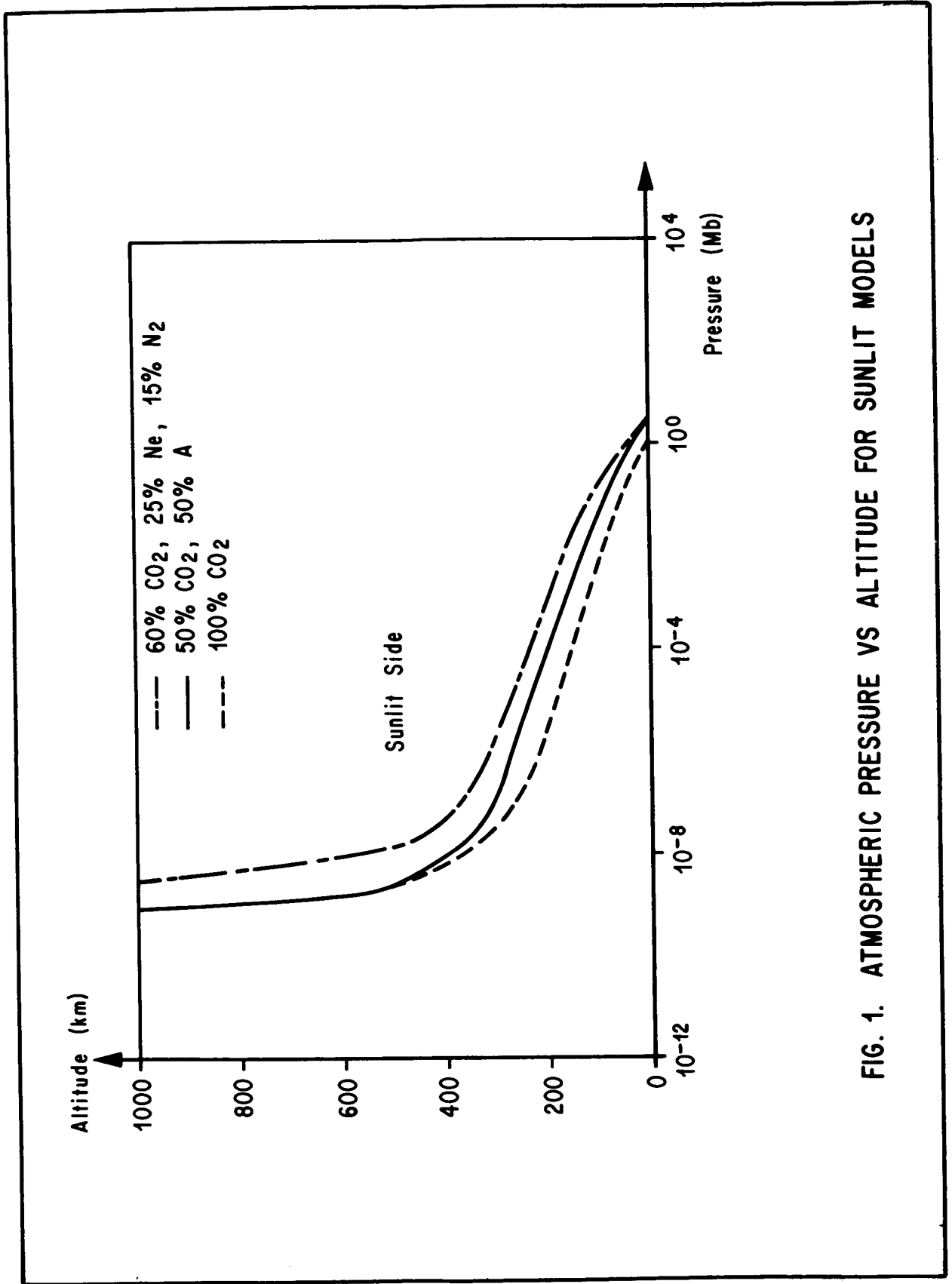


FIG. 1. ATMOSPHERIC PRESSURE VS ALTITUDE FOR SUNLIT MODELS

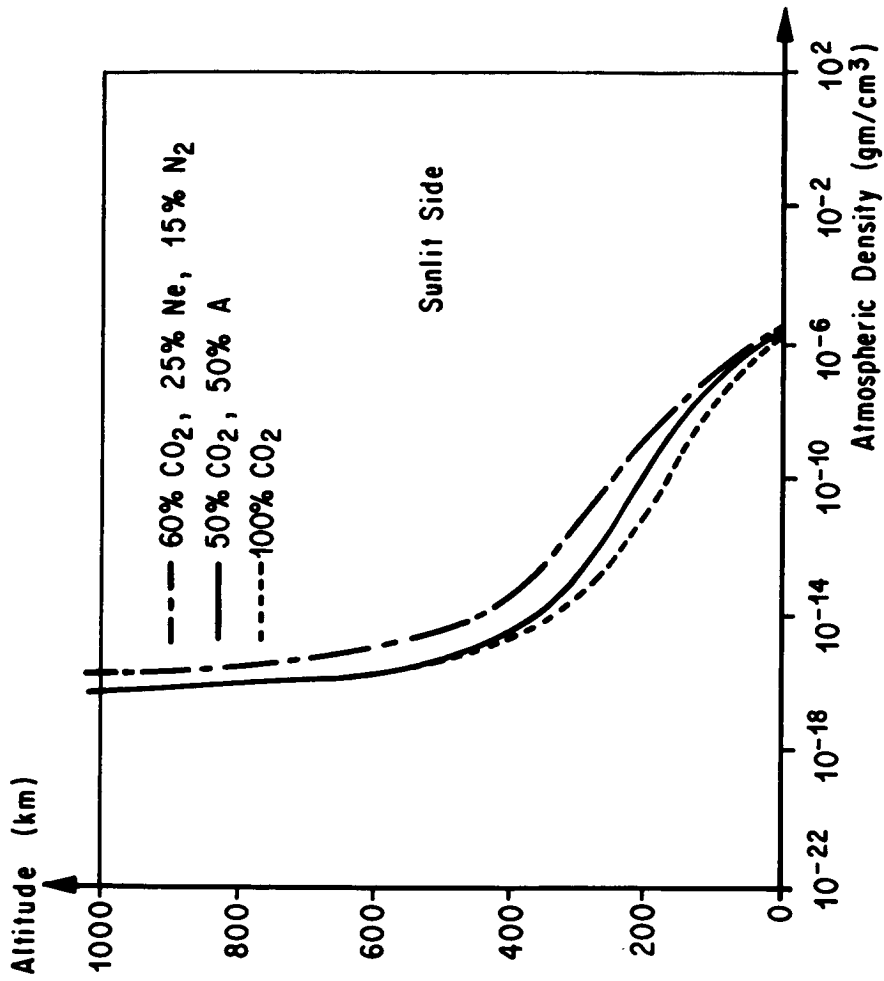


FIG. 2. ATMOSPHERIC DENSITY VS ALTITUDE FOR SUNLIT MODELS

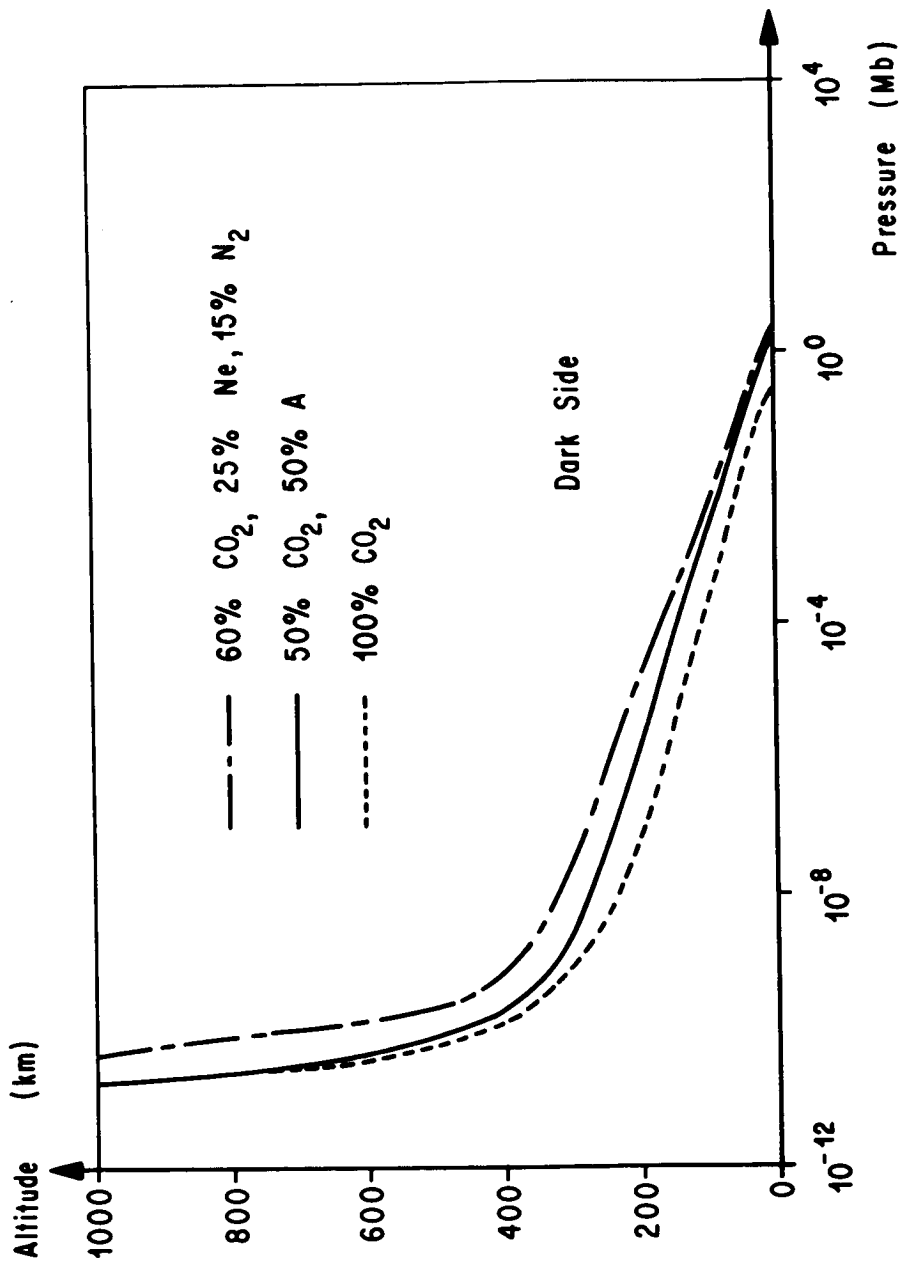


FIG. 3. ATMOSPHERIC PRESSURE VS ALTITUDE FOR DARK SIDE MODELS

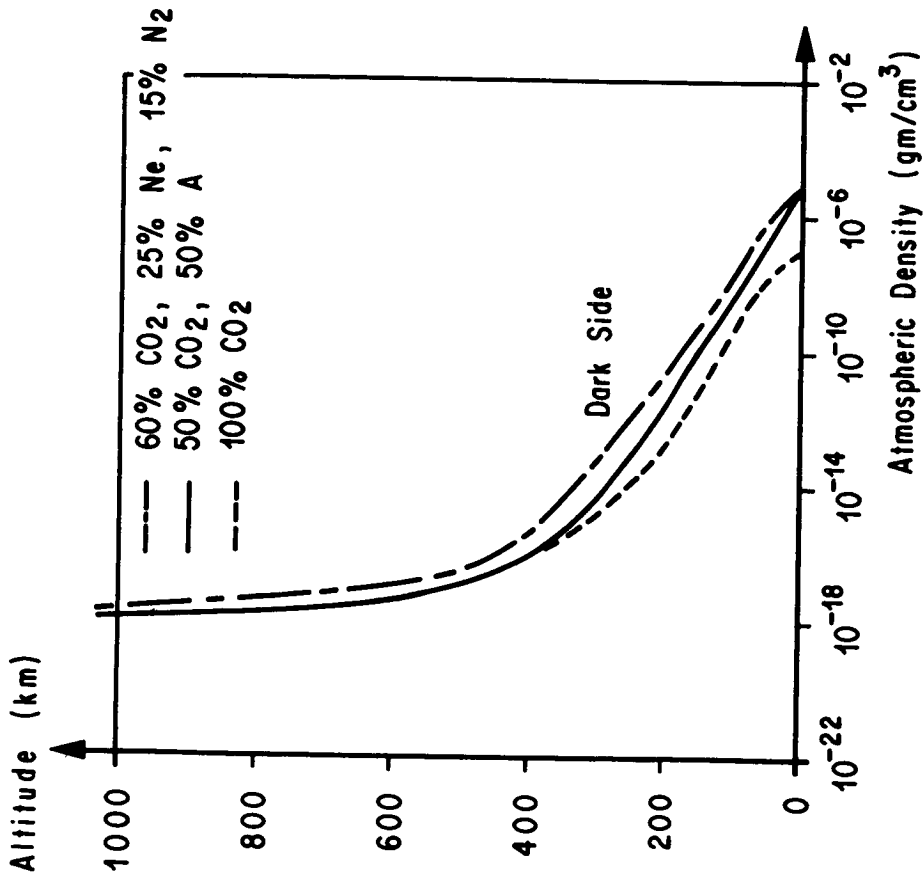


FIG. 4. ATMOSPHERIC DENSITY VS ALTITUDE FOR DARK SIDE MODELS

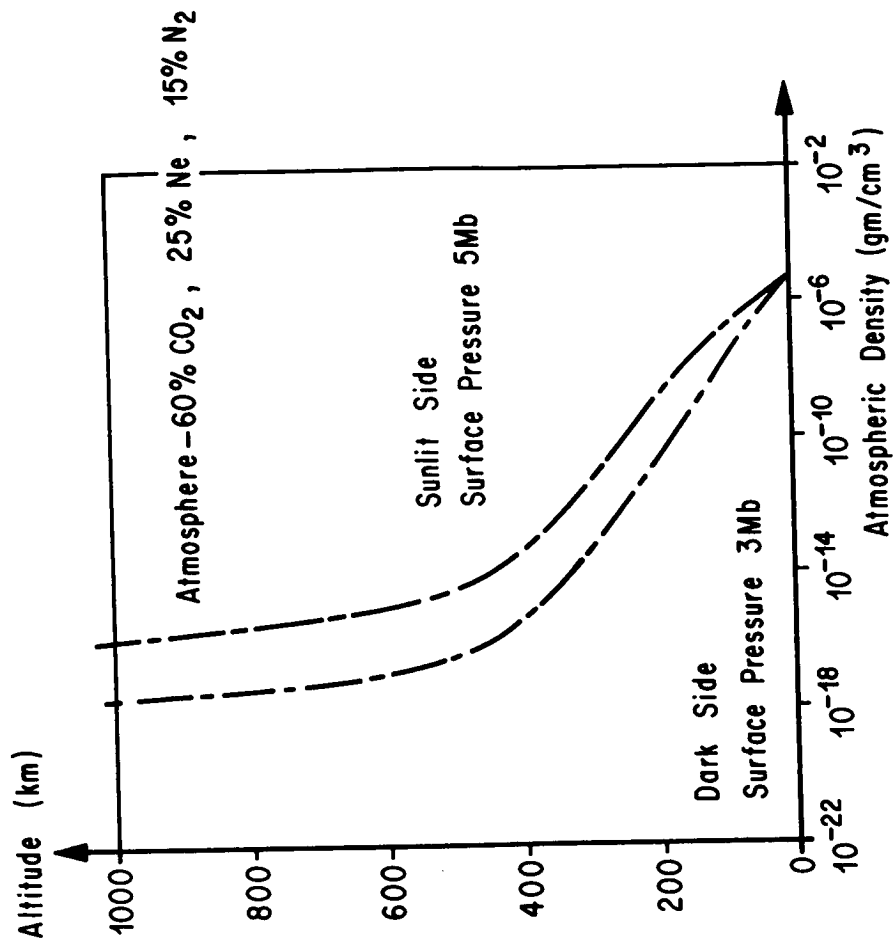


FIG. 5. ATMOSPHERIC DENSITY OPERATIONS ENVELOPE
FOR MAXIMUM DENSITY MODEL

REFERENCES

1. Kuiper, G. P., "The Earth as a Planet," Chicago, Illinois, The University of Chicago Press, Vol. 2, 1954.
2. Kuiper, G. P., and B. M. Middlehurst, "Planets and Satellites," Chicago, Illinois, The Univ. of Chicago Press, Vol. 3, 1961.
3. Kuiper, G. P. and B. M. Middlehurst, "The Moon, Meteorites, and Comets," Chicago, Illinois, The Univ. of Chicago Press, Vol. 4, 1963.
4. Sandner, W., The Planet Mercury, Faber and Faber, London, 1963.
5. Heath, M. B. B., "The Brightness of Mercury at Its Greatest Elongations," Journal of the British Astronomical Association, Vol. 68, 1958, pp. 30-32.
6. Kiess, C. C. and K. Lassovsky, "The Known Physical Characteristics of the Moon and the Planets," Air Research and Development Command, Wright-Patterson AFB, Ohio, July 1958, TR-11, AD115617, Uncl.
7. Krause, H. G., "Astronomical Constants of the Solar System," Unpublished manuscript, 1965, MSFC, Huntsville, Ala.
8. Dollfus, A., "Polarization Studies of Planets," in Planets and Satellites, Solar System II, G. P. Kuiper and B. M. Middlehurst, Chicago, Illinois, The University of Chicago Press, 1961.
9. Foreign Technology Division, Wright-Patterson AFB, "News about Mercury (Carbon Dioxide has Been Revealed in This Planet's Atmosphere)," October 1965, TT-65-64151, AD-622-361, FTD-TT-65-1240, Uncl.
10. Kozyrev, N. A., "The Atmosphere of Mercury," Sky and Telescope, Vol. 27, pp. 339-341, 1964.
11. Rasool, S. I., S. H. Gross, and W. E. McGovern, "The Atmosphere of Mercury," NASA TM X-57322, Goddard Space Flight Center.
12. Barrett, A. H., "Microwave Spectral Lines as Probes of Planetary Atmospheres," Mem. Soc. Roy. Sci. Liege 7, 1962, pp. 197-219.
13. Kozyrev, N., "The Atmosphere of Mercury," The Journal of the British Astronomical Association, Vol. 73, 1963, pp. 345-346.

REFERENCES (Continued)

14. Field, G., "The Atmosphere of Mercury," New York, New York, John Wiley and Sons, Inc., 1964, pp. 269-276, A65-33300. (The Origin and Evolution of Atmospheres and Oceans; Proceedings of a Conference, National Aeronautics and Space Administration, Goddard Space Flight Center, Goddard Inst. for Space Studies, New York, N.Y., 8-9 April 1963; A65-33289 21-30.)
15. Spinrad, H. and P. W. Hodge, "An Explanation of Kozyrev's Hydrogen Emission Lines in the Spectrum of Mercury," *Icarus*, Vol. 4, April 1965, pp. 105-108, A65-23491.
16. Spinrad, H.; G. B. Field, and P. W. Hodge, "Spectroscopic Observations of Mercury," *Astrophysical Journal*, Vol. 141, 1 April 1965, pp. 1155-1160, A65-25226.
17. Ray, Archie E., "Foundations of Astrodynamics," Macmillan Co., New York, New York.
18. Pettengill, G. H. and R. B. Dyce, "A Radar Determination of the Rotation of the Planet Mercury," Arecibo Ionospheric Observatory, Puerto Rico, 1965, AD 629 334, Contract No. AF 49(638)-1156, (published in *Nature*, Vol. 206, No. 4990, 19 June 1965, p. 1240), Uncl.
19. Pettengill, G. H., "Recent Arecibo Observations of Mercury," Symposium on Planetary Atmospheres and Surfaces, Dorado, Puerto Rico, 24-27 May 1965, *Journal of Research, Section D - Radio Science*, Vol. 69D, December 1965, pp. 1627-1628, A66-20119.
20. Peale, S. J. and T. Gold, "Rotation of the Planet Mercury," *Nature*, Vol. 206, 19 June 1965, pp. 1240-1241, A65-27014.
21. McGovern, W. E., S. H. Gross, and S. I. Rasool, "Rotation Period of the Planet Mercury," *Nature*, Vol. 208, 23 October 1965, p. 375, A66-12891.
22. Walker, J. C. G., "The Thermal Budget of the Planet Mercury," *Astrophysical Journal*, Vol. 133, January 1961, pp. 274-280.
23. Barrett, A. H., "Passive Radio Observations of Mercury, Venus, Mars, Saturn, and Uranus," Symposium on Planetary Atmospheres and Surfaces, Dorado, Puerto Rico, May 24-27, 1965. *Journal of Research, Section D - Radio Science*, Vol. 69D, December 1965.

REFERENCES (Continued)

24. Welch, W. J. and D. D. Thornton, "Recent Planetary Observations at Wavelengths Near 1 cm," *Astronomical Journal*, Vol. 70, No. 2, 1965, pp. 149-150.
25. Howard, W. E., A. H. Barrett, and F. T. Haddock, "Measurement of Microwave Radiation from the Planet Mercury," *The Astrophysical Journal*, Vol. 136, 1962, pp. 995-1004.
26. Epstein, E. E., "Disk Temperatures of Mercury and Mars at 3.4 mm," *Astrophysical Journal*, Vol. 143, February 1966, pp. 597-598.
27. Epstein, E. E., J. P. Oliver, and R. A. Schorn, "Further Observations of Planets and Quasi-Stellar Radio Sources at 3 mm," Technical Report 10 April 1965, to 29 April 1966, Aerospace Corp., Laboratory Operation, El Segundo, Calif., July 1966, Report No. TR-669 (9230-04)-1, SSD TR-66-122, Unclassified, AD-487-702, Contract No. AF 04(695)-669, NAS7-100.
28. Kaftan-Kassim, M. A. and K. I. Kellermann, "Temperature of Mercury," *Sky and Telescope*, April 1967.
29. Colombo, G., "Rotational Period of Mercury," *Nature*, November 6, 1965, pp. 575.
30. Colombo, G., and I. Shapiro, "The Rotation of the Planet Mercury," *Astrophysical Journal*, July 1966, Vol. 145.
31. de Vaucouleurs, G., "Geometric and Photometric Parameters of the Terrestrial Planets," *Icarus* 3, pages 187-235, 1964.
32. Brandt, J. C. and P. W. Hodge, "Solar System Astrophysics," McGraw-Hill Book Co., Inc., New York, N. Y., p. 367, 1964

LIMITATIONS IN KNOWLEDGE OF THE
THERMODYNAMIC PROPERTIES OF THE
MARTIAN ATMOSPHERE

by

Wallace W. Youngblood
Nortronics-Huntsville
Huntsville, Alabama

N68-18845

SUMMARY

Current knowledge of the thermodynamic properties of the Martian atmosphere is reviewed, with consideration given to the vertical profiles of composition, temperature, number density, and pressure. There are major uncertainties in these profiles; in particular, a significant area of disagreement resides in identifying the main ionospheric layer measured by the Mariner IV occultation experiment as being analogous to a terrestrial F₂, F₁, or E layer. The latest values of the optical properties of the atmosphere and surface, the thermal properties of the surface, and the convective heat transfer coefficient of the atmosphere near the surface are briefly reviewed and compared.

A brief discussion of potential experiments is given and includes polarization studies of CO₂ and H₂O frosts, determination of the upper atmospheric reaction rate coefficients for temperatures approaching 80°K, and determination of the convective heat transfer coefficient near the Martian surface.

I. INTRODUCTION

The thermodynamic properties of the Martian atmosphere which are considered to have significant importance to spacecraft design and which may lend themselves to laboratory simulation are reviewed. The major objectives of this study were: (1) To review current knowledge of the thermodynamic properties of the Martian atmosphere, (2) To identify and briefly define the significant parameters and their interrelationships, and (3) To suggest experiments that could be performed to clarify or augment existing knowledge of the thermal properties of the Martian atmosphere.

Much of the information concerning the planet Mars is still basically hypothetical, and this lack of definitive data has led to different, even opposite, interpretations of the same observations, and often extrapolations approaching speculation.

Selected for investigation and evaluation were several thermally related parameters, many of which relate to other technical areas and which cannot be easily separated because of their interdependence. A prime example of this,

Prepared for NASA/MSFC under Contract NAS8-20082.

which is of particular interest to this task, is that of dissociation and ionization. These reactions taking place above about 60 km can have a significant effect on the heat balance of the atmosphere and are dependent upon the atmospheric composition, altitude, energy spectrum and flux, recombination rate, etc.

Although most of the thermodynamic experiments suggested in this report could probably be performed in the same basic facility or laboratory, experiments involving larger-scale effects, such as the transport of dust by horizontal winds and cyclonic disturbances, require different types of laboratory apparatus including a low speed, low density flow facility.

II. DISCUSSION

Brooks has published an excellent comprehensive survey paper [1] of the complete Martian atmosphere. Although Brooks' paper is useful as a quick reference for the latest information, it does not expand on the major inconsistencies and uncertainties that remain and which are of great concern in the present study. Where possible, areas that may lend themselves to experimental verification and simulation will be pointed out here. The more significant thermodynamic parameters are discussed in the following paragraphs.

A. Present Knowledge of Selected Thermodynamic Properties

1. Surface (Atmosphere) Temperatures. The term "surface atmosphere temperature" refers here to the temperature of the Martian "air" only a few meters above the solid lithosphere surface. This specification is necessary since it is believed that there can be a large variation in the surface atmosphere temperature and the surface (solid lithosphere) temperature [2]. In fact, as a result of the radio occultation experiment of Mariner IV [3] the surface atmosphere temperature was deduced as approximately $180 \pm 20^\circ\text{K}$, while the surface temperatures were suggested to be approximately 240°K for the relative time, conditions, and location of the Mariner IV measurements. However as discussed in the next paragraph, the surface temperature was based on radiometric observations made before 1956 [4]. Therefore, it is only conjecture at this time that the temperature differential was as high as suggested, although, by analogy, Gifford established that the diurnal variation of the air temperature at 2 meters above the Gobi desert (Earth) in June is only about 25 percent of that at the surface.

The surface atmosphere temperature was calculated from the equation

$$T = H m g/k \quad (1)$$

where H is the number density scale height, m is the mean molecular mass, g is the gravitational acceleration (at Mars' surface), and k is the Boltzmann constant. The scale height (H) was measured by the Mariner IV occultation experiment and the mean molecular mass was based on the assumption that the bulk of the atmosphere is carbon dioxide. Of course, the justification for

the preponderance of carbon dioxide results from the total surface pressure deduced from the occultation experiment being approximately the same as the partial pressure of carbon dioxide (4 to 6 mb) measured spectroscopically from Earth [5 and 6].

Knowing the surface atmosphere temperature and the total molecular number density (n), we can calculate the total surface pressure from the equation of state

$$P = nkT. \quad (2)$$

Obviously, then, the data required to measure the surface atmosphere temperature - other than direct measurements using landing vehicles - is the number density scale height and the surface mass density.

Hopefully, additional instrumented flights will be capable of making similar measurements from which the temperature may be deduced, or even better, measured directly.

2. Surface (Lithosphere) Temperatures. Most of the available knowledge of the surface temperature of Mars comes from radiometric observations assembled by Gifford [4] and Sinton and Strong [7]. Figure 1 [8] gives the observed diurnal temperature variation from observations taken in 1954 [7], when the planet was near perihelion, nearest to the Sun and Earth. The values given in Figure 1 include tentative corrections to the data of Sinton and Strong as made by Opik [9] for imperfect emissivity. The dashed portion of the curve for the nocturnal temperatures represents estimations by Opik [8], who suggests that the large diurnal temperature amplitude indicates a low thermal conductivity of the upper surface materials.

The observations of Sinton and Strong [7] support an extreme diurnal temperature variation of about 100°C at the equator. This extends considerably the diurnal variation from 50°C as reported earlier by Gifford [4]. It has been postulated [2] that the noontime equatorial surface temperature for Mars could be 75°K higher than the air temperature near the surface which indicates very poor thermal coupling between the atmosphere and lithosphere. This poor thermal coupling is attributed in part to a very low thermal conductivity for the surface material [8].

Some more recent average temperature values (Table 1), reported by Johnson [10], are based on observations made at the Mt. Wilson and Lowell observatories using vacuum thermocouples.

Table 1. SURFACE TEMPERATURE DATA FOR MARS

Event	Temperature (°K)
Mean temperature of illuminated disk	248
Tropical diurnal temperature	
Sunrise	225 to 215
Midday	265 to 285
Sunset	280 to 265
Polar Caps	
Average	205
Limbs	260

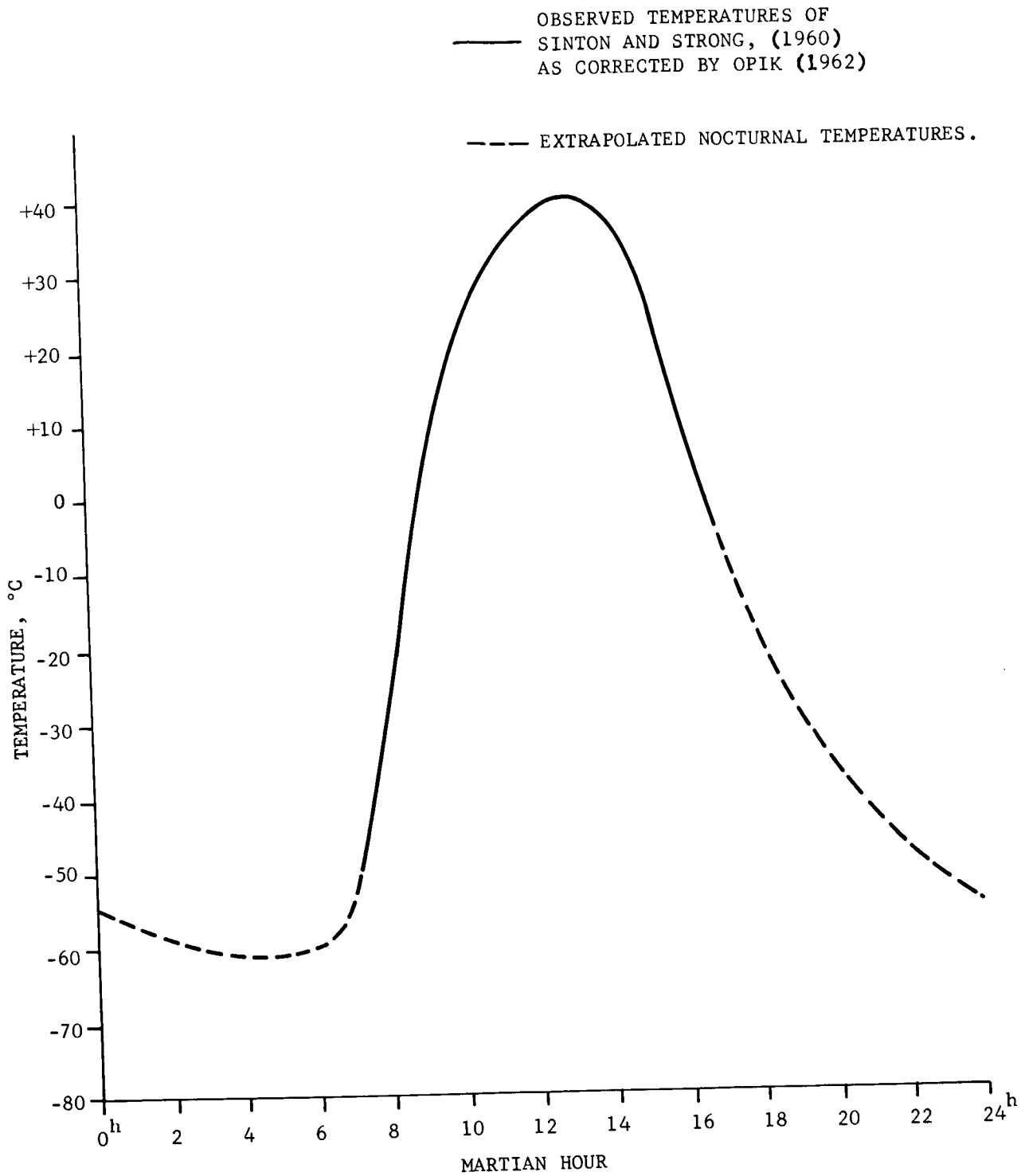


Figure 1. DIURNAL VARIATION OF SURFACE TEMPERATURE ON THE MARTIAN EQUATOR AT PERIHELION

Values of surface thermal conductivity, specific heat, reflectivity, etc., are required to provide a basis for mathematically predicting the surface temperatures. Radiometric observations from orbital vehicles and direct temperature measurements are encouraged. Additional laboratory investigations of the thermo-physical properties of possible Martian surface materials would provide more useful information concerning the composition of the lower atmosphere.

3. Optical Properties of the Atmosphere and Surface.

a. Transmissivity and specific scattering of the atmosphere, and surface reflectivity. Table 2 provides more data on the transmission coefficient (p) and specific scattering (a) of the Martian atmosphere, and the reflectivity (s) of the surface. These values were compiled by Opik [9 and 11] from Russian observations made with a small (6-inch) telescope [12] .

Table 2. SOME SELECTED OPTICAL PROPERTIES
OF THE MARTIAN ATMOSPHERE AND SURFACE

Wavelength (Å)	p	a	s
4600 (Blue)	0.33	0.20	0.25
5200 (Green)	0.54	0.22	0.25
5430 (Green-Yellow)	0.60	0.23	0.34
5800 (Yellow)	0.69	0.24	0.40
6400 (Red)	0.74	0.20	0.53

b. Albedo. According to Opik [8], the albedo for the Martian atmosphere in the blue and violet range is about 0.15. Thus, only about 15 percent of the violet light stopped by the atmosphere is truly scattered in all directions, while 85 percent is absorbed and converted into heat. On the basis of a paper by Kuiper [13], Johnson [10] lists a value of 0.148 for the integrated visual albedo.

However, the acceptance of a value of 0.15 or 0.148 for the integrated albedo seems inadvisable. According to G. de Vaucouleurs [14], "...new data on the spectral reflectivity curve of Mars, in conjunction with the spectral energy curve of the Sun, lead to a value of 0.25 for the radiometric or integral albedo of Mars. This is significantly higher than the visual value of 0.15 often used in the past in theoretical calculations on the heat budget of the planet ...; hence, somewhat less solar energy, in the ratio 0.75/0.85, is available at and near the surface of Mars than we thought previously."

The foregoing paragraph requires careful consideration since some authors are still using albedo values of 0.15 while others are using values of 0.25 to 0.26. For example, Neubauer [15] used a value of 0.26 for the integrated albedo in his study of the thermal convection in the Martian atmosphere, while Leovy [16] used an albedo value of 0.15 in his study of the thermal properties of the Martian surface. This appears to be a serious inconsistency and is a problem area that should be resolved before any further serious studies are made of the overall heat budget.

4. Thermal Properties of the Martian Surface. Most of the following values for the thermal properties of the Martian surface are based on the assumption that the surface near the equator is a fairly homogeneous layer of finely powdered goethite or limonite having a characteristic size of not more than a few microns. Table 3 is a tabulation of some of these latest derived and assumed values and their sources.

Table 3. THE THERMAL PROPERTIES OF MARS SURFACE

Quantity	Units	Value	Reported By Whom	Derived or Assumed Parameter
ρ_d (Density)	gm/cm ³	2.7	Neubauer [15]	Assumed
ρ_d (Density)	gm/cm ³	2.0	Leovy [16]	Assumed
$k\rho_d c$	cal ² /sec cm ⁴ °K ²	1.53×10^{-5}	Neubauer [15]	Derived
$k\rho_d c$	cal ² /sec cm ⁴ °K ²	5.76×10^{-6}	Leovy [16]	Derived
k (Thermal conductivity)	cal/cm sec °K	3.3×10^{-5}	Neubauer [15]	Derived
k (Thermal conductivity)	cal/cm sec °K	2.0×10^{-5}	Leovy [16]	Derived
c (Specific heat)	cal/gm °K	0.173	Neubauer [15]	Assumed
h_c (Convective heat transfer coefficient)	cal/cm ² sec °K	0.35×10^{-4} to 1.1×10^{-4}	Leovy [16]	Derived

a. Density at the surface. Johnson [10] reports calculations made by MacDonald [17] which give a mean surface density of 3.8 to 3.9 gm/cm³ at zero depth. The later values taken by Leovy [16] and Neubauer [15] were based on the assumption that the Martian surface material is similar to finely powdered goethite or limonite (Table 3).

b. The parameter ($k\rho_d c$). A value of 1.53×10^{-5} cal²/sec cm⁴ °K² was calculated by Neubauer [15] from a heat balance based on a temperature curve obtained from Planets and Satellites [18]. The temperature curve used belonged to one of the bright areas believed to consist of goethite or limonite. Leovy [16] calculated a value for $k\rho_d c$ of $\sim 5.76 \times 10^{-6}$ cal²/sec cm⁴ °K² by a similar procedure using a diurnal temperature curve from Sinton and Strong [7]. Their temperature curve was based on observations, all of which were taken within a few latitudinal degrees of the equator.

The value of $k\rho_d c$ derived by Neubauer [15] is larger than the value derived by Leovy [16] by a factor of more than 2. Part of this discrepancy may be due to the different values taken for the albedo (0.15 for Leovy and 0.26 for Neubauer), as discussed above in the section on albedo. Another possible reason for the discrepancy may be the assumption by Neubauer that the

main constituent of the Martian atmosphere is nitrogen rather than carbon dioxide. This does not invalidate the analysis of Neubauer, but the work should be updated with the latest values of pressure and composition.

c. Specific heat. Neubauer [15] obtained the value of specific heat for the surface material from an extrapolation of a table for c (T) of goethite in Landolt-Bornstein [19]. The value taken by Neubauer was $c = 0.173$ cal/gm °K. Leovy [16] cited a value of $\rho_d c \sim 0.30$ cal/cm³ °K which was said to be considered representative of powdery limonite, or of fine quartz sands. Leovy assumed that this product could be broken into $\rho_d = 2$ gm/cm³ and $c = 0.15$ cal/gm °K. The source of Leovy's data was not listed.

d. Thermal Conductivity. The value of $k = 3.3 \times 10^{-5}$ cal/cm sec °K as reported by Neubauer [15] was derived from the product $k\rho_d c$ and the values for goethite and limonite. Likewise, the value of $k \sim 2 \times 10^{-5}$ cal cm sec °K determined by Leovy [16] was determined from the product $k\rho_d c$ as explained previously.

e. Convective heat transfer coefficient. Leovy [16] suggested that the order of the convective heat transfer coefficient should be $h_c \sim 10^{-4}$ cal/cm² sec °K. He was able to conclude this from a heat balance where it was assumed that the linear convective heat-flux was a good approximation for forced convection with steady winds.

5. Surface-to-Atmosphere Thermal Coupling. The thermal coupling in question refers to how well heat is transferred between the surface and the atmosphere. From the literature reviewed thus far, it is apparent that only a very limited amount of knowledge exists on this subject. Most conjectures appear to agree with that of Anderson [2], who suggests that great convective instability can occur in the lowest layers of the atmosphere. As mentioned previously, the wide diurnal temperature variations and the possibly large surface-to-atmosphere temperature differentials could create unstable convective layers near the surface.

The most recent theoretical analyses reviewed concerning thermal convection near the surface of Mars are those by Leovy [16] and Neubauer [15]. Neubauer's paper supports the highly interesting contention that convective instability near the surface can give rise to small-scale cyclonic disturbances (dust devils) and that these disturbances explain the yellow clouds observed on Mars.

Direct measurements of the temperature profiles in these lowest convective layers may be possible if performed by landing vehicles. Measurements obtained from the radio occultation experiment fail because of the uncertainty of the height of specific topographical features along the limb.

6. Atmospheric Composition. Although nitrogen was originally thought to be the major atmospheric constituent of Mars, it is now believed that carbon dioxide is the major constituent because it is compatible with both the Mariner IV occultation experiment and spectroscopic measurements [3].

Brooks [1] summarizes the gaseous composition as follows: "... The gases and vapors can be grouped in three classes according to estimates of

their abundances: (1) CO₂, A, Ne, N₂; (2) O, O₂, H₂O, CO; and (3) O₃, NO, NO₂, N₂O₄, and all others. The total abundances of the groups are of the order of magnitude of 100 m-atm, 5 cm-atm, and 5 micron-atm, or 99.95 percent, 0.05 percent, and 0.000005 percent, respectively, of the total atmosphere. With considerable uncertainty, it can be stated that CO₂ accounts for about 70 percent, argon and/or neon about 20 percent, and N₂ about 10 percent, but it is realized that CO₂ may constitute more than 90 percent of the atmosphere if the total pressure is found to approach the CO₂ partial pressure."

7. Temperature Versus Altitude Profile.

a. Temperature versus altitude profile above the tropopause. There is general agreement among several investigators regarding important temperature points inferred and deduced from the Mariner IV radio occultation experiment. Specifically, agreement exists on a surface atmosphere temperature of approximately $180 \pm 20^\circ\text{K}$ and a temperature of approximately 80 to 85°K in the region near 100 km above the surface [2, 3, 20, and 21]. However, there are two areas of disagreement that should be noticed, one of which appears to be of considerably more consequence than the other.

First, the temperature-versus-altitude profiles below about 100 km are generally in poor agreement although they all tend to follow the same trend (Figure 2). The region of greatest disagreement below 100 km appears to be between approximately 50 km and 90 km. The main explanation given for this disagreement [22] is that the exact sublimation and diffusion times for CO₂ are not completely known for this region. Fjeldo, et al. [3] assumed an F₂ model allowing the temperature below 100 km to dip well below the saturation temperature for CO₂. Johnson [23] also assumed an F₂ ionization model; however, he assumed that the temperature profile from the top of the convective layer (~ 14 km) up to about 100 km approximately follows the vapor-pressure curve for dry ice.

The second, and possibly the most significant, area of disagreement is the temperature-versus-altitude profile in the region of the ionosphere and above. The disagreement resides in identifying the main ionospheric layer measured by Mariner IV as being analogous to a terrestrial F₂, F₁, or E layer. Several investigators including Johnson [23] and Fjeldbo et al. [22] have suggested an F₂ model while Chamberlain and McElroy [24] support the E model. The large and very serious disagreement in the range of temperatures predicted by the two models is shown in Figure 2. The ambiguous interpretations of the Mariner IV radio occultation data at ionospheric heights result in proposed neutral number densities differing by factors up to 10^4 and upper-atmospheric temperatures varying from about 100°K to more than 400°K [22]. This disastrously wide range of values is not a result of design criteria parametric studies, but is, rather, a result of a variety of interpretations of the occultation experiment.

b. Adiabatic lapse rates to the tropopause. Based on the results of Mariner IV, Johnson [23] suggested the F₂ model shown in Figure 2. He assumed that the fall in temperature from the surface atmosphere value to the tropopause through the convective layer should be adiabatic. He suggested that the temperature through most of the atmosphere should run along the dry-ice vapor-pressure line which sets the temperature at the tropopause altitude (~ 14 km) at 140°K . Thus, with a surface atmosphere temperature of 210°K , the adiabatic lapse rate is about $5^\circ\text{K}/\text{km}$ for an atmosphere assumed to consist mainly of carbon dioxide.

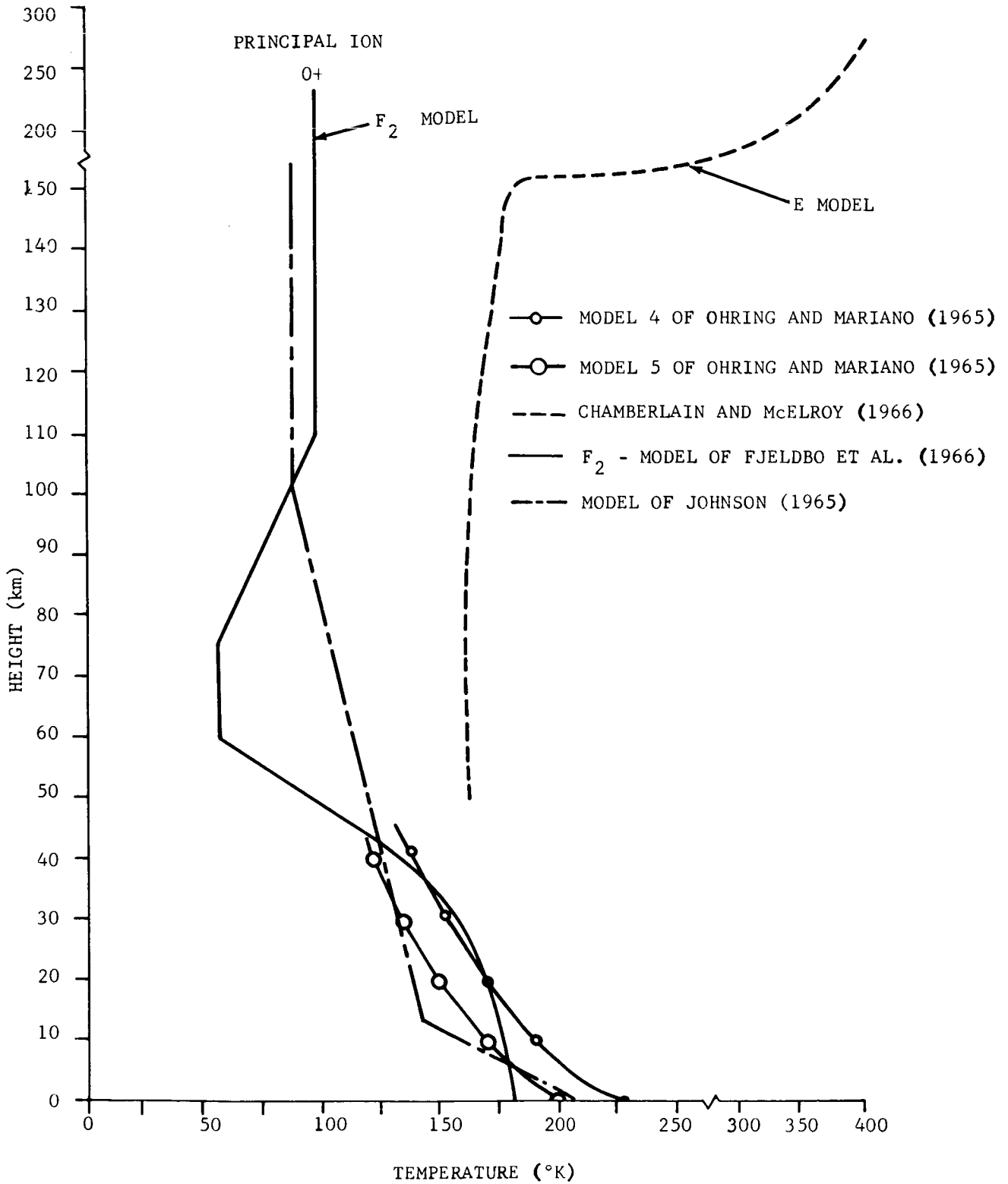


Figure 2. TEMPERATURE VERSUS ALTITUDE FOR SOME SELECTED ATMOSPHERIC MODELS

Models 4 and 5 of Ohring and Mariano [25] are in fair agreement with the model of Johnson [23] in the troposphere and the lower part of the atmosphere to approximately 45 km. Ohring and Mariano assumed adiabatic convective lapse rates to the tropopause, but computed the radiation temperature change rates as a function of altitude. Therefore, the temperature profiles of Ohring and Mariano do not exhibit linear adiabatic lapse rates.

The adiabatic lapse rate calculation by Anderson [2] for a surface atmosphere temperature of 210°K is 5.44°K/km, which is in fair agreement with the 5°K/km determined by Johnson [23]. The adiabatic lapse rate can be determined from

$$A = g/C_p,$$

where g is the acceleration of gravity and C_p is the mean value of the specific heat capacity at constant pressure.

8. Density and Pressure Versus Altitude Profiles. Figures 3 and 4 show comparisons of the number density and pressure versus altitude profiles for various atmospheric models. These models generally represent the results of assuming different atmospheric compositions and making different assumptions about the heat transfer processes taking place.

The models of Weidner and Hasseltine [21] and Evans et al. [26] represent the extreme variability in the Martian atmosphere for the design of spacecraft, and should not be considered as representative of the actual Martian atmosphere. Three model atmospheres of differing atmospheric composition, surface pressure, and surface temperature were assumed by Weidner and Hasseltine (the upper density model - 48.8 percent CO₂ and 51.2 percent N₂; the mean density model - 75 percent CO₂ and 25 percent N₂; and the lower density model - 100 percent CO₂). (The MSFC Planetary Atmosphere Computer Program was used in generating these models.) The lower density model appears to agree quite well with that of Fjeldbo et al., [3] because of the large (100 percent) percentage assumed for carbon dioxide. Weidner and Hasseltine assumed that the atmosphere at 60 km would change from a purely mixed medium to a gas undergoing strong dissociation and diffusive equilibrium. The assumption was made that, when the carbon dioxide is dissociated, the resulting atomic oxygen and carbon monoxide begin to undergo diffusive separation.

The number density profile of Chamberlain and McElroy [24] is based on an available radiative model of Prabhakara and Hogan [27] having a surface pressure of 10 millibars and an assumed composition of 44 percent CO₂ and 56 percent N₂ (including 0.4 percent O₂). They insist that the lifetime of a CO₂ molecule against photodissociation "... is 3×10^6 seconds, or about 1 month, high in the atmosphere. But in the main dissociation region the lifetime is much longer. For example, with photochemical equilibrium...the optical thickness to ultraviolet is 0.4 at the O₂ peak, so that here a CO₂ molecule could survive intact for 10^3 years." In addition, Chamberlain and McElroy assumed that the constituent gases were homogeneously mixed throughout the atmosphere although it was admitted that this is an oversimplification and represents the opposite extreme to models based on complete dissociation. Even when models with much lower densities and temperatures are assumed at the base of the ionosphere, the temperatures calculated for the ionospheric peak and the thermosphere are still

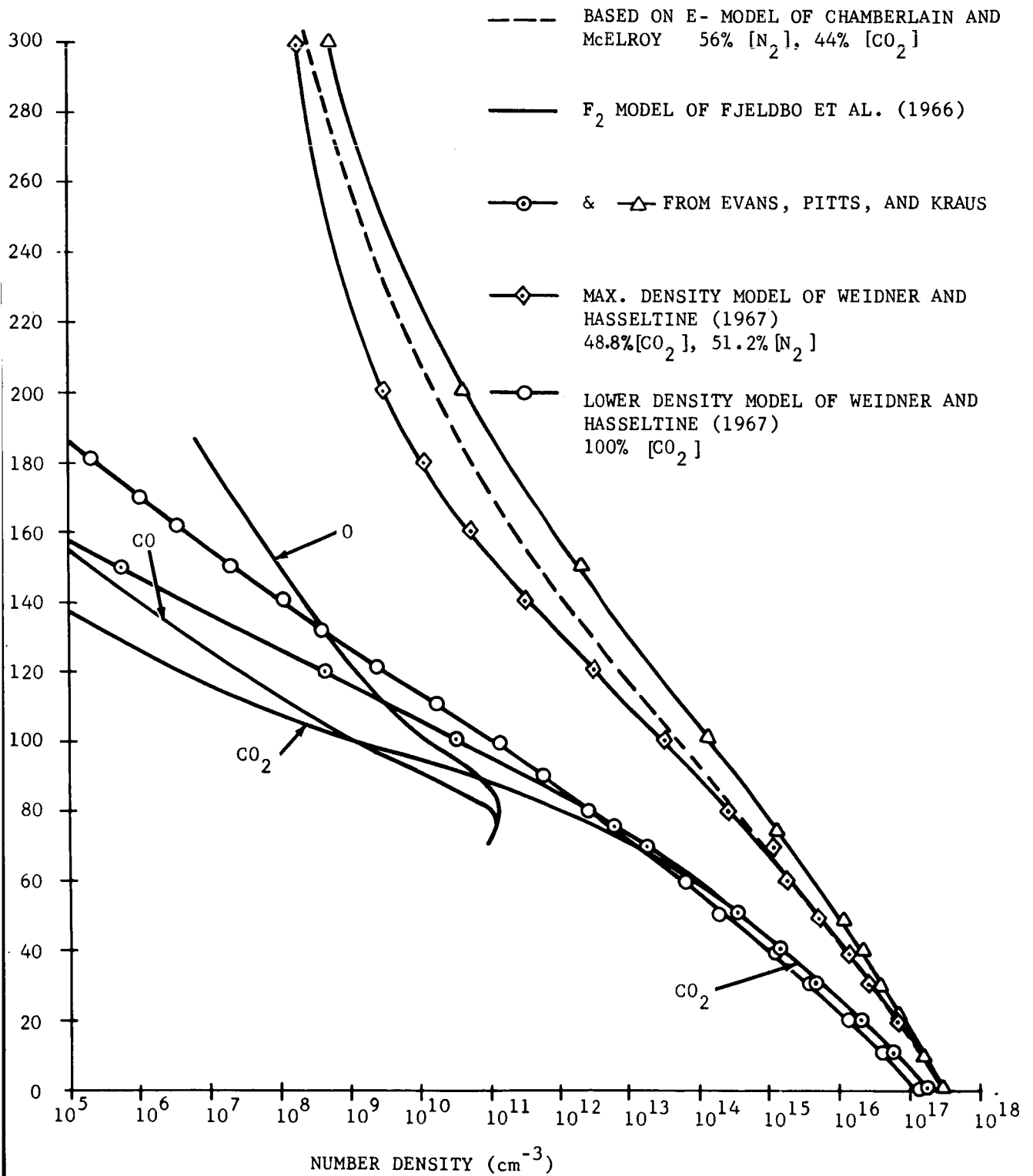


Figure 3. NUMBER DENSITY VERSUS ALTITUDE FOR SOME SELECTED ATMOSPHERIC MODELS

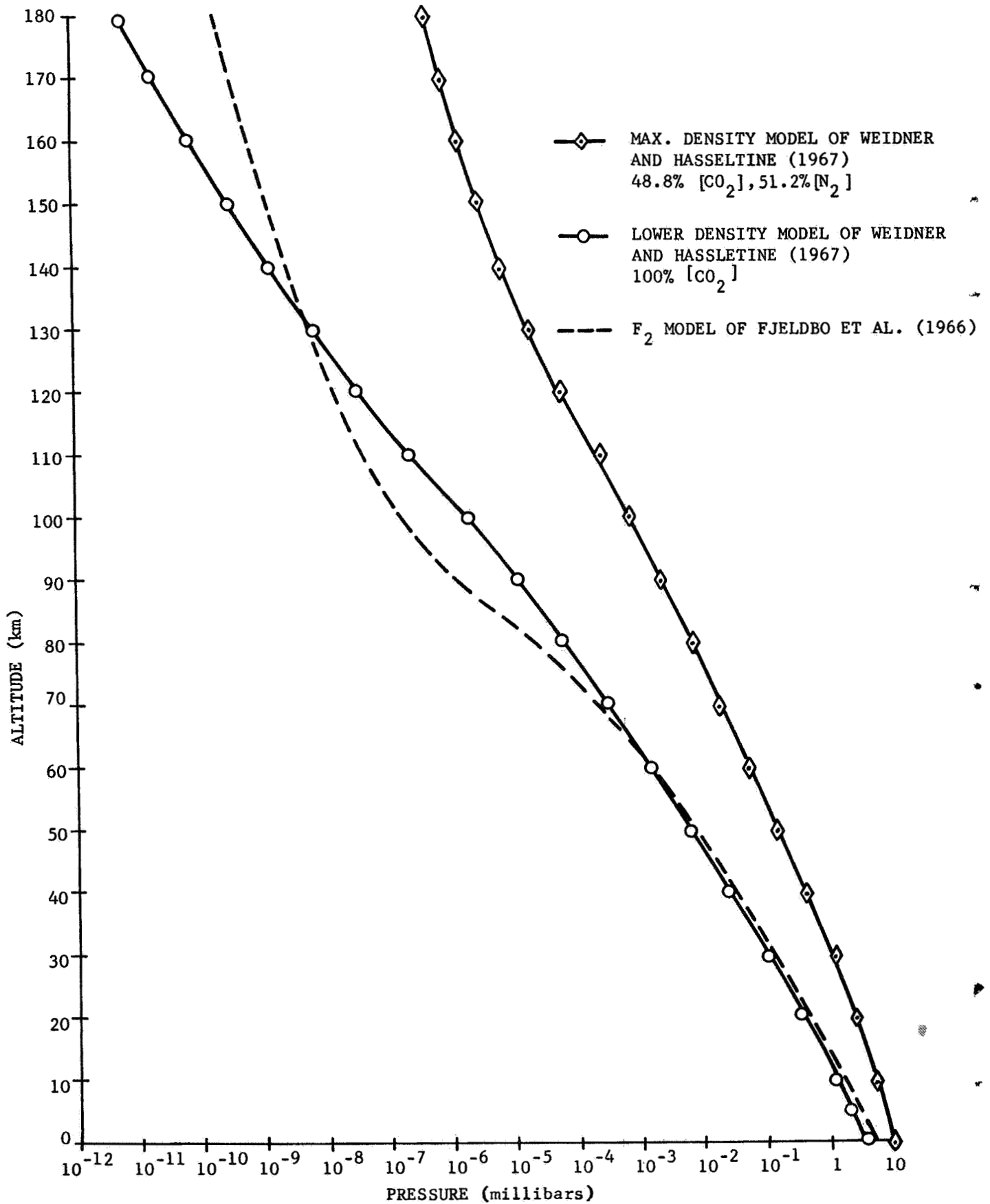


Figure 4. PRESSURE VERSUS ALTITUDE FOR TWO DIFFERENT INVESTIGATORS

extremely high compared to models of other investigators. In particular, Chamberlain and McElroy assumed the temperature (100°K) and density at 70 kilometers as used by Johnson [23] to test the effect of lower temperatures and densities on their model. The height of 70 kilometers was chosen since Johnson suggested that the onset of diffusive separation began at this level and, also, that it was the level at which direct solar heating became important. Chamberlain and McElroy subsequently calculated a temperature of 285°K at 125 kilometers (in the region near the observed ionospheric peak) and an exospheric temperature of 375°K, both of which are in serious disagreement with the nearly isothermal temperature of 85°K as suggested by Johnson.

The previous paragraph concerning the large disagreement in the ionosphere and exosphere temperatures has been included here because it is tied so strongly to the assumed models of density and composition. Model I of Prabhakara and Hogan [27], used in the calculations of Chamberlain and McElroy, seems inconsistent with the generally accepted density and composition models of other investigators who assume the atmosphere to be composed mainly of carbon dioxide [2, 3, and 23].

B. Potential Experiments

The review of present knowledge concerning the Martian atmosphere has pointed out several experiments that could aid in clarifying and explaining certain anomalies and unknowns of the atmosphere. In fact, several assumptions made concerning the Martian atmosphere are based on incomplete data from laboratory experiments performed on Earth.

The potential experiments outlined below are believed to be within the present state-of-the-art and most can be performed in small laboratory facilities.

1. Polarization Studies of CO₂ and H₂O Frosts. There is still a considerable amount of uncertainty concerning the composition and physical make-up of the "polar caps" and the so-called "blue haze." According to G. de Vaucouleurs [28], the polar caps were definitely proven to be "ice" (frozen water) by Gerard P. Kuiper. From Kuiper's direct spectrophotometer investigations, it was theorized that the polar ice caps were not thick snow and ice fields, but were only thin coverings of frost. This theory was still supported as late as 1964 [29].

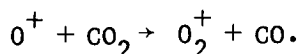
The radio occultation experiment of Mariner IV has shown the surface pressure to be about 4 to 5 mb. This experiment, along with earlier determinations of the partial pressure of CO₂ on Mars, has substantiated the theory that CO₂ is the major constituent of the Martian atmosphere. Also, more accurate surface pressure measurements have resulted in better estimates of the surface (lithosphere) and surface atmosphere temperatures. This new information has prompted the theory that the polar caps are composed mainly of precipitated carbon dioxide with possibly a very thin film of water ice covering the solid carbon dioxide. This theory has been suggested by Leighton and Murray [30] who state that "...CO₂ should precipitate out and accumulate at the higher latitudes during local winter." They felt that the possibility of a thin film of the frozen H₂O at the top of the receding CO₂ polar caps might alter the "...reflective properties of the cap enough to make it appear to be composed of water ice."

Thus, a very simple experiment could be performed to investigate the nature and amount of polarized light given off by various combinations of solid carbon dioxide and water frost formed under the predicted temperature and pressure environment of the Martian polar caps. However, this study would not be entirely conclusive until more accurate surface temperatures are obtained for the regions under consideration.

Although possibly more difficult to simulate under laboratory conditions, additional polarization studies of "clouds" formed of frozen crystals of H₂O and CO₂ may shed new knowledge concerning the so-called "blue-haze" of Mars. Carbon dioxide as well as carbon and hydrocarbon smoke have been suggested by Salisbury [31] as possible candidates for the "blue-haze."

2. Determination of the Reaction Rate Coefficients, k_1 , at Temperatures Approaching 80°K. The Mariner IV occultation experiment has provided new and highly instructive information about the Martian atmosphere. A great deal of conjecture remains concerning the reactions taking place in the Martian upper atmosphere and ionosphere. One such model has been formulated [3] based on present information about the critically important rate coefficients for ion loss processes. The significance of this model is the choice of the critically important reaction and rate coefficient for the loss of ionized oxygen in the main ionospheric layer. Atomic oxygen was chosen to be the principal constituent above some altitude because of its lightness compared to CO, N₂, O₂, Ar, and CO₂. According to Fjeldbo et al., "...the most promising model for the upper atmosphere appears to be the one in which reaction (5) ($O^+ + CO_2 \rightarrow O_2^+ + CO$, $k_1 \approx 10^{-9}$ cm³/sec) is the dominant rate mechanism in the main ionospheric layer." (Rate coefficient, k_1 , times particle density equals loss rate.) However, the rate coefficient (k_1) was taken as that measured at 300°K rather than at 80°K (the predicted ionospheric temperature) and the temperature dependence on the rate coefficient is not well known. Therefore, this atomic-oxygen/carbon-dioxide model of the upper atmosphere may have to be revised when new information is obtained on the temperature dependence of the rate coefficients.

An intensive study should be made of the temperature dependence of the most suitable rate coefficients. This could very possibly be done in a cryogenically cooled vacuum chamber. As discussed earlier, the most important rate coefficient to be investigated is that associated with the loss of ionized atomic oxygen as depicted by the equation



3. Determination of the Characteristic Time Constant for CO₂ Sublimation. Fjeldbo et al. [3] have deduced a temperature versus altitude profile (Figure 2) based on the assumption that all of the CO₂ in the atmosphere is supercooled. However, they suggested that this may well not be the case and that some CO₂ sublimation might take place. They showed that the temperature and number density profiles may deviate widely from the supercooled case if varying amounts of sublimation are allowed. The exact amount of sublimation taking place could not be predicted since the characteristic time constant for the process is not known.

It is suggested that the relative amounts of sublimation nuclei could be determined for different degrees of supercooling in a simulation facility. Such

a facility would require the ability to maintain selected pressures and temperatures while simultaneously being able to determine the degree to which the gas is supercooled. The major problems anticipated with such a study are as follows:

1. Accounting for the gas and sublimation nuclei that condense on the cool chamber walls.
2. Measurement of the actual number of sublimation nuclei present per unit volume for any given condition of temperature and pressure.

It is believed that solutions to these problems can be found. For example, the mass of carbon dioxide being deposited continuously on the cooled walls of the facility may be measured by cryogenic quartz crystal microbalances. The amount of sublimation nuclei present may possibly be measured by visualization techniques such as ultraviolet fluorescence.

4. Determination of the Convective Heat Transfer Coefficient Near the Surface of Mars. One of the most recent calculations of the convective heat transfer coefficient near the surface of Mars was made by Leovy [16]. Leovy suggested a range for this coefficient of $\sim 0.35 \times 10^{-4}$ to $\sim 1.1 \times 10^{-4}$ cal/cm² sec^oK. It was assumed that the linear, convective-heat-flux law could be expected to be a good approximation for forced convection with steady winds. The basic exchange of heat among the ground, atmosphere, and space was assumed to be expressed by

$$h(T_o - T_h) = \epsilon \sigma T_o^4 - R_b + h_c(T_o - T_a),$$

where T_o is the Martian surface temperature, h and T_h are parameters related to radiative processes as well as to conduction and convection in the atmosphere, ϵ is the infrared emissivity of the ground, σ is Stefan's constant, R_b is the flux of back radiation, and h_c is a convective heat-transfer coefficient. The parameter T_a depends on the temperature distribution in the atmosphere.

The convective heat-transfer coefficient near the surface of Mars could be simulated along with the Martian wind and dust storms in the same facility. This should pose little problem since the temperature profile above the surface of the flow facility can be measured readily at several stations. Likewise, measurements of the radiation arriving at the surface of the facility may be taken or estimated.

A major importance of such a measurement of the convective heat transfer coefficient is its relationship to the initiation of winds and dust devils through natural convection. Before performing the aforementioned convective heat transfer tests, the proper scaling laws must be investigated for natural and forced convection under similar circumstances. This could, perhaps, result in the suggestion of smaller-scale tests that could furnish the desired information more efficiently and economically.

III. CONCLUSIONS

The present knowledge of Mars resulting from Earth-based observations and the Mariner IV flyby falls somewhat short of satisfactory design criteria.

Strong disagreements still persist on even the most fundamental aspects of the Martian environment. Thus, the following conclusions may be listed as a result of the present review:

- The main disagreement concerning the vertical structure of the Martian atmosphere involves specification of the main ionization layer observed by Mariner IV as analogous to the terrestrial E, F₁, or F₂ layers.
- Uncertainties still persist in specification of a self-consistent model of atmospheric composition.
- The exact composition of the polar "ice" caps is unknown.
- The correct value for the integral albedo of Mars is unknown.
- The temperature dependency of most atmospheric rate coefficients is unknown for processes taking place at temperatures well below 300°K.
- The temperature and number density profiles are not accurately known even for the region below diffusive separation since the characteristic time constant for carbon dioxide sublimation is not known.

It may also be concluded that the following list of experimental studies would provide useful information concerning the Mars atmosphere.

- Experimental and analytical investigations leading to more accurate and reliable values of the cross sections and rate coefficients for the suspected reactions in the Martian atmosphere.
- Investigations concerning the nature and amount of polarized light given off by various combinations of solid carbon dioxide and water frost formed under the predicted temperature and pressure environment of the Martian polar caps.
- Experimental and theoretical studies to determine the characteristic time constant for the sublimation of CO₂, to better specify the number density and temperature profiles of the Martian lower atmosphere from the tropopause to the lower level of the ionosphere.
- Experimental and theoretical studies to determine the thermal conductivity of the Martian surface and the convective heat transfer coefficient of the near surface atmosphere.

REFERENCES

1. Brooks, E. M., "Comprehensive Summary of the Available Knowledge of the Meteorology of Mars and Venus," NASA Contractor Report, NASA CR-786, May 1967.
2. Anderson, A. D., "A Model for the Lower Atmosphere of Mars Based on Mariner IV Occultation Data," Lockheed Palo Alto Research Laboratory, Palo Alto, California, Rep. No. 6-75-65-62, December 1965.

3. Fjeldbo, G., Fjeldbo, W. C., and Eshleman, V. R., "Models for the Atmosphere of Mars Based on the Mariner IV Occultation Experiment," Stanford Electronics Laboratories, SEL-66-007, January 1966 (1966a).
4. Gifford, F. A., Jr., "The Surface-Temperature Climate of Mars," The Astrophysical Journal, Vol. 123, January-May 1956, pp. 154-161.
5. Kaplan, L. D., Munch, G. and Spinrad, H., "An Analysis of the Spectrum of Mars," Astrophysics Journal, 139, 1964, pp. 1-15.
6. Kuiper, G. P., "Infrared Spectra of Stars and Planets, IV: The Spectrum of Mars, 1-2.5 Microns, and the Structure of its Atmosphere," Communication of the Lunar and Planetary Laboratory, 2, 1964, pp. 79-112.
7. Sinton, W. M. and Strong, J., "Radiometric Observations of Mars," Astrophysics Journal, Vol. 131, 1960, pp. 459-569.
8. Opik, E. J., "The Martian Surface," Science, Vol. 153, No. 3733, 1966.
9. Opik, E. J., Progress in the Astronautical Sciences, Vol. 1, North-Holland, Amsterdam, 1962, p. 282.
10. Johnson, R. W., "Terrain and Soil of Mars," Ninth Annual Meeting of the American Astronautical Society, Edited by: E. Burgess, 15-17 January 1963, p. 406.
11. Opik, E. J., "Journal of Geophysical Research," Vol. 65, 1960, p. 3057.
12. Barabashev, N. P. and Chekirda, A. T., Circ. Kharkov Observ., No. 9, 1952.
13. Kuiper, G. P., "The Atmosphere of the Earth and Planets," American Journal of Physics, Vol. 28, October 1960, pp. 618-622.
14. DeVaucouleurs, G., "Optical Studies of the Surface and Atmosphere of Mars," In: Exploration of Mars, Advances in the Astronautical Sciences, Vol. 15, Edited by G. W. Morgenthaler, 1963, pp. 519-532.
15. Neubauer, F. M., "Thermal Convection in the Martian Atmosphere," Journal of Geophysical Research, Vol. 71, No. 10, 15 May 1966, pp. 2419-2426.
16. Leovy, G., "Note on Thermal Properties of Mars," Icarus, Vol. 5, 1966, pp. 1-6.
17. MacDonald, G. J. F., "On the Internal Constitution of the Inner Planets," Journal of Geophysical Research, Vol. 67, July 1962, pp. 2945-2974.
18. Kuiper, G. P., Ed., Planets and Satellites, University of Chicago Press, 1961, p. 434.

19. Landolt-Bornstein, Zahlenwerte and Funktionen aus Physik, Chemie, Astronomie, Geophysik und Technik, Vol. 3, Springer-Verlag, Berlin, Göttingen, Heidelberg 1952.
20. Kliore, A., Cain, D. L., Levy, G. S., Eshleman, V. R., Fjeldbo, G., and Drake, F. D., "Occultation Experiment: Results of the First Direct Measurement of Mar's Atmosphere and Ionosphere," Science, Vol. 149, 1965, pp. 1243-1248.
21. Weidner, D. K. and Hasseltine, C. L., "Natural Environment Design Criteria Guidelines for MSFC Voyager Spacecraft for Mars 1973 Mission," NASA TMX-53616 Marshall Space Flight Center, Huntsville, Alabama, June 1967.
22. Fjeldbo, G., Fjeldbo, W. C., and Eshleman, V. R., "Atmosphere of Mars: Mariner IV Models Compared," Science, Vol. 153, No. 3743, 23 September 1966 (1966b), pp. 1518-1522.
23. Johnson, F. S., "Atmosphere of Mars," Science, Vol. 150, 1965, pp. 1445-1448.
24. Chamberlain, J. W., and McElroy, M. B., "Martian Atmosphere: The Mariner Occultation Experiment," Science, Vol. 152, No. 3718, 1 April 1966, pp. 21-25.
25. Ohring, G., and Mariano, J., "The Vertical Temperature Distribution in the Martian Atmosphere," Journal of Atmospheric Sciences, Vol. 23, No. 2, March 1966.
26. Evans, D. E., Pitts, D. E., and Kraus, G. L., "Venus and Mars Nominal Natural Environment," National Aeronautics and Space Administration, NASA SP-3016, 1967.
27. Prabhakara, G. and Hogan, J. S., "Ozone and Carbon Dioxide Heating in the Martian Atmosphere," Journal of Atmospheric Sciences, 22, March 1965, pp. 97-109.
28. DeVaucouleurs, G., "Mars," Scientific American, May 1953, p. 65.
29. Owen, R. B., "The Martian Environment," National Aeronautics and Space Administration, NASA-TMX-53167, November 19, 1964.
30. Leighton, R. C. and Murray, B. C., "Behavior of Carbon Dioxide and Other Volatiles on Mars," Science, Volume 153, 8 July 1966, pp. 136-144.
31. Salisbury, F. B., "Martian Biology," Science, Volume 136, Number 3510, April 6, 1962, page 17.

SIMULATION STUDY OF MARTIAN ATMOSPHERIC COMPOSITION

by

T. S. Chang
Nortronics-Huntsville

N68-18846

SUMMARY

The feasibility of obtaining information related to the Martian atmospheric composition by simulating the atmosphere of Mars in an absorption tube is studied. The physical requirements for such an experiment and an existing multiple-reflection absorption tube system are briefly discussed.

I. INTRODUCTION

Our knowledge of the composition of the Martian atmosphere obtained from ground-based observations has been derived primarily from spectrograms taken of Mars. Interpretation of the spectrograms was guided by our understanding of their analogy with spectrograms of the terrestrial atmosphere and comparison with laboratory simulation experiments. The essence of the laboratory simulation experiments is to make an artificial Martian atmosphere, produce its absorption spectrum, and compare this spectrum with that actually taken of Mars. The constituents of the artificial Martian atmosphere are placed in an absorption tube with a solar (or selected) radiation source at one end and an infrared spectrograph at the other. By varying the constituents of the artificial Martian atmosphere, as well as its physical conditions (temperature, pressure, and path length), a variety of spectrograms can be obtained. Comparison of those spectrograms with those actually taken of Mars will show how close the artificial Martian atmosphere is to the real one. In earlier laboratory work, absorption tubes of high pressure (up to 50 atm) and long path (up to 45 meters) were used. However, because of the high pressure broadening of the spectral lines, a reliable gas content could not be obtained [1].

The success of the art of simulation, as we have seen, depends primarily on our ability to create an artificial Martian atmosphere which is as close as possible to the real Martian atmosphere.

Prepared for NASA/MSFC under Contract NAS8-20082.

The first consideration is that the observed Martian spectra are a blend of a solar, telluric, and Martian absorptions. The simulation of these spectra would best be made by channeling natural sunlight, received through the Earth's atmosphere, through the absorption tube that simulates the Martian atmosphere, although one cannot reproduce in this way the apparent radial velocity of the planet [2].

Secondly, the artificial Martian atmosphere in the absorption tube is made up so that the composition, pressure, temperature, and path length are sufficiently close to the actual Martian atmosphere and at its observed conditions. The composition and temperature of the mixture will be chosen from a given Martian atmosphere model. The partial pressure of each constituent times the path length is its abundance, and is chosen from observed data.

II. DISCUSSION

The gas pressure in the absorption tube, to achieve simulation, must be consistent with the pressure exerted by a unit column of such gas mixture transferred to the surface of the planet. The appropriate relation is furnished by the Curtis-Godson approximation, which states that the mean pressure along the absorbing path in a planetary atmosphere is equal to one-half the surface pressure [3]. Thus, for example, with a CO₂ abundance of 55 m-atm and a maximum surface pressure of 5.2 mb, the CO₂ pressure in the absorption tube is 2.6 mb and the required path length, ℓ , of the absorption tube will be

$$\ell = \frac{55}{5.2/2/1000} = 21,200 \text{ meters.}$$

This path length is typical of the requirement for simulation. This did not seem feasible until 1942, when J. U. White [4] developed a multiple-reflection-type absorption tube which could provide, in a reasonably short tube, an absorbing path comparable to the solar spectrum in the Martian atmosphere. An absorption tube used in the Yerkes Observatory, University of Chicago, is depicted in Figure 1. In this apparatus, there are three spherical, concave mirrors of equal radius of curvature. Two of these, A and B, are cut from one circular mirror, as shown in Figure 1b, and are mounted at one end of the tube; the third, C, shaped as indicated in Figure 1c, is mounted at the other end at a distance equal to the radius of curvature. Light from an automobile headlight bulb, or, for ultraviolet work, light from a hydrogen discharge tube, is focused on an entrance slit at 0 in Figure 1a, and 1c. From there, the light falls on the two mirrors, A and B, which form images of the slit at 1 and -1, respectively, the latter being discarded. The mirror C is so adjusted that the light from A received at 1 is reflected to B. With proper adjustment, A is imaged on B, and no light is lost except for reflection losses. The mirror B then forms an image of 1 at 2, whereupon the light is reflected to A, and so on, until the light emerges at 8 after having traversed the space between the mirrors sixteen times. By turning mirror A, small increments about an axis perpendicular to the plane of the paper in Figure 1a, the number of images on mirror C can be readily changed. Using this system with a small glass tube 5 cm in diameter

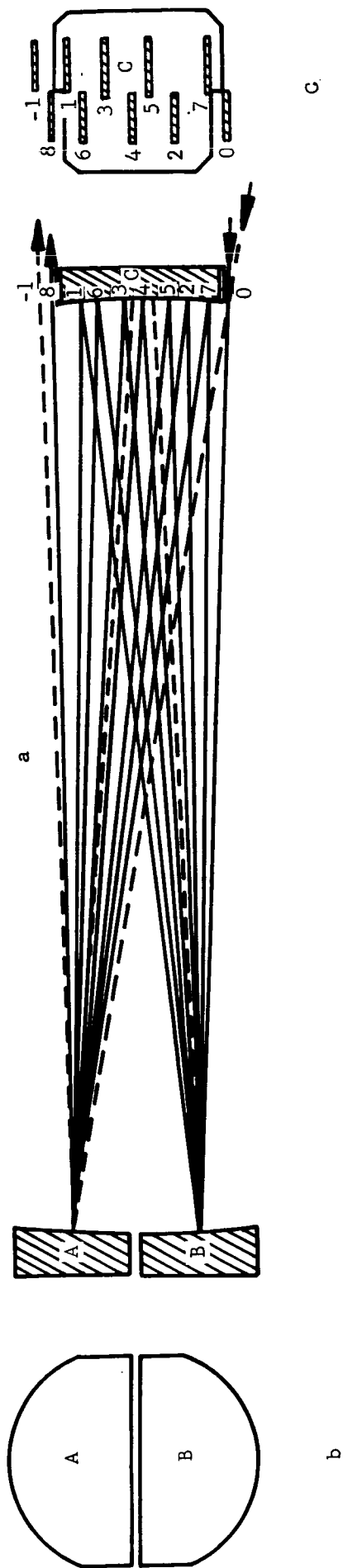


Figure 1. OPTICAL ARRANGEMENT FOR ABSORPTION TUBE, YERKES OBSERVATORY

with mirrors of 150-cm radius of curvature, we can obtain a path length of 60 meters. With a metal pipe 10 inches in diameter and mirrors of 22-meters radius of curvature, a path length of 5500 meters can be obtained. The limit to the number of traversals is set by the reflection losses and by the number of images that can be accommodated on mirror C. If the latter presents no difficulty, the number of traversals through the tube that can be made without decreasing the efficiency of the system can be calculated from the formula

$$R^n = \frac{1}{e},$$

where R is the reflectivity of the mirror, n is the number of traversals, and e is the base of natural logarithms [5].

Figure 2 shows such a long-path gas absorption tube attached to a spectrometer for obtaining infrared absorption spectrum [6].

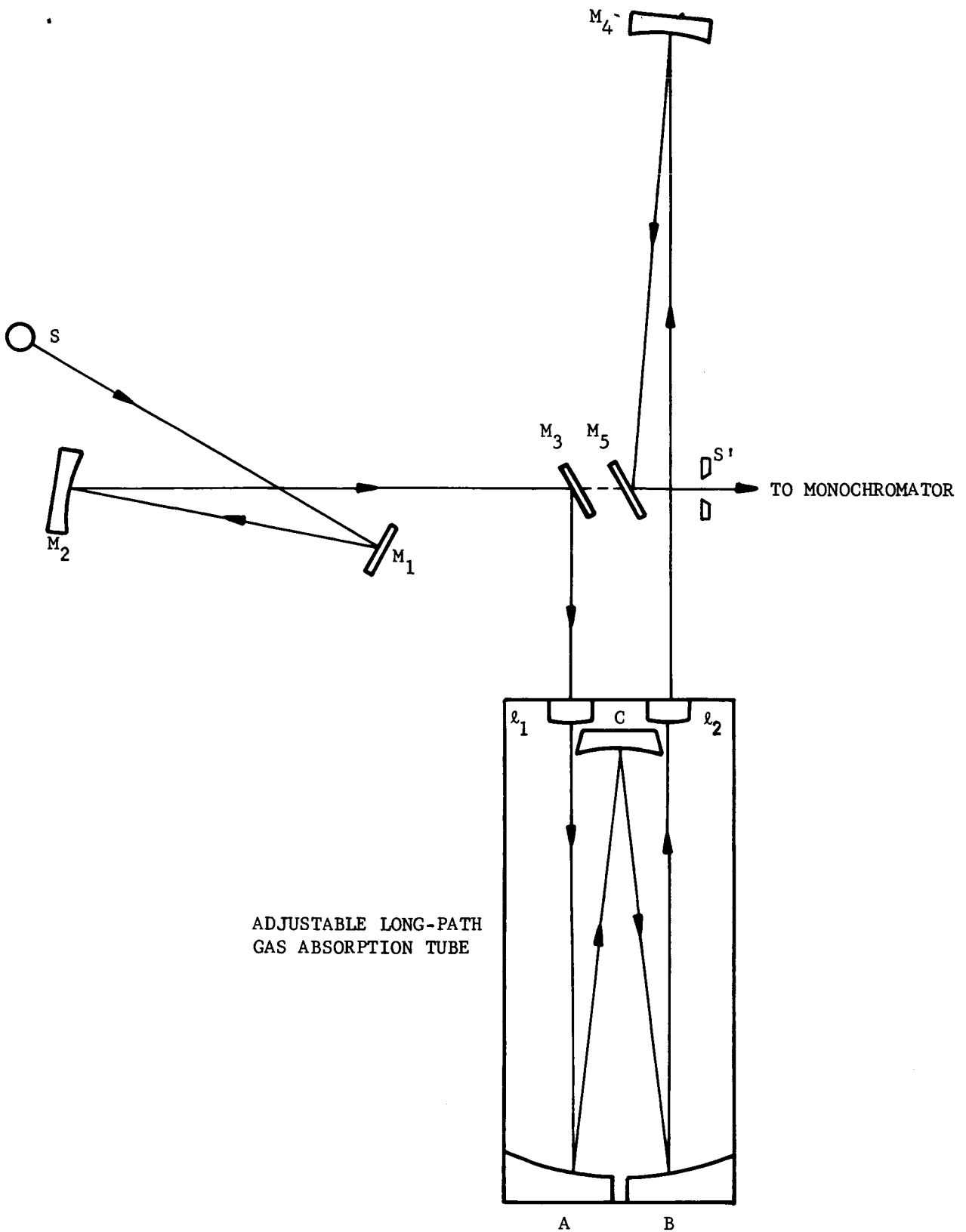
The main function of the windows ℓ_1 and ℓ_2 is to provide a vacuum and pressure seal. Of necessity, the material must be infrared transmitting (generally KBr or NaCl). All mirrors within the tube are prealigned optically and bonded to metal mounting posts. The mirrors A and B are prealigned to the principal optical plane of C and bonded to metal posts with provisions for a push-pull rotational adjustment by screws. Focal adjustment is obtained by movement of the assembly holding A and B. The mirrors M_3 and M_5 are integral to a sub-base, which is kinematically mounted to the main base of the tube and thus can be readily removed. This allows a frequent measure of the radiation without the tube and will permit clearance to the polarizing attachment and sample tubes of other types.

This technique has been used by Herzberg [1] and Kuiper et al. [2].

III. CONCLUSIONS

Presently, because of the tenuous nature of the Martian atmosphere, employing the technique used by Herzberg and Kuiper for its study requires modification. Since partial pressures of the constituents of the Martian atmosphere, as well as path lengths, are important to its study, they must be included in any simulation, and the study must be done at low pressures. In the case of CO_2 the pressure is no higher than 10 mb, that is one-hundredth of the Earth's atmospheric pressure. The path length required for simulating a CO_2 atmosphere will be thousands of meters. For gases other than CO_2 , the partial pressure will be even lower, and correspondingly, the path lengths will be greater. The tenuous Martian atmosphere also prevents astronomers from obtaining clear absorption lines of constituents other than CO_2 which are needed for comparative purposes. These, then, present known problems which must be overcome for successful simulation experiments.

These simulation experiments will give us a better understanding of the Martian atmosphere, which, in turn, will stimulate further activities for the other planets.



ADJUSTABLE LONG-PATH
GAS ABSORPTION TUBE

Figure 2. A LONG-PATH GAS ABSORPTION TUBE INSTALLED FOR OBTAINING INFRARED ABSORPTION SPECTRUM

REFERENCES

1. Herzberg, G., "Laboratory Absorption Spectra Obtained with Long Path," The Atmosphere of the Earth and Planets, Ed. by Kuiper, G. P., Chapter XIII, University of Chicago Press, 1952.
2. Kuiper, G. P., "Infrared Spectra of Stars and Planets, IV: The Spectrum of Mars, 1-2.5 Microns, and the Structure of its Atmosphere," Communications of the Lunar and Planetary Laboratory, Vol. 2, No. 31, The University of Arizona, 1964.
3. Owen T. C., and Kuiper, G. P., "A Determination of the Composition and Surface Pressure of the Martian Atmosphere," Communications of the Lunar and Planetary Laboratory, Vol. 2, No. 32, The University of Arizona, 1964.
4. White, J. U., "Long Optical Path of Large Aperture," Journal of Opt. Soc. of America, Vol. 32, May 1942.
5. Skymanski, H. A., and Alport, N. L., IR Theory and Practice of Infrared Spectroscopy, Plenum Press, New York, 1964.
6. Pilston, R. G., and White, J. U., "A Long Path Gas Absorption Cell," Journal of Optical Society of America, Vol. 44, No. 7, July 1954.

SIMULATION OF THE TRANSPORTATION AND
DEPOSITION OF DUST AND SAND
BY MARTIAN ATMOSPHERIC PROCESSES

by

W. C. Lucas
W. W. Youngblood

Nortronics-Huntsville
Huntsville, Alabama

N 68-18847

SUMMARY

The feasibility of simulating the transportation and deposition of dust and sand under Martian environmental conditions is examined with a view to developing design criteria for Martian missions. The dynamic processes active in the acquisition, transportation, and deposition of unconsolidated material are analyzed and shown capable of producing dust storms and meaningful landforms on the Martian surface.

The basic conditions necessary for the movement of unconsolidated material on the Martian surface are the presence of the material and winds with velocities high enough to move the material. Consideration of the possible geologic processes active on the Martian surface indicate that volcanic, meteoritic impact, and weathering processes would produce unconsolidated material ranging from clay-size particles to boulders. Theoretical calculations made concerning the pertinent dynamic atmospheric processes indicate that threshold velocities one meter above the surface may be as low as 55 m/sec, and that the minimum velocities are for medium-grained sand which should be plentiful. Previous theoretical studies have predicted peak surface wind velocities as high as 143 m/sec. Thus the transportation and deposition of unconsolidated material on the Martian surface is shown as a probability. Consideration of the typical landforms composed of wind-blown sand indicates that the classical desert barchan and seif dunes can be expected on the Martian surface, and that their characteristic shapes will reveal much about the wind direction and velocity. Significantly, these features can be observed remotely and their interpretation used to evaluate photographic data returned from probes and to improve design criteria for later missions. Simulation of the acquisition, transportation, and deposition of dust under Martian environmental conditions is considered feasible within the present state-of-the-art techniques, and promises immediate improvement in design criteria.

I. INTRODUCTION

Present estimates of wind velocities, circulation patterns, and related atmospheric phenomena on Mars are based on observations from Earth, and the results of sparse theoretical studies. These estimates, however, are no more than broad approximations and there is a definite need for improvements to meet the

design criteria requirements for Martian missions. Some improved estimates are expected through further Earth-based observations, better theoretical techniques, and planetary probe data; however, more immediate and reliable gains can be made through vacuum chamber and wind tunnel simulation of the Martian atmospheric processes. Such simulation studies can contribute much to developing empirical and theoretical techniques, particularly for exploring the interrelationships between the atmosphere and surface materials. The nature of an atmosphere, terrestrial or planetary, governs the effectiveness of weathering, wind erosion, and deposition. In turn, dust clouds and eolian (wind) landforms, which may be observed remotely, are products of atmospheric processes and surface geologic characteristics. Thus, the dust clouds and eolian landforms are important because they can be observed remotely and interpreted for what they reveal of the related atmospheric processes.

This study considers the previous experimental and theoretical work on the transportation and deposition of sand and dust by atmospheric processes as a point of departure, then develops the applicable theories to the point necessary to determine the feasibility of meaningfully simulating those processes of the Martian atmosphere.

A brief review of the physics of eolian processes is made from which appropriate theories are developed to determine whether unconsolidated material exists on the Martian surface, and whether the winds could have velocities high enough to move the material. The determination includes consideration of horizontal, vertical, and cyclonic (dust devil) winds as possible transporting agents. Sand dunes, as typical eolian surface features, are reviewed and their shapes related to winds as a means of determining the atmospheric significance of eolian surface features.

In addition, the types of facilities necessary to simulate the various atmospheric processes are investigated and summarized in the study.

II. PHYSICS OF EOLIAN PROCESSES

The problem of particle movement in air, or in fluids in general, has not been studied in any great depth except in limited areas to meet the needs of a particular discipline or problem. The deposition of silt and sand in rivers and harbors, rock ingestion in jet engines, pipeline transportation of particles, determination of the geological history and formation of sedimentary rocks, and the interpretation of eolian landforms are just a few of the areas that have been investigated. Only in two areas have comprehensive investigations been made: the acquisition, transportation, and deposition of sand (0.1 - 1.0 mm diameter) in a desert environment [1] and the rate of fall of individual particles through a fluid at rest [2, 3]. In both areas, theoretical and experimental approaches were used. The laboratory investigations of sand movement [1] also were supplemented by field investigations.

Bagnold's studies [1] are of particular interest because they show that a combined theoretical and experimental program can reasonably predict the behavior of spherical sand-size particles under various wind conditions. His extensive work covers such areas as the various factors influencing the acquisition of particles (particle characteristics, wind direction and velocity, surface

characteristics, gravity, etc.); transportation of particles (suspension, saltation, and surface creep); and deposition of the particles (true sedimentation, accretion, and encroachment).

An extensive investigation of the physics of particle movement in the Martian environment was not undertaken in this study; rather, only those areas are discussed that would furnish clues to the probability of movement of sand and dust by Martian winds and that would aid in determining the test requirements of a simulation facility.

Two basic conditions must be met before the movement of sand and dust can take place on Mars: (1) the presence of unconsolidated material, and (2) winds with velocities high enough to move the material. The presence of unconsolidated material on the Martian surface was established in reference 4. The quantity and characteristics of the unconsolidated material are directly related to the rock types present and the geologic processes active on the surface. Typical rock types expected to be found on the Martian surface are basalt, andesite, obsidian, stoney-iron meteorites, etc. The three geologic processes which are readily seen as sources of unconsolidated material are volcanism, meteoritic impact, and gradation.

The unconsolidated material on Mars formed during meteoritic impacts and volcanic eruptions should closely resemble that found on Earth. However, this is not thought to be true in the case of sediments formed by Martian gradation processes because, on Earth, chemical weathering, physical weathering, and a variety of erosional agents (water, wind, ice, etc.) are active. Water, through erosion and chemical weathering, is the dominant influence in determining the characteristics of most terrestrial sediments and, in particular, the formation of clay-size particles. The apparent absence of large amounts of water indicates that, while clay-size particles (<0.0039 mm) may be present, the extent and quantity will be much less than found on Earth.

Many investigators believe [5, 6] that the Martian surface is smooth when compared to the Earth. Ryan, in his paper on Martian yellow clouds [7], considered the maximum grain diameter of surface material to be less than 100μ and probably less than 50μ . However, careful consideration of possible Martian geologic processes indicates a much broader range of grain sizes. For example, volcanism and meteoritic impacts would produce unconsolidated material ranging from clay-size particles to boulders. Also, physical weathering would generally produce coarse grained material, with the actual grain size determined largely by type and texture of the parent rock. Grain sizes as large as 2 to 4 mm should not be uncommon. The unconsolidated material furnished by these sources then would be transported and deposited over much of the planet's surface by winds. Thus, we believe that unconsolidated material may be wide-spread on the Martian surface and that the material may occur as well- to poorly sorted sediments. The well-sorted sediments are expected to consist mostly of clay- and sand-size particles, while the poorly sorted sediments may include particles ranging from clay sizes to boulders.

Winds with velocities high enough to move the unconsolidated material and form sand and dust clouds also appear to be present on the Martian surface. Yellow clouds have been observed on the Martian surface, usually in the lower latitudes and predominantly in the southern hemisphere. The clouds are generally local in extent and dissipate in a matter of a few days. However, there have

been occasions (1956) when the entire disc was covered for several weeks. Photometric and polarization studies imply that the yellow clouds are composed of solid particles.

The velocities of these cloud movements have been measured telescopically (accuracy $\pm 25\%$) on numerous occasions [8]. The maximum velocity, observed in 1956, is 24.69 m/sec. Numerous other measurements have shown velocities in the 10 to 12 m/sec range. If Earth analogy is valid, it is probable that winds within the clouds are higher than the velocity of the cloud movement itself. Theoretical studies have produced estimates of peak surface wind velocities as high as 143 m/sec [9].

Two types of phenomena which may be responsible for the movement of unconsolidated material on Mars are horizontal and vertical winds associated with large-scale climatic disturbances and small-scale cyclonic systems (dust devils).

A. Horizontal and Vertical Winds as Agents for Transporting Martian Unconsolidated Material

Only a few investigators have approached the problem of sand and dust movement on Mars from a theoretical point of view in any degree of detail. Ryan, [7], using 25-mb and 80-mb atmosphere models, discussed the winds required to initiate grain motion and to maintain them aloft, the range of particle sizes that may make up dust and sand clouds, and the probable result of the depositional phase of the eolian processes. A JPL document [8] basically updates the Ryan paper by recalculating many of the results, using pressure values of 14 mb and 40 mb.

Ryan's conclusions concerning the Martian threshold velocities are the results of calculations based on Bagnold's fluid threshold equation (Prandtl's rough surface law). The calculations made in this report are also based upon this basic equation and the numerical data in Table 1. Bagnold's fluid threshold equation is

$$v_t = 5.75A \sqrt{\frac{\sigma - \rho}{\rho} gd} \log \frac{z}{k} \quad (1)$$

where

v_t = Threshold fluid velocity at any height

A = Dimensionless parameter

σ = Particle density

ρ = Atmospheric density

g = Gravity field strength

d = Particle diameter

z = Height above the ground

k = Roughness factor ($\approx 1/30$ the effective grain diameter).

This equation may be restated as

$$v_t = 5.75 V_{*t} \log \frac{z}{k} \quad (2)$$

where V_{*t} , the threshold velocity gradient, is equal to

$$A \sqrt{\frac{\sigma - \rho}{\rho} g d} \quad (3)$$

Bagnold found experimentally that the dimensionless parameter A was primarily dependent on the Reynolds number (Re) which is defined as

$$Re = \frac{(\text{velocity } V_{*t})(\text{size dimension } d)}{(\text{kinematic viscosity } \gamma)} \quad (4)$$

The critical Reynolds number value was found experimentally to be 3.5. For particles with Reynolds numbers greater than 3.5, A is nearly constant. In air on Earth this value of A is approximately 0.1. For particles with Reynolds numbers less than 3.5, the value of A, which was found by Bagnold through experimentation, is not constant.

No experimental work has been performed under Martian environmental conditions to determine values of A. Thus, we assume in this study that the fluid threshold equation is valid for Mars and that the dimensionless parameter A for Mars (A_m) is approximately equal to the dimensionless parameter A on Earth (A_e) for a given Reynolds number. The relationships of the Reynolds number to coefficient A_e were calculated using equations (3) and (4) from data found in reference 1. The Re to A_m to d relationships for Mars were then determined using the following equation:

$$Re = \frac{d}{\gamma} \left[A \left(\frac{\sigma - \rho}{\rho} g d \right)^{\frac{1}{2}} \right] \quad (5)$$

Equation (5) is solved for d using numerical data for the two atmospheric models [9] given in Table 1 and terrestrial values of Re and A. With the relationships between Re, A_m , and d known, the fluid threshold velocities then can be found using equation (1) for various heights above the surface and for different roughness factors.

Table 1. MARTIAN ENVIRONMENTAL DATA

	Gravity (cm/sec ²)	Atmosphere (Surface)						
		Density (gm/cm ³)	Pressure (mb)	Composi- tion %		Kinematic Viscosity (cm ² /sec)	Mean Free Path (m)	Coefficient of Viscosity (kg/m-sec)
				CO ₂	N ₂			
Model 1	375	1.5657	10	50	50	11.0	6.414x10 ⁻⁶	1.7252x10 ⁻⁵
Model 2	375	1.2096	4	100	0	9.8	1.020x10 ⁻⁶	1.1827x10 ⁻⁵

As discussed earlier, we disagree with the general opinion that Mars is extremely smooth and consider it to be as rough or rougher than the Earth. With this assumption, we calculated the fluid threshold velocities at a height of one meter above the surface using recent Martian atmosphere data (Model 1 and Model 2 given in Table 1). The four different values (0.03, 0.05, 0.1, and 0.2 cm) for the roughness factor (k), which were used in the calculations, represent surfaces composed of particle sizes ranging from 9 to 60 mm in diameter. The results of these calculations are shown in Figures 1 and 2.

The high wind velocities indicated by these calculations are not the minimum wind velocities necessary to cause sand and dust movement on the Martian surface. There exists a critical wind velocity, less than the fluid threshold velocity of a given surface, where saltation once set in motion can just maintain itself indefinitely down-wind of the disturbance. This critical velocity was termed by Bagnold as the "impact threshold velocity." Bagnold's experimental results show that impact threshold velocities are approximately 20 percent lower than those for the fluid threshold. Upon the assumption that this phenomenon is valid for Mars, the minimum impact threshold velocity based on the data in Table 1 would be approximately 55 m/sec. Considering the possibility of a high gust of wind, an earthquake, meteor impact, landslide, etc., originating the saltation of particles, it is possible for these movements to grow into dust or sand storms, and to form eolian landforms. Additional calculations by the authors to determine the effect of grain density on the fluid threshold velocities showed that the difference in densities between feldspar (2.5 g/cm^3) and pyroxene (3.6 g/cm^3) had little influence on the fluid threshold velocity of a particular surface. However, while the fluid threshold velocity is practically unaffected, the impact threshold velocity may be noticeably lower. This possibility, however, has not been confirmed and will require additional study.

The vertical winds required to keep particles aloft must be considered along with the fluid threshold velocities required to initiate particle movement. Using the Cunningham-Stokes equation for particles less than 10μ , the Stokes equations between 10 and 100μ , and graphically solving for particles greater than 100μ , Ryan [7] determined that vertical wind velocities required to maintain particles aloft on Mars are less than for Earth over a large range of sizes (1 to 300μ for an atmospheric pressure of 80 mb , and 4 to 200μ for 25 mb).

Using Models 1 and 2, we recalculated these vertical wind velocities showing (Figure 3) that even with a 4-mb atmosphere, particles ranging in size from $\approx 14 \mu$ to $\approx 140 \mu$ in diameter will require lower vertical wind velocities to maintain them aloft on Mars.

The significance of these calculations is seen when the probable Martian surface and environmental conditions are considered. The unconsolidated material on the Martian surface is believed to be typically composed of a wide range of grain sizes resulting from the action of volcanic, meteoritic impact, and gradation processes. Assuming such a surface and a Martian wind with velocities great enough to initiate and sustain movement of grains 0.4 to 0.6 mm in diameter, it is logical that clay-size particles present will be dislodged and carried into the atmosphere. Once these small particles are air-borne, their settling rates, implied by the vertical wind velocities shown in Figure 3, will be similar to and in some cases less than on Earth.

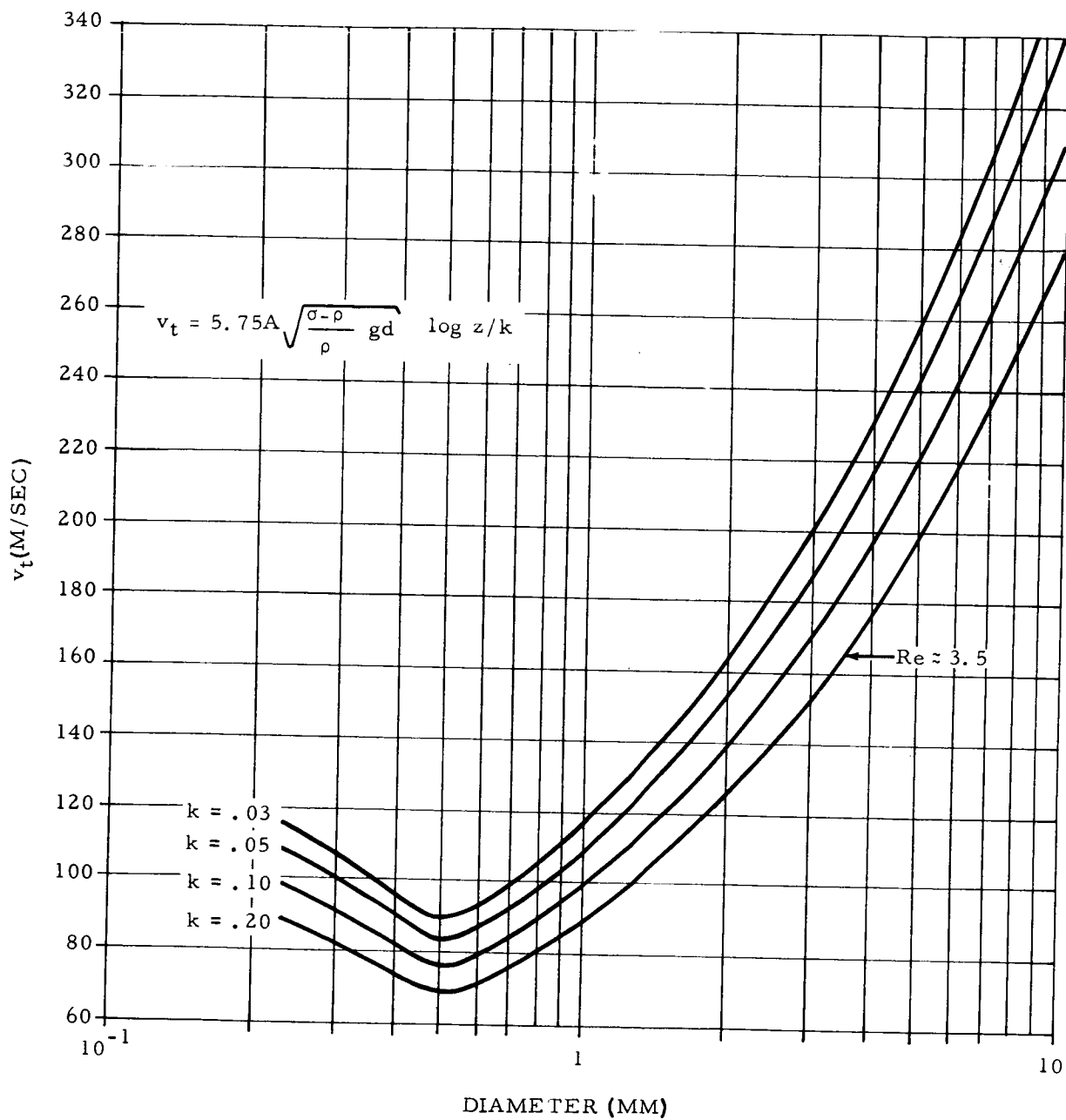


Figure 1. FLUID THRESHOLD VELOCITY AS A FUNCTION OF PARTICLE SIZE FOR ATMOSPHERE MODEL 1 AT A HEIGHT OF ONE METER ABOVE THE SURFACE

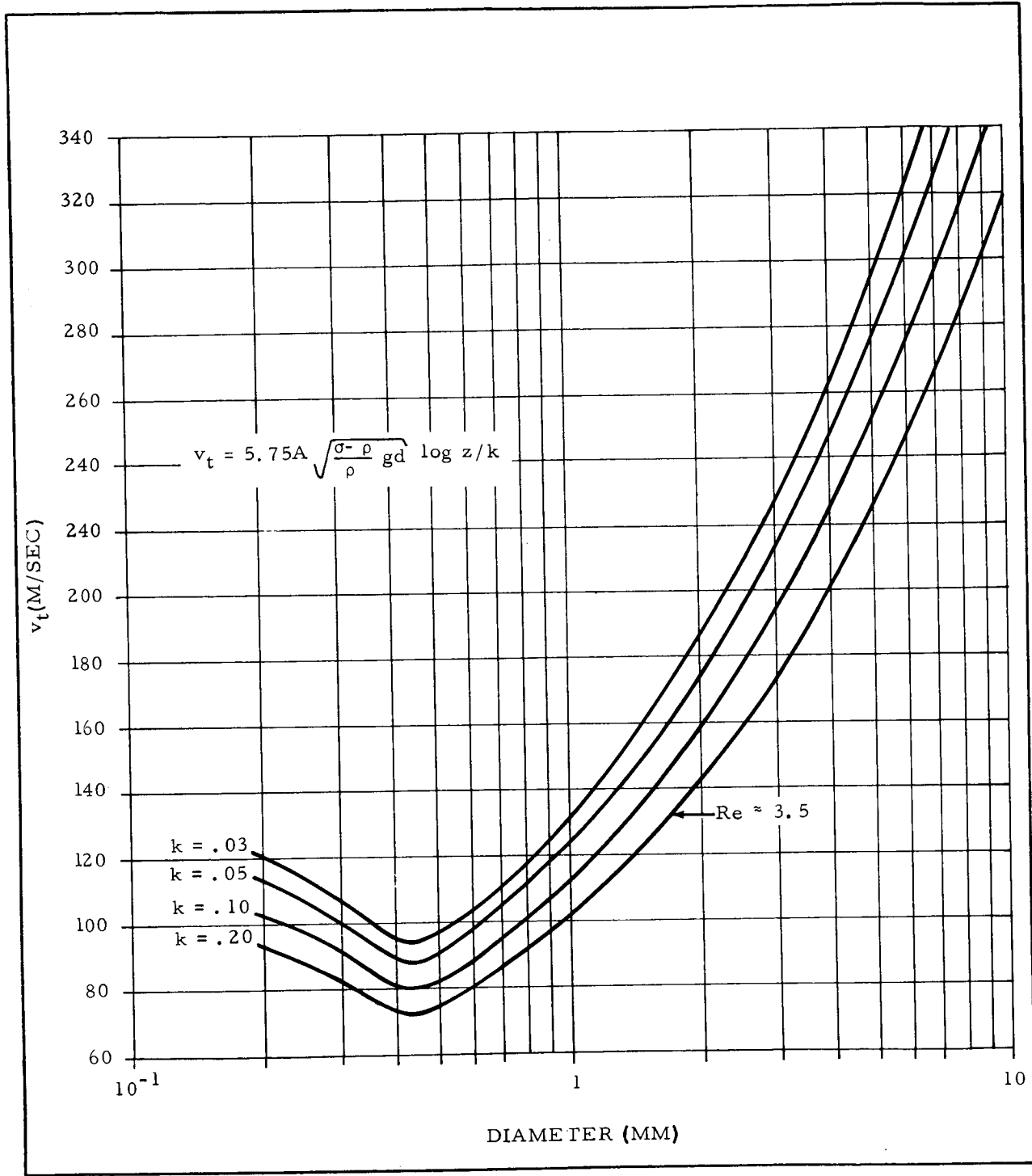


Figure 2. FLUID THRESHOLD VELOCITY AS A FUNCTION OF PARTICLE SIZE FOR ATMOSPHERE MODEL 2 AT A HEIGHT OF ONE METER ABOVE THE SURFACE

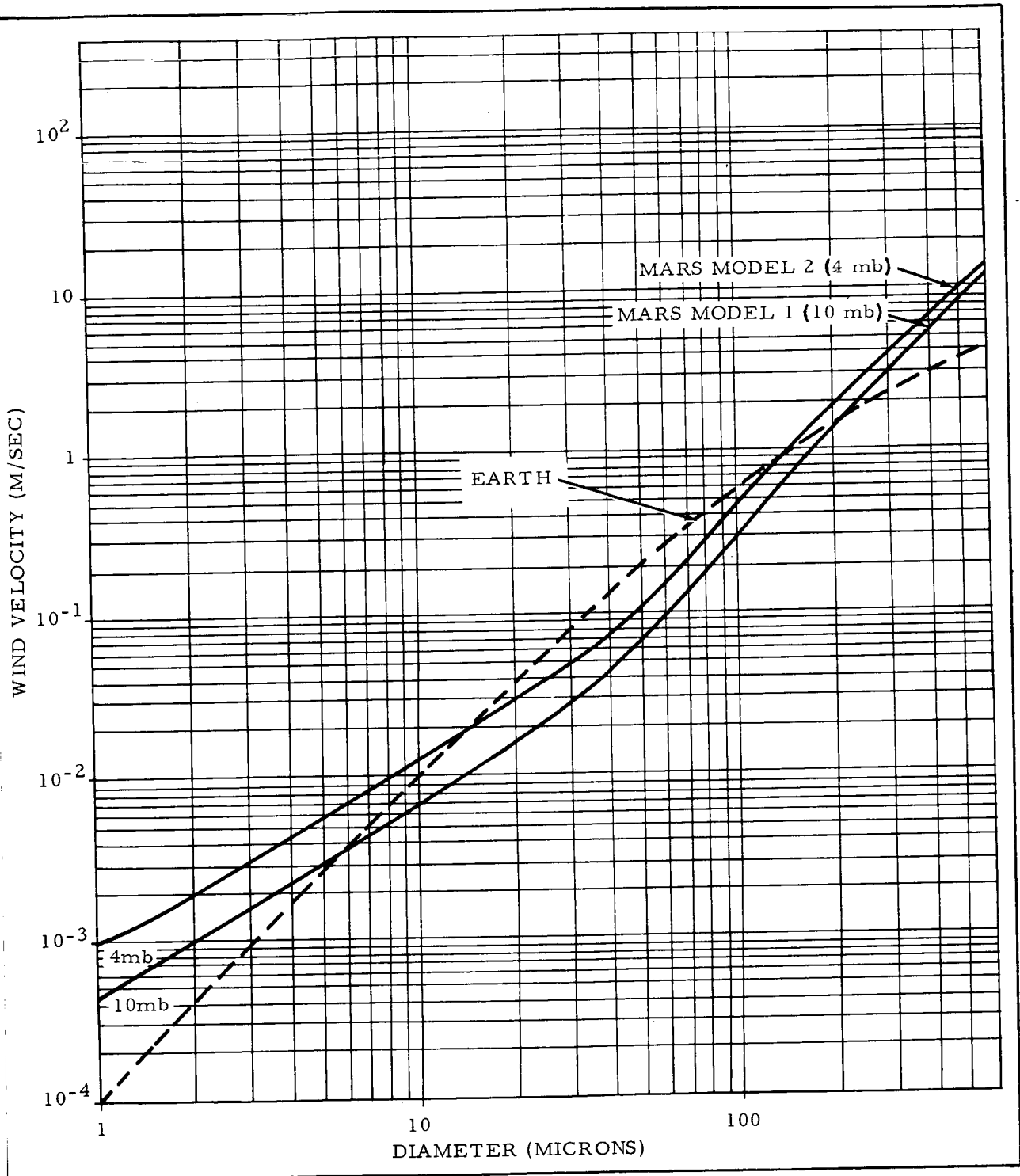


Figure 3. MINIMUM VERTICAL WIND VELOCITIES NECESSARY TO MAINTAIN PARTICLES ALOFT AS A FUNCTION OF GRAIN SIZE

From the results of the preceding calculations and discussion, it appears that Martian atmospheric and surface conditions will be conducive to both the formation of dust clouds and eolian surface features.

B. Dust Devils as Agents for Transporting Martian Unconsolidated Material

The yellow clouds on Mars have been explained in several ways. Of these explanations, horizontal wind storms appear to be the most likely cause of the large-scale phenomena. Smaller-scale disturbances, below the resolving power of Earth-based observations, probably exist also. The source of many of these small-scale phenomena may be dust devils.

Sinclair [10], in his studies, observed high horizontal and vertical wind velocities near the ground. Similarly, Ives [11] observed the transport of large amounts of dust to high altitudes through the agency of dust devils. This has been taken by Neubauer [12] as a strong argument for proposing that small-scale cyclonic wind systems are a possible explanation for the yellow clouds.

Neubauer [12] proposed that "...small scale cyclonic wind systems can explain the formation of dust clouds, even in the absence of strong large scale wind systems." His calculation of the time-dependent vertical temperature profile for the region very close to the Martian surface indicate "...a very steep temperature gradient near the ground around the time of temperature maximum."

Neubauer extended his analysis to the mechanism of the dust devils. His analysis of the dust devil is based on a simple integration of the equation of motion from the Martian surface to the top of the dust devil. The major relationship resulting from the analysis was the maximum wind velocity at the top of the dust devil

$$v_{\max}^2 = 2g \Delta T_0 / \bar{T}_0 b \quad (6)$$

where g is the acceleration of gravity (375 cm/sec^2 on Mars), ΔT_0 is defined as $T_0 - \bar{T}_0$, T_0 is the surface atmospheric temperature, \bar{T}_0 is the daily mean surface atmospheric temperature, and b is proportional to $1/D$ where D is the dust devil diameter. By analogy to Earth dust devils, Neubauer obtained the relationship $bD \approx 4/15$ and, therefore,

$$v_{\max} \approx 2.5(gD\Delta T_0 / \bar{T}_0)^{1/2}. \quad (7)$$

However, the results of Neubauer should be checked since he assumed the main constituent of the Martian atmosphere to be nitrogen rather than the now generally accepted carbon dioxide.

Thus, according to Neubauer "...the critical parameter for the wind velocities in a dust devil is $g\Delta T_0 / \bar{T}_0$. Furthermore, one would expect the number of dust devils created per unit area and unit time to increase as $\Delta T_0 / \bar{T}_0$ increases." To support his argument for the enhanced occurrence of dust devils on Mars, Neubauer calculated a $\Delta T_0 / \bar{T}_0$ of 0.21 for the maximum value resulting from his analysis of the temperature profile near the ground and compared this value with a typical value for Earth of 0.12 (given by Ives [11]). This comparison

shows that the initiation of dust devils should occur more easily on Mars than on the Earth.

Sinclair [10] and Ives [11] suggest that the up-currents of dust devils can reach the very high altitudes, of 5 to 9 km. This is also the altitude at which de Vaucouleur's [13] has observed dust clouds on Mars.

Tang [14] calculated the maximum surface wind speed on Mars that might exist in a storm. He suggested that the maximum surface wind velocity on Mars would be found in a tornado, assuming that such storms could exist. The calculations were based on a formula for the maximum surface wind velocity for a convective vortex as derived by Kuo [15]

$$V_{\max} = \gamma RT_o \left\{ \frac{2}{\gamma-1} \left[1 - \left(\frac{p_c}{p_o} \right) k \right] \right\}^{\frac{1}{2}} \quad (8)$$

where

V_{\max} = Maximum tangential velocity

γ = The ratio of specific heat at constant pressure to that at constant volume

R = Gas constant for the atmosphere

p_c = Surface pressure at the center of the vortex (central pressure)

p_o = Surface pressure at a distance where the wind velocities are nil (surrounding pressure)

k = Poisson constant

T_o = Surface temperature.

Tang obtained a maximum surface wind velocity of 114 m/sec in the vortex of a Martian tornado when assuming a surface pressure of 25 mb and a pressure drop to the center of the vortex of 2 mb.

III. SIGNIFICANCE OF EOLIAN SURFACE FEATURES

Interpretation of present or past climatic conditions from eolian surface features is common in geological analysis and should be applicable to a better understanding of the Martian and other planetary atmospheres. Numerous studies have been made concerning conditions and factors entering into the formulation of ripples, dunes, sand drifts, regs, sand sheets, and other related eolian phenomena. Again, as in the physics of particle movement, comprehensive studies of these problems should consist of theoretical, experimental, and field approaches.

Although sand ripples have interested scientists for many years, explanations for their existence and physical characteristics still remain controversial. Early attempts assumed that the formation of eolian and fluvial sand

ripples were analogous. Experimental studies, however, indicated that the similarities between the two types of ripples are superficial, and that fundamental differences exist in the processes and conditions under which they are formed.

Bagnold [1] recognized that combinations of various factors were responsible for eolian sand ripples: wind, saltation, size of surface grains, surface relief, and the state of sand movement (erosional or depositional phases). Because these factors are mutually interactive, they underlie the numerous interpretations of the ripple phenomena.

In recent work, Sharp [16] concludes that ripple dimensions (height, wave length, and index) are controlled by the size of grains traveling by surface creep and wind velocity. He found that the degree of asymmetry of individual sand ripples varies inversely with wind velocity and directly with grain size. Of particular interest were Sharp's observations of the rate of movement of ripples. Under wind velocities ranging from 16 to 40 mph, ripples were observed to move at velocities of 0.35 to 3.2 inches per minute. By observing the rate of movement of a particular ripple, the wind direction can be determined, and wind velocity and ripple particle size can be calculated if values are known for one of them. The possibility of applying this approach to observations made from a Mars probe is intriguing.

Of the large-scale eolian features, sand dunes are the most valuable in determining present climatic conditions. Their shapes, sizes, and rates of movement are indicative of wind direction and velocity. Careful analysis of aerial photographs of sand dunes not only can supply information concerning the winds that formed the dunes, but may also indicate the characteristics of the material composing the dunes.

The classical dune shapes develop best in desert regions where wind direction and velocity are the primary controlling factors. Dunes also develop in riverine and coastal areas where other factors enter into their forms. For example, the characteristics of riverine and coastal dunes are greatly influenced by moisture and vegetation which contribute to confused forms. Most dunes, however, are complex features and may occur alone or in groups.

The barchans and seif dunes common to desert regions are perhaps the best known eolian features. The barchan, for example, is indicative of a moderate wind with a nearly constant direction. The well-developed barchan is a crescent-shaped feature with the horns trailing off downwind. Barchans are usually migratory and range in size from a few meters to 90 meters in height and up to 400 meters across. Rates of movements as high as 50 feet per year have been measured. Bagnold, using his wind tunnel experiments as a basis, formulated the following equation for predicting the forward movement of barchans:

$$C = \frac{q}{\gamma H} \quad (9)$$

where

C = Displacement (m/hr)

γ = Bulk specific gravity of the sand (tons/m³)

H = Height of the dune (m)

166 q = Rate of sand transportation by the wind (metric tons/linear meter/hr).

The rate of sand transportation (q) is defined as

$$q = 1.5 \times 10^{-9} (v - v_t)^3 \quad (10)$$

where

v = Effective wind velocity at heights z (m/sec)

v_t = Threshold velocity (m/sec).

The results of field studies have generally confirmed the validity of Bagnold's equations.

Seif dunes are relatively large features that may extend for hundreds of miles and may reach heights as great as 200 meters. Because they line up approximately parallel to the prevailing wind, seifs are often referred to as longitudinal dunes. Bagnold maintained that two winds were involved in the formation of the dunes. A prevailing gentle wind parallel to the trend of the seif chain is responsible for the lengthening of the chain. Sand-bearing storm winds blowing out of a single quarter controlled the height and width of the dunes.

Assuming the availability of source material and the presence of high-velocity winds, it appears reasonable that barchan, seif, and other dunes can exist on Mars. Thus, analysis of photographs of Mars obtained by spacecraft could supply valuable information concerning the direction and velocity of surface winds.

IV. SIMULATION FACILITIES

Simulation experiments are a necessary part of any comprehensive study of eolian processes. The results of analysis of eolian processes and the problem of interpreting eolian landforms indicate that two types of simulation facilities would be desirable. These are a horizontal wind facility capable of simulating both terrestrial and Martian environments for studying the acquisition, transportation, and deposition of rock fragments; and a facility for simulating terrestrial and Martian dust devils.

A. Horizontal Wind Facilities

Before the problem of Martian eolian processes can be approached with confidence, it is necessary to increase our knowledge of eolian processes on Earth. Investigators, particularly Bagnold, have shown the feasibility of wind tunnel experiments from both a scientific and engineering point of view when the experiments are coupled with both theoretical and field studies.

Recent advancements in simulation technology and measuring techniques make it possible to improve the accuracy and to expand the scope of earlier studies to include a large variety of samples (density, size, shape, etc., of particles) and environmental conditions.

Although there has been very little simulation work done in the study of Martian eolian processes, some preliminary simulation was performed by Hertzler et al., [17]. These studies were concerned mainly with threshold velocities required to pick up various types of dust, and with the resulting abrasion on some selected surface coatings. However, the facilities used did not permit adequate studies to fully define the flow field. The velocity gradients du/dz were not determined, nor were the particulate density profiles. In fact, the flow bed was not long enough to determine whether the flow was fully developed, and no mention was made of the surface boundary layer. A longer flow bed would have permitted (at least qualitatively) an investigation of the particle saltation, surface creep, rate of particle movement, and small-scale surface features.

1. Terrestrial Wind Simulation Facility. The design requirements of a facility to simulate terrestrial dust storms must be considered first. The physical requirements are far easier to meet in the case of a terrestrial dust storm simulator since the facility may be exhausted directly to the atmosphere. The major design parameters are listed in Table 2.

The suggested facility size is based only on preliminary estimates. Final design would be based on considerations of the boundary layer thickness, attainment of fully developed flow, and of the overall facility cost. The terrestrial wind simulation facility would be much simpler to design, fabricate, and operate because there is no requirement for vacuum pressures or for recovery of the flow medium. The suggested major components of the facility are the flow conditioning system (including filtration, heating or cooling, and humidification or dehumidification), axial flow fan, flow straightening section and test bed section (including heating or cooling systems), and monitoring instrumentation.

2. Martian Wind Simulation Facility. Ranges of the design requirements for a facility to simulate Martian dust storms (Table 2) were acquired through a review of the latest analytical efforts on the subject. The cost of vacuum pumping equipment capable of handling the required flows may largely dictate facility size. Added to this problem is the increased boundary layer thicknesses that would be experienced by this facility over the facility required to simulate terrestrial dust storms. The problems involved with construction of a Martian wind simulation facility include at least the following: the facility must be able to withstand vacuum pressure; the vacuum pumping system must maintain a relatively large mass flow rate for extended periods of time; test section must be large enough to compensate for boundary layer growth; and a pumping system may be required for the recovery and recompression of the special flow medium. Thus, the design requirements for a facility to simulate the Martian surface winds are far more stringent than for the terrestrial simulator.

Table 2. TERRESTRIAL AND MARTIAN WIND SIMULATION FACILITIES DESIGN REQUIREMENTS

Parameter	Terrestrial	Martian
Flow Medium	Air	CO ₂ and N ₂
Static pressure	1 atmosphere	4-25 mb
Wind Velocity	0-160 km/hr	0-400 km/hr
Test bed temperature	240-328°K	175-300°K
Air (wind) temperature	240-328°K	175-300°K
Air (wind) relative humidity	≈0-100%	≈0
Test section area	122 cm x 122 cm	122 cm x 122 cm
Test section length (min.)	12.2 m	12.2 m
Particle sizes	≥1 μ	≥1 μ

3. Required Measurements. To specify completely the conditions at any position in the facility, it is necessary to determine the local velocity, static pressure, temperature, Reynolds number, and particulate density (concentration of the small particles entrained in the flow). These conditions may be specified by obtaining the following measurements: freestream static pressure, p ; stagnation pressure, p_0 ; stagnation temperature, T_0 ; sand flow, q ; and particulate density, ρ_p . Pressures and temperatures probably can be measured with little difficulty by conventional instrumentation (except for the contaminating influence of the dust particles). Determination of the particulate density will be decidedly more difficult. It may be necessary to use flow measurement techniques such as high-speed motion pictures, shadowgraph, or rake probe, to obtain useful particulate density profiles. Although the high-speed motion pictures, shadowgraphs, and similar flow visualization techniques may provide useful information, they will probably give only qualitative results. It is believed that the rake probe will produce density profiles of a more quantitative nature.

Determination of the remaining flow parameters can be accomplished by conventional instrumentation. Entrainment of dust particles will cause some changes in the flow parameters, and measurement of these effects is expected to be relatively difficult for low entrainment rates. High entrainment rates may cause larger changes in the flow field; however, the flow parameters may be more difficult to measure because of the abrasive and clogging action of the dust.

B. Dust Devil Simulation Facility

It appears that an effort should be made toward improving the theoretical analysis of dust devils before the design of a simulation facility, which necessarily follows from theory, is undertaken. To accomplish this, the following effects should be added to Neubauer's analysis: surface friction, the influence of the dust content of the air on the dynamics of the dust devil, and the decrease of air density with height. As mentioned earlier, Neubauer assumed the major constituent of the Martian atmosphere to be nitrogen rather than the recently accepted carbon dioxide. Thus, the analysis should reflect the latest generally accepted values.

A facility to simulate terrestrial and Martian small-scale cyclonic disturbances (dust devils) would be considerably different from the conventional low speed wind tunnels used to create horizontal wind velocities. The maximum velocities to be attained at the top of the facility would be in the range of 10 to 60 m/sec or possibly higher depending on the grain (particle) diameter and density of the flow medium [18]. The mass flow rate of the facility will be small compared to the facility simulating horizontal winds.

The facility would be constructed with its flow channel mounted in a vertical position to allow the natural and induced convection to create the required flow patterns. The heat required to warm the base of the facility (simulating the soil surface) could be provided by resistance heaters located in the base, or by quartz lamps directed at the base from above. Resistance heaters in the base would be far simpler. The cyclonic motion of the outer flow layer (simulating the outer perimeter of the disturbance) could be

induced by a series of jets mounted to introduce the flow tangentially. An alternate would be to create cyclonic motion by fans (possibly of the centrifugal type) located on the outer perimeter of the facility and use very-low-speed jets for mass addition. The latter method would be resorted to only if the required velocities could not be attained by the tangentially mounted jets.

Parametric design studies would have to be performed to establish the size of the facility. Although it would be desirable to use the same facility to simulate both terrestrial dust devils and the Martian dust devils, there are several reasons to believe that this may not be feasible. As mentioned earlier the terrestrial simulation facility using air as a flow medium could use a large, relatively low-speed fan exhausting to the atmosphere. The Martian simulation facility would not be nearly so simple because attainment of the correct static pressure would require inducing a vacuum to the level of approximately 5 to 7 mb by means of steam ejectors or similar pumps. In addition, it may be necessary to find an economical means of reclaiming the flow of gaseous carbon dioxide for the Martian facility. The low static pressure of the Martian facility would require much heavier construction than would the facility for terrestrial simulation.

Design of facilities to simulate terrestrial and Martian dust devils must rely on observation of terrestrial dust devils and subsequent scaling to predict the dust devils assumed to exist on Mars. It is believed that the problems of attaining reasonable cyclonic motions and temperature and pressure profiles can be overcome. Construction of the Martian dust devil simulator should be no more difficult than that of the typical medium-size altitude chamber.

V. CONCLUSIONS

The small amount of available information concerning the Martian atmosphere, particularly wind velocities, circulation patterns, probability of sand and dust storms, and related phenomena, is far from being satisfactory design criteria. However, until more and higher quality information is obtained by direct sensing methods, this deficiency can be partly alleviated by data obtained from vacuum chambers and wind tunnel simulation experiments. Also, these studies would improve the accuracy of interpretation of data returned from early planetary probes. Correct interpretation of sand and dust storms and eolian landforms could supply information concerning Martian wind velocities, circulation patterns, and particle densities long before planetary probes penetrate the Martian lower atmosphere.

The principal objectives of the simulation studies are to analyze the dynamic processes in the acquisition, transportation, and deposition of rock fragments, and to investigate methods for determining the direction and velocity of the dominant winds of a region by the analysis of the small- and large-scale eolian terrain features. A more detailed, although not necessarily complete, list of objectives are to estimate Martian wind velocities based on dust cloud simulation; to determine range of particle sizes (shape and mineralogy determined by geologic studies) likely to compose Martian dust clouds and eolian surface features; to determine particle settling rates; to determine the effects of surface roughness on surface winds and particle movement; to study the effects of sand and dust movement on the surface winds; and to acquire a better understanding of particle motion (suspension, saltation, and surface creep) in general.

Although the results of theoretical studies are of great value, these studies must be supplemented by experimental data to fully evaluate the eolian phenomenon both on Earth and on Mars. For example, the application of Bagnold's threshold velocity equations to grain sizes smaller than 0.04-mm diameter under Earth conditions is highly speculative. Experimental data is also needed to accurately determine vertical wind velocities required to maintain particles with diameters $>100\mu$ aloft under Martian atmospheric conditions. In general, there is a need for simulation experiments to verify the application of the principles of terrestrial physics of particle movement to the Martian environment.

The results of this study indicate that conditions necessary for the transportation and deposition of dust and sand and the formation of characteristic eolian landforms are probably present on Mars. Theoretical calculations indicate that impact threshold velocities one meter above the surface range from 75 m/sec to 55 m/sec. The higher value was calculated using a 4-mb atmospheric model and a roughness factor equivalent to a rough terrestrial desert while, a 10-mb atmospheric model and a roughness factor approximately seven times rougher were used in calculating the lower value. Since these minimum velocities are for medium-grain sands, sand dunes probably exist on Mars. While these velocities are high, they are within the range of velocities predicted for Martian surface winds, and do not unduly tax the state-of-the-art of simulation technology. In recent years, advancements in simulation technology and measuring techniques make it possible to improve the accuracy and to expand the scope of earlier studies to include a large variety of samples (density, size, shape, etc. of particles) and environmental conditions. Three types of simulation facilities are desirable, a horizontal wind facility, a dust devil simulator, and an unconsolidated material physical properties laboratory. Each facility should be capable of simulating both terrestrial and Martian environmental conditions.

Several areas needing further investigation are (1) evaluation and updating previous theoretical studies for use as a guide for planning and evaluating simulation experiments and facilities; (2) simulation of eolian processes using horizontal wind and dust devil facilities under both terrestrial and Martian environmental conditions; (3) supplementing these experiments with experiments concerning the physical properties of unconsolidated material; (4) theoretical and experimental studies of electrostatic effects; and (5) field studies to validate theoretical and experimental studies.

REFERENCES

1. Bagnold, R. A., The Physics of Blown Sand and Desert Dunes, Methuen and Co., Ltd, London, 1965.
2. Krumbein, W. C., "Settling Velocity and Flume-Behavior of Nonspherical Particles," Am. Geophys. Union, Trans., 1942.
3. Krumbein, W. C., and Pettijohn, F. J., Manual of Sedimentary Petrography, Appleton-Century Co., Inc., New York, 1938.
4. Blair, J. T., Lucas, W. C., Stanley, J. T., and Tatom, F. B., "Analytical Model of the Martian Surface," Northrop Space Laboratories, Contract NAS8-20082, Report No. TR-793-7-142, 1967.

5. Dollfus, A., "Visual and Photographic Studies of the Planets at the Pic du Midi," Planets and Satellites, B. M. Middlehurst, ed., University of Chicago Press, 1961.
6. Johnson, R. W., "Terrain and Soil of Mars," Ninth Annual American Astronautical Society Meeting, Los Angeles, California, 1963.
7. Ryan, J. A., "Notes on the Martian Yellow Clouds," Journal of Geophysical Research, Vol. 69, No. 18, September 1964.
8. JPL Technical Memorandum No. 33-234, 1966.
9. Weidner, D. K. and Hasseltine, C. L., ed., "Natural Environment Design Criteria Guidelines for MSFC Voyager Spacecraft for Mars 1973 Mission," NASA TM X-53616, 1967.
10. Sinclair, P. S., "Some Preliminary Dust Devil Measurements," Monthly Weather Review, Vol. 92, No. 8, August 1964.
11. Ives, R. L., "Behavior of Dust Devils," Bull. Am. Meteorol. Soc., Vol. 28, 1947.
12. Neubauer, F. M., "Thermal Convection in the Martian Atmosphere," Journal of Geophysical Research, Vol. 71, No. 10, 15 May 1966.
13. de Vaucouleurs, G., Physics of the Planet Mars, Faben and Faben, Ltd., London, 1954.
14. Tang, W., "Some Aspects of the Atmospheric Circulation on Mars," NASA Contractor Report, NASA CR-262, July 1965.
15. Kuo, H. L., "Dynamics of Convective Vortices and Eye Formation," The Atmosphere and the Sea in Motion, The Rockefeller Institute Press (New York) in Association with Oxford University Press, 1959.
16. Sharp, R. P., "Wind Ripples," Journal Geology, Vol. 71, 1963.
17. Hertzler, R. B., Wang, E. S. J., and Welbers, O. J., Development of a Martian Environmental Simulation Facility, McDonnell Aircraft Corporation, St. Louis, Mo., 1966.
18. Anderson, A. D., "Spherical Particle Terminal Velocities in the Martian Daytime Atmosphere from 0 to 50 Kilometers," Lockheed Palo Alto Research Laboratory, Palo Alto, California, LMSC 6-76-66-21, September 1966.

A COLLECTION OF PAPERS RELATED TO PLANETARY METEOROLOGY

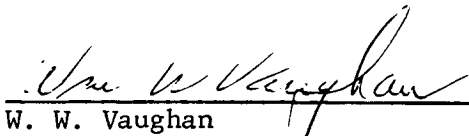
Edited by Don K. Weidner

The information in this report has been reviewed for security classification. Review of any information concerning Department of Defense or Atomic Energy Commission programs has been made by the MSFC Security Classification Officer. This report, in its entirety, has been determined to be unclassified.

This document has also been reviewed and approved for technical accuracy.



R. E. Smith
Chief, Space Environment Branch



W. W. Vaughan
Chief, Aerospace Environment Division



E. D. Geissler
Director, Aero-Astrodynamic Laboratory

DISTRIBUTION

DEP-T

Dr. Rees

R-DIR

Mr. Weidner

R-SE

Mr. L. Richards (2)

R-ASO

Mr. Williams (2)
Mr. H. S. Becker
Mr. Carter
Mr. Huber
Mr. Hamby
Mr. Danenberg
Mr. Spears
Mr. Woodcock
Mr. Bradford
Mr. Brown
Mr. Madewell
Mr. Schaefer
Mr. Tidd

R-ASTR

Dr. Haeussermann
Mr. Digesu (2)
Mr. Hamilton
Mr. Hosenthien
Mr. Dodds
Mr. Moore
Mr. Wagnon
Mr. Brandner
Mr. Horton

R-EO

Dr. Johnson (2)

R-ME

Mr. Kuers
Mr. Maus
Mr. Groth

I-DIR

Brig. Gen. O'Connor

R-P&VE

Dr. Lucas
Mr. Hellebrand
Mr. Palaoro
Mr. Goerner
Mr. Johns
Mr. Darwin
Mr. Laue
Mr. deSanctis
Mr. Vaccaro
Mr. Paul
Mr. Kroll
Mr. Brooksbank

R-QUAL

Mr. Grau

R-SS

Dr. Stuhlinger (2)
Mr. Downey
Mr. Bensko
Dr. Hale
Dr. Shelton
Dr. Dozier
Mr. Heller (2)
Dr. Becher

I-SAA

Mr. Belew

I-MO-MGR

Dr. Speer

R-COMP

Dr. Hoelzer
Mr. E. Seely
Mr. P. Harness

RSIC

MS-IP
MS-IL (8)
MS-H
I-RM-M
CC-P
MS-T (5)